MESOSCALE VARIABILITY ON THE NEW JERSEY SHELF: EFFECTS OF TOPOGRAPHY, SEASONS, WINDS, AND OFFSHORE FORCING ON CIRCULATION, HYDROGRAPHY, AND TRANSPORT

BY

DONGLAI GONG

A dissertation submitted to the

Graduate School—New Brunswick

Rutgers, The State University of New Jersey

In partial fulfillment of the requirements

For the degree of

Doctor of Philosophy

Graduate Program in Oceanography

Written under the direction of

Scott M. Glenn

And approved by

_____

_____

_____

_____

_____

New Brunswick, New Jersey

October, 2010

ABSTRACT OF THE DISSERTATION

Mesoscale Variability on the New Jersey Shelf: Effects of Topography, Seasons, Winds, and Offshore Forcing on Circulation, Hydrography, and Transport

by Donglai Gong

Dissertation Director: Scott M. Glenn

Continental shelf transport and shelf-slope exchange processes are driven by a combination of meteorological, oceanographic and topographic forcing mechanisms. The varied response of the water column to particular forcing combinations can lead to either cross-shelf dominated or along-shelf dominated shelf transport on different time scales. Using data from a coastal ocean observatory, this study investigates how different physical forcing mechanisms such as changing seasons, wind stress, storms, slopewater eddies/rings, river plumes and large scale alongshelf forcing affect the hydrography and circulation at the mid- to outer New Jersey Shelf. The NJ Shelf undergoes large changes in stratification from well mixed during the winter to highly stratified during the summer. The stratification controls the response of the water column to wind forcing. The wind-driven surface flow oscillates between being alongshelf dominated during spring and autumn, and cross-shelf dominated during winter and summer. Cross-shelf

transport takes place on the time scale of 1 to 5 weeks.

When multiple watermasses converge at the shelf-slope front (SSF), complex hydrographic patterns and flow behaviors can emerge, especially during the stratified summer season. The SSF has a characteristic along-shelf scale of 10-30 km and a characteristic cross-shelf scale of 5-20 km. The different types of slopewater salinity intrusions at the outershelf drive the variability of the SSF and stratification on tidal to intra-seasonal time scales. Four types of salinity intrusions outlining the SSF were identified based their hydrographic properties. Along-shelf wind stress affects the location of the foot of the front, river discharge and offshore eddies affect the strength of surface and pycnocline intrusions. Eddies can also drive frontal movement and influence secondary circulation below the pycnocline. Upwelling and downwelling associated with the SSF connect the bottom boundary layer with the pycnocline, bringing heat and salt into the water column interior. Tropical and extra-tropical storms at the beginning of the autumn entrain the heat and salt advected onto the shelf through vigorous transport and mixing, marking the beginning of transition from a summer stratified to a winter well-mixed regime.

List of Tables

List of Figures

Acknowledgements

I would like to thank my Ph.D. dissertation advisor, Dr. Scott M. Glenn, without his support, this study would not be possible. He took me in as a student, and guided me to become a teacher and a colleague, for that I am forever grateful. I also would like to thank my dissertation committee, Dr. Robert Chant, Dr. Glen Gawarkiewicz, Dr. Oscar Schofield and Dr. John Wilkin, for their helpful comments and constant support. My colleagues and collaborators at RUCOOL not only enabled my study with their support and hard work but also made my study enjoyable. I would like to thank Dr. Josh Kohut, Dr. Hugh Roarty, Chip Haldeman, Jennifer Bosch, Elias Hunter, John Kerfoot and Courtney Kohut who offered me invaluable help countless number of times. I am very proud to be part of the RUCOOL family. I also would like to thank Dr. Peter Rona, Dr. Vince Guida and Dr. Dennis McGillicuddy for teaching me to becoming a seagoing oceanographer. I want to thank Dr. Paul Falkowski for pushing me to think beyond 'moving chairs'. Two of my teachers that I would to especially thank are my Sifu Lawrence Hill and my middle school algebra teacher Mrs. Bishop. They inspire me to become a teacher myself. Finally, I would like to give a special thanks to my mom Yingming Zhao, my dad Leiguang Gong and my wife Livia Gong for their inspiration, sacrifice, and support. I would like to thank the Office of Naval Research for supporting me throughout my graduate study.

Dedication

To my parents, Yingming and Leiguang, and my wife Livia.

Table of Contents

Chapter 1

Introduction

The continental shelf is the interface between the land and the open ocean. A significant amount of transport from and mixing between the human-influenced riverine water, often loaded with nutrients, pollutants, and sediments, and the open ocean water, typically nutrient poor, low in pollutants and sediments, takes place on the continental shelves around the world. Various types of physical forcing mechanisms such as solar insolation, river discharge, winds, storms, topography, upstream forcing, and offshore rings/eddies affect the type and the rate of mid-latitude shelf-slope transport and exchange processes. My dissertation focuses on characterizing and understanding the subtidal temporal and spatial variability of these processes acting on the central portion of the Mid-Atlantic Bight (MAB).

In Chapter 2, the spatial structure of the mean and seasonal surface circulation in the central region of the Mid-Atlantic Bight (New Jersey Shelf) are characterized using six years of CODAR Long Range HF Radar data (2002-2007). The mean surface flow over the NJ Shelf was 3-12 cm/s downshelf and offshore to the south. The detided Root Mean Squared (R.M.S.) velocity variability ranged from 11 to 20 cm/s. The variability was on the order of the mean current offshore and several times that of the mean current nearshore. The Hudson Shelf Valley (HSV) and the shelfbreak acted as dynamical boundaries that define the NJ Shelf. The surface flow on the NJ Shelf

depended on topography, seasonal stratification and wind forcing. The flow was in the approximate direction of the wind during the unstratified season and more to the right of the wind during the stratified season. During the stratified summer season, the dominant along-shore upwelling favorable winds from the SW drove cross-shelf offshore flow. During the unstratified winter season, the dominant cross-shore NW winds drove cross-shelf offshore flows. During the transition between the stratified and the mixed seasons in the spring and autumn, along-shore NE winds, often associated with storm events, drove energetic downshelf alongshelf flows. The surface transport pathways are either cross-shelf dominated during summer and winter, or along-shelf dominated during the transition seasons. The residence time of surface Lagrangian drifters on the NJ Shelf ranged from 1 to 7 weeks with summer and autumn showing faster transport than winter and spring. This chapter has been published in the Journal of Geophysical Research (*Gong et al.*, 2010). The co-authors are myself, Dr. Josh Kohut and Dr. Scott Glenn.

In Chapter 3, the subtidal to intra-seasonal variability of cross-shelf exchange processes on the outer New Jersey Shelf is characterized for summer 2006 using data from a suite of moorings, satellite, and gliders. The key results are: (1) The structure and location of the shelf-slope front (SSF, represented by the isohaline of 34) varied on tidal to intra-seasonal time scales due to the combined forcings of seasonal heating, wind stress, river discharge, tides, offshore rings/eddies, frontal interactions, and storms. Among these, the high summertime discharge from the Hudson River, wind forcing, the presence of slope water eddies, and storms had the most significant effect on shelf-slope exchange. (2) Different forcing mechanisms affected the different parts of the water column. Along-shelf wind stress affected the location of the foot of the front,

river discharge and slope water eddies affect the surface and pycnocline hydrographic structure, and frontal movements affected secondary circulation in the water column interior. The combination of the different physical forcing mechanisms led to unique configurations and dynamical states of the SSF. (3) The slope water intrusions were 3-D structures that varied in time. Along-shelf features were coherent on the 10-30 km scale, and cross-shelf features were coherent on the 5-20 km scale, although pieces of intrusions could be observed up to 40 km shoreward of the 100 m isobath. Temporal variability was predominantly in the semidiurnal, inertial and 4-8 days bands. (4) Outershelf stratification was correlated with the intensity of nonlinear internal wave activity. Strong shelf stratification coincided with a period of strong internal tide, which induced a peak in nonlinear internal wave activity on the NJ shelf during August 17-19, 2006. This chapter is to be submitted to the Journal of Geophysical Research. The co-authors are myself, Dr. Josh Kohut, Dr. Renato Castalao, Dr. Oscar Schofield, and Dr. Scott Glenn. In particular, Dr. Renato Castalao contributed key insight and data in the analysis of the effect of wind forcing on the location foot of the SSF.

In Chapter 4, secondary circulation at the SSF is studied in detail. A double thermohaline interface of the shelf-slope front (SSF) was observed to form on the outer New Jersey Shelf during the onshore approach of a warm core ring in August 2006. Shoreward movement of the SSF brought saltier offshore water onshore. Applying the methods of accumulated temperature change (*Pickart*, 2000) and inspection of the vertical temperature gradient (dT/dz) on high resolution cross-shelf glider hydrographic observations indicated that there were two regions of bottom boundary layer (BBL) detachments and that upwelling/downwelling in the vicinity of the SSF were occurring on the outershelf. The two observed BBL detachment regions were separated by 10 km

in the cross-shelf and were coherent in the along-shelf for at least 10 km but less than 30 km. A temperature change of 2 °Cand salinity change of 1 were observed across both interfaces with a characteristic width of 5 km. Intrusion of salty offshore water ($S > 34$) was prevalent in the water column below the pycnocline during the onshore excursion of the SSF. The observed hydrographic features connecting the BBL and the thermocline suggests that enhanced secondary circulation during front-eddy interactions could drive increased vertical mixing and transport of heat, salt, and nutrients at the outer continental shelf during the stratified season. This chapter is to be submitted for publication. The co-authors are myself and Dr. Scott Glenn.

Chapter 2

Seasonal Climatology of Wind-Driven Circulation on the New Jersey Shelf

2.1 Introduction

The Middle Atlantic Bight (MAB), a shallow and wide continental shelf located off the east coast of the United States, is bounded by Cape Cod to the northeast and Cape Hatteras to the southwest (Figure 2.1). It is a highly productive shelf that exhibits strong seasonal cycles in both physical and biological processes (*Bigelow*, 1933; *Bigelow and Sears*, 1935; *Beardsley and Boicourt*, 1981; *Yoder et al.*, 2002). Several major urban estuaries such as the Connecticut River, the Hudson River, the Delaware River and the Susquahana River discharge into the bays and sounds connected to the MAB, delivering fresh and nutrient rich water onto the shelf. Transport of nutrients and organic material can determine the timing and distribution of shelf primary production and the subsequent response in the higher trophic levels (*Yoder et al.*, 2002; *Schofield et al.*, 2008). An important objective of recent research projects is to characterize and quantify the cross-shelf exchange mechanisms and transport pathways on the MAB (*Biscaye et al.*, 1994; *Castelao et al.*, 2008a; *Chant et al.*, 2008; *Zhang et al.*, 2009). This transport is critical to the understanding of shelf marine ecosystem dynamics. The dynamics of shelf circulation are governed by the combined interactive forcing of many factors such as stratification (*Lentz*, 2001; *Flagg et al.*, 2002; *Castelao et al.*, 2008b),

winds (*Allen*, 1980; *Beardsley et al.*, 1985; *Lentz*, 2001; *Whitney and Garvine*, 2005), storms (*Keen and Glenn*, 1995; *Kohut et al.*, 2006a; *Glenn et al.*, 2008), river discharge (*Fong and Geyer*, 2002; *Byoung-Ju and Wilkin*, 2007; *Chant et al.*, 2008), topography (*Harris et al.*, 2003; *Zhang et al.*, 2009), bottom boundary layers (*Gawarkiewicz and Chapman*, 1992; *Chapman and Lentz*, 1994; *Keen and Glenn*, 1994; *Garvine*, 2004), upstream forcing (*Mountain*, 2003), and offshore forcing (*Gawarkiewicz et al.*, 1996a; *Linder and Gawarkiewicz*, 1998; *Churchill et al.*, 2003; *Lentz*, 2003). The seasonal variability of the dominant processes impacts the coupled seasonal biological response. The set of forcing factors driving the dynamics of the midshelf or the outershelf is often different from that of the innershelf. Whereas buoyancy forcing and bottom friction play major roles in the innershelf dynamics, winds and changing stratification are the major drivers of the dynamics at the mid to outershelf. In this study, a 6-year time series of HF Radar surface current data from Rutgers University Coastal Ocean Observation Lab (*Glenn and Schofield*, 2009) is used to characterize the effect of topography, seasonal stratification and wind forcing on the surface subtidal circulation and transport at the mid to outer portion of the New Jersey Shelf. In particular, the surface flows during the transition seasons of spring and autumn are characterized and compared with the stratified summer as well as the unstratified winter. A seasonal climatology of the wind-driven surface current response is constructed and the seasonal transport patterns and residence times are examined.

This paper is structured as follows. In section 2.2, we review the relevant physical processes affecting circulation and transport on the NJ Shelf. In section 2.3, we describe the 6-year Rutgers HF Radar and NOAA NDBC weather buoy dataset used in this analysis. In section 2.4.1 we characterize the mean and the subtidal variability

of surface flow. In section 2.4.2, we characterize the low-wind background flow and effect of topographic features such as the Hudson Shelf Valley (HSV) and the Fortune/Tiger Shore (FTS). In section 2.4.3, we discuss the effect of seasonal variability in stratification and wind on the mean flow over seasonal time scales. In section 2.4.4, we discuss the response of surface flow to seasonal wind forcing. In section 2.4.5, we present the seasonal climatology of the wind-current correlation. In section 2.4.7, we calculate the seasonal cross-shelf transport pathways and shelf residence time. Finally in section 2.4.6, we explore the interannual variability of the current response to changes in seasonal forcing. The results are discussed in section 4.4 and summarized in section 2.6.

2.2 Background

2.2.1 Mean flow & upstream sources

Studies using geochemical tracers have shown that the upstream source of MAB shelfwater originates from southern Greenland with a volume flux of 4-5 Sverdrups (*Chapman and Beardsley*, 1989). Most of this water exits the shelf as it travels downshelf. By the time the coastal current enters the MAB the mean volume flux drops to approximately 0.4 Sverdrups (*Beardsley et al.*, 1985). Historically, the depth-averaged mean flow on the MAB is shown to be 3-7 cm/s downshelf towards the southeast based on current meter moorings (*Beardsley and Boicourt*, 1981). A recent study using an expanded dataset of current meter measurements shows that the mean depth-averaged alongshore flow on the shelf is constant along-isobath and is linearly correlated with the depths of the isobaths, decreasing towards shore (*Lentz*, 2008a). This alongshelf flow has been largely attributed to a basin scale alongshelf pressure gradient (*Beardsley and*

Winant, 1979; *Lentz*, 2008a). A climatological study of MAB hydrography found that shelfwater volume (characterized by salinity < 34) on the NJ Shelf varied seasonally with a magnitude on the order of the mean shelfwater volume (*Mountain*, 2003). Variability about the mean shelf flow is significant on various temporal and spatial scales ranging from tidal to inter-annual and from internal Rossby radius to shelfwide length scales (*Beardsley et al.*, 1985; *Lentz*, 2008b; *Dzwonkowski et al.*, 2008a).

2.2.2 Topography

Topographic variations on the shelf-wide scale can play an important role on along-shelf and cross-shelf transport. The Hudson Shelf Valley (HSV) is the only remaining submarine shelf valley that cuts perpendicularly across the entire width of the MAB shelf. The Fortune/Tiger Shore (FTS) (*Knebel and Spiker*, 1977; *Thieler et al.*, 2007), an ancient shoreline to the south of the HSV, is outlined by the 40 m isobath (Figure 2.1). The steep topography between the 40 and 60 m isobaths at the outershelf edge of this shoreline makes the FTS one of the most prominent features on the shelf besides the HSV. The HSV/FTS system has significant influence on the cross-shelf transport. The HSV acts both as a conduit for cross-shelf flow as well as a dynamical boundary for along-shelf flow. Winds from the NW can drive a strong up valley return flow along the HSV during the winter mixed season (*Harris et al.*, 2003). Analysis of CODAR surface current and ADCP mooring data deployed in the HSV during the Langrangian Transport and Transformation Experiment (LaTTE) showed a clear two layer exchange flow during the spring time (*Chant et al.*, 2008). During the Shallow Water 2006 (SW06) experiment (*Tang et al.*, 2009), satellite Sea Surface Temperature (SST), surface drifters and CODAR surface currents showed that a significant quantity of fresh riverine water

was transported rapidly offshore from the innershelf to the outershelf along a pathway south of the HSV (*Castelao et al.*, 2008a). All this evidence suggests that the flow in the HSV/FTS region can deviate from the long term mean shelfwide flow, depending on the wind and stratification regimes.

2.2.3 Wind Forcing

Wind forcing has long been recognized as an important driver of circulation and transport on continental shelves (*Allen*, 1981; *Winant*, 1980). Studies of the wind-driven response at the innershelf have shown that the surface flow is highly correlated with the wind during the stratified season, consistent with an Ekman-type response, and less correlated with the wind when the water column is mixed (*Kohut et al.*, 2004; *Dzwonkowski et al.*, 2008a). Alongshore winds drive significant cross-shelf transport during the stratified seasons on the North Carolina Shelf (*Lentz*, 2001) while cross-shore wind is found to be the main driver of surface cross-shelf flow on the inner New England Shelf (*Fewings et al.*, 2008). Idealized modeling exercises have also shown that cross-shore wind is a significant driver of cross-shelf flow in a weakly stratified water column (*Tilburg*, 2003). The different depths and external forcing at the inner and outer shelf result in different dynamical balances reflected in the cross-shelf variability of the shelf flow. Prior studies have focused on the circulation and dynamics at the innershelf and the outershelf.

2.2.4 Innershelf

The innershelf dynamics are dominated by buoyancy driven river plumes for most of the year while coastal upwelling becomes more important during the summer time (*Song*

et al., 2001). Coastal river plumes can carry a high concentration of nutrients and pollutants. The response of a buoyancy trapped river plume, such as the Hudson's, to wind forcing, topography and background flow determines both its initial development (*Chant et al.*, 2008) and downstream evolution (*Yankovsky and Garvine*, 1998; *Yankovsky et al.*, 2000), which can then affect the whole shelf ecosystem (*Schofield et al.*, 2008). Extensive research efforts have focused on the effect of upwelling and downwelling favorable alongshore winds on coastal plume dynamics and plume transport (*Fong and Geyer*, 2002; *Chant et al.*, 2008). A springtime CODAR virtual drifter study during the Langrangian Transport and Transformation Experiment (LaTTE) 2005 experiment revealed multiple pathways for Hudson River water leaving the innershelf Bight apex, either along the Long Island coast, the New Jersey coast, or a cross-shelf pathway south of the HSV (*Gong et al.*, 2006; *Zhang et al.*, 2009). Coastal upwelling driven by winds from the southwest brings nutrient rich water near the surface, driving summer time primary production at the innershelf (*Glenn et al.*, 2004). Alongshore downwelling favorable winds, on the other hand, are associated with development of an alongshore coastal plume (*Chant et al.*, 2008). Wind-driven Ekman transport associated with coastal upwelling has been proposed as a dominant mechanism for cross-shelf transport from the innershelf to the outershelf during the stratified season, with much less influence in the mixed season. (*Lentz*, 2001).

2.2.5 Outershelf

At the outershelf, the dynamics are dominated by the shelf-slope frontal interactions. The interface between the shelf water and the slope water on the MAB is porous and highly dynamic. A shelfbreak frontal jet exists at the interface throughout the

year, although its structure varies seasonally with changing hydrography (*Linder and Gawarkiewicz*, 1998). The equatorward along-shelf transport associated with the shelf-break jet is on the order of the shelf wide transport for the MAB, with stronger summer transport than winter transport observed (*Linder and Gawarkiewicz*, 1998). Cross-shelf exchange of shelf and slope water at the shelfbreak is enhanced during the stratified season when the isopycnals are nearly horizontal from the mid-shelf to the shelfbreak. Offshore features such as eddies and Warm Core Rings in the slope sea can modify the velocity structure of the shelfbreak jet (*Gawarkiewicz et al.*, 2001) and enhance the cross-frontal exchange by pulling surface shelf water offshore and/or bring slope water onshore via sub-surface intrusions (*Flagg et al.*, 1994; *Hare et al.*, 2002).

Although there have been case studies of cross-shelf transport pathways on shorter time intervals (*Castelao et al.*, 2008a; *Dzwonkowski et al.*, 2008b), the spatial and temporal variability of the shelf flow is not well known on the seasonal to interannual time scales. The mid-shelf region and the vicinity of a cross-shelf valley such as the HSV are also much less studied. Furthermore, most previous studies of shelf circulation have divided the shelf into a stratified regime and a mixed regime. That approach misses the flow response to winds and changing stratification during the crucial transition seasons. The transition between the stratified and the well-mixed water column is not instantaneous across the entire shelf, but progresses from shallow to deep water over several weeks or months. A complete seasonal climatology of surface circulation for all four seasons over the full shelf is needed to understand the temporal and spatial variability of shelf scale transports and their impact on the observed variability in the shelf ecosystem (*Xu et al.*, 2009).

2.3 Methods & Data

2.3.1 Surface Current

The NJ Shelf has a cross-shelf distance of 90 to 130 km from the innershelf to the shelfbreak and an along-shelf distance of approximately 300 km from the tip of Long Island to Delaware Bay (Figure 2.1). Surface current data were collected on the NJ Shelf from the start of 2002 to the end of 2007 using radial data from three 5 MHz Long Range CODAR (Codar Ocean Sensors SeaSonde HF Radar system) sites along the New Jersey coast: Sandy Hook (HOOK), Loveladies (LOVE), and Wildwood (WILD) (Figure 2.1, black dots). HF Radar uses the Doppler Shift of a radio signal backscattered off the ocean surface to measure the component of the flow in the direction of the antenna (*Barrick*, 1971a,b; *Teague*, 1971). These systems have supported various studies on the New Jersey Shelf including nearshore studies using a 25 MHz standard range system consisting of two shore stations with a coverage area of approximately 30 by 40 km and a resolution of 1.5 km (*Kohut et al.*, 2004, 2006a). Shelf-wide studies have been done using the long range 5 MHz system consisting of three shore stations with an approximate coverage area of 250 km by 160 km and a resolution of 6 km (*Ullman et al.*, 2006; *Hunter et al.*, 2007; *Castelao et al.*, 2008a; *Dzwonkowski et al.*, 2008b, 2009).

Hourly radial data from each station are transfered to the Coastal Ocean Observation Lab at Rutgers University, where the radial vector maps (Radials) are combined to make 2-D current maps (Totals) every 3 hours. Potential ionospheric contamination is eliminated using the manufacturer (CODAR Ocean Sensors) supplied filter applied to each individual Doppler spectra. If ionospheric characteristics are found, data from

the entire range cell are removed. Our approach is consistent with the data processing procedures used in previous studies of the NJ Shelf (*Kohut et al.*, 2006b; *Ullman et al.*, 2006; *Hunter et al.*, 2007; *Dzwonkowski et al.*, 2008b). The resolution of the CODAR radial spectra is dependent on the operating frequency, sweep rate, and FFT length used in processing. Using a standard 1 Hz sweep rate, an operating frequency of 4.55 MHz, and a 1024 point FFT gives a radial velocity resolution of 3.22 cm/s. This operating frequency implies an effective depth of the surface velocity of 2.4 m (*Stewart and Joy*, 1974). When radial data from several sites are combined to estimate a total vector, any non-orthogonal angles would introduce some geometric uncertainty. To eliminate less reliable Totals due to poor radial site geometry, we set a threshold for the estimated Geometric Dilution of Precision (GDOP) (*Chapman and Graber*, 1997). For this analysis we adopt a community recommended geometric mapping error value of 1.5 or less to identify the vectors with acceptable GDOP (*Dzwonkowski et al.*, 2009). This value is chosen based on current comparison studies using CODAR and ADCPs (*Kohut et al.*, 2006a) and CODAR and drifters (*Ohlmann et al.*, 2007). These studies show that when subgridscale spatial variability is accounted for, the adjustable CODAR current resolution is matched to the uncertainty level in the observed currents. The spatial resolution of the final total vector current maps is 6 km with a cross-shelf range of 150 km. The averaged current fields are constructed using the 3 hourly Total vector maps. A minimum of 50 percent temporal coverage over the entire 6 year record is required to be included in the following analysis (Figure 2.2(a)).

Diurnal differences in the CODAR coverage area do occur due to the increase in the background noise levels at night. To assess their potential impact, the standard error of the mean flow was calculated for the full field. The 50% coverage line for the

larger day time and smaller nighttime fields are added to the standard error plot in Figure 2.2(b). In all cases, the standard error remains in the range of 0.25 to 0.35 cm/s with little difference from the intermediate value chosen for this study. The HF Radar coverage area is also affected by the roughness of the sea state, which has been shown to increase with larger wind waves (*Barrick*, 1971a). The theoretical study of *Barrick* (1971a) showed that the returned signal is enhanced in stronger winds up to 15 knots for HF Radar systems operating below 10 MHz. On average, persistent NW winds during winter are stronger than SW winds during summer (*Mooers et al.*, 1976). As a result the CODAR coverage area is often increased during the windy winter compared to the calmer summer.

All CODAR surface currents are detided using the T_TIDE Matlab package (*Pawlowicz et al.*, 2002) before further analysis is performed. Since the outershelf is least affected by the diurnal variations of sea/land breeze due to its distance from shore (*Hunter et al.*, 2007), and the time scale of our study is from monthly to interannual averaging over many tidal, diurnal and inertial cycles, we believe that the higher frequency effects of diurnal coverage difference, sea/land breeze, and tidal/inertial influences will not measurably bias the result of our present study.

2.3.2 Winds

Wind data from five NOAA NDBC buoys (ASLN6, 44025, 44009, 44017, 44004) including four on the NJ Shelf and one offshore in the slope sea (44004) are used for the wind analysis (Figure 2.1, open diamonds). Cross-correlations of the 5 buoys are performed on low-pass filtered (Hamming filter with a 33 hour window) hourly wind data over the 6 years from 2002 to 2007. The cross-correlation coefficients and the temporal lags

of the wind velocity among the five buoys are tabulated in Table 2.1 and Table 2.2, respectively. Over the length scale of the NJ Shelf, winds are highly correlated (> 0.7) at sub-tidal time scales among all four sites on the shelf (Table 2.1). The southern buoys lead the northern buoys and the inshore buoys lead the offshore buoys in time on the order a few hours (Table 2.2). The observed temporal lag is consistent with the fact that most frontal systems propagate northeastward on the MAB shelf. The velocity correlation of shelf wind buoys with the offshore wind buoy are weaker, but are still greater than 0.5 between all sites. The correlation analysis suggests that under many conditions, the wind field of the Mid-Atlantic Bight region had a correlation scale at least the size of the NJ Shelf. For the analysis presented in the following sections, we will be focusing on wind data from NOAA NDBC Buoy 44009 (38.46 N 74.70 W) due to its good temporal coverage and proximity to the center of the study region near the Tuckerton Endurance Line.

2.4 Results

2.4.1 Mean Current & Variability

Mean:

The mean surface flow on the NJ Shelf over a period of 6 years (2002 to 2007), as measured by the Rutgers Long Range CODAR network, is generally offshore and downshelf with a speed of 3-12 cm/s (Figure 2.3(a)). The mean surface flow contained along-shelf and cross-shelf flow structures with velocity ranges from 2 cm/s at the innershelf, to 6 cm/s at the midshelf, to 12 cm/s at the shelfbreak. The weakest flow regions, with a speed of 3 cm/s or less, are observed at the inner to mid-shelf south of the Hudson

Shelf Valley (HSV) and in an area north of the HSV. A band of higher velocity flow 30 to 50 km wide, with an average current speed of 5-7 cm/s, is seen just to the south of the HSV. The fastest surface flow is seen offshore of the 80 meter isobath near the shelfbreak (8-12 cm/s). Just north of the HSV, the flow is weakly downshelf towards the SW. South of the HSV at the innershelf, the flow is offshore, directed towards the SE. At the outershelf, the flow veered clockwise heading downshelf towards the SW. The mean surface flow is largely consistent with the along-isobath, equatorward depth-averaged flow as measured by current meter moorings (*Beardsley and Boicourt*, 1981; *Lentz*, 2008a).

The HSV appears to separate the flow regimes geographically and exert topographic control over local circulation. There is a clear difference in the surface current velocities between regions to the north and to the south of the HSV, with enhanced flow velocity observed to the south compared to the north (Figure 2.3(a)). A divergence map of the mean surface flow illustrates that the 6 year mean flow is divergent over the HSV and north near the midshelf and convergent south of the HSV (Figure 2.3(b)). The persistent divergence zone suggests an enhanced upwelling of sub-surface material. In regions away from the influence of the HSV, the alongshelf component of the flow velocity increases linearly with the water column depth, a result consistent with a simple 2-D shelf model assuming geostrophic balance plus wind forcing for the alongshelf direction (*Csanady*, 1976; *Lentz*, 2008a). The flow in these regions shows no coherent structure in the divergence, though the amplitude of the divergence fluctuations is of the same order of magnitude as the HSV region.

Variability:

Consistent with historical current meter analysis (*Beardsley and Boicourt*, 1981), the variability in the surface current is significant compared to the mean. The root mean square (RMS) of the detided surface current ranges from 11 cm/s at the upper portion of the HSV to 17 cm/s at midshelf regions to the south of the HSV (Figure 2.3(c)). Two regions of high variability are noted, one centered along the 40m isobath near 39.5 N, 73.5 W just south of the HSV, and the other located further to the south near latitude 38.5 N, with RMS of 17 to 20 cm/s. Near the HSV, on the other hand, the RMS speed has much lower values of 12 to 15 cm/s. The average RMS for the whole field is 15.5 cm/s.

Different forcing mechanisms can affect the spatial variability at different scales. Earlier analyses of the spatial correlation of winds and different seasonal stratification suggest that coherent wind forcing and stratification operate at shelf-wide scales while the shelf topography can vary on scales of a few kilometer to tens of kilometers, a fraction of the shelf size. For temporal variability, we hypothesize that wind forcing is the dominant factor after the tidal contribution has been removed. The RMS current speed for the low wind conditions from 2002 to 2007 with an average value of 12.2 cm/s (Figure 2.3(d)) is significantly lower than the total RMS (Figure 2.3(c)). In the following sections we examine how different wind conditions and changing stratification affect the temporal and spatial variability of the surface circulation in the NJ Shelf. The first step is to determine the topographically modulated background flow in the absence of winds so that the effect of large scale forcing can be separated from that of the winds and stratification.

2.4.2 Background Flow & Topography

The large scale along-shelf flow over the length of the MAB has long been observed (*Bumpus*, 1973; *Beardsley et al.*, 1976). Since the very early studies of the MAB shelf, the alongshelf flow has been hypothesized to be driven by a large scale along-shelf pressure gradient imposed at the shelfbreak (*Csanady*, 1976) setup by the large scale circulation in the western North Atlantic (*Beardsley and Winant*, 1979). Such a background flow would exist on the shelf in the absence of wind and other local forcing such as river discharge. To calculate an estimate of the background shelf surface flow due to the large scale alongshelf pressure gradient, the 2002-2007 surface current data was averaged conditionally for winds less than 2 m/s (Figure 2.4(a)). The directional distribution of the winds in this weak wind regime is approximately uniform for all seasons with a mean wind speed of 0.1 m/s. The effect of the sloping cross-shelf topography is clearly seen in the background surface flow, away from the HSV/FTS. The along-shelf flow speed increases from 2-4 cm/s at the innershelf to 6-10 cm/s at the outershelf. Compared to the 6-year mean field (Figure 2.3(a)), the low-wind flow field has a weaker offshore flow component at the inner to mid-shelf.

Assuming maximum velocities of 6-10 cm/s (Figure 2.4(a)), $f = 10^{-4}\ s^{-1}$ and a curvature length scale of $L \sim 50\ km$ derived from the maximum curvature of the flow along the axis of the HSV, the Rossby number of the flow is $Ro = U/fL = 0.025$ or less. This indicates a geostrophic balance dominating these low wind regimes. Even for the larger flow speeds of 30 cm/s occasionally observed on the shelf under strong wind conditions, the Rossby number remains small and less than 0.1, indicating that the nonlinear advective terms in the momentum equation do not contribute significantly to the momentum balance over the seasonal time scale.

A two-dimensional model for the mean circulation on the MAB that assumed a geostrophic balance in the cross-shelf direction and an Ekman balance in the along-shelf direction produced a depth-averaged along-shelf velocity that is a linear function of the depths of the isobaths (*Csanady*, 1976; *Lentz*, 2008a). To evaluate the dynamical importance of winds below 2 m/s, we compare the contributions to the momentum equation by the large scale pressure gradient ($g\,\theta$) and by the mean wind stress ($\tau/\rho_0 h$) for winds below 2 m/s, where $\theta = \Delta\eta/\Delta y$ is the slope of sea surface, τ is the wind stress and h is the depth of the surface mixed layer. Using a mean along-shelf sea surface slope of 3.7×10^{-8} as estimated by *Lentz* (2008a), a mean wind stress of 1.5×10^{-5} N/m^2 (corresponding to a mean wind speed of 0.1 m/s) and a surface mixing layer thickness of $h = 15$ m, the pressure gradient contribution to the momentum equation of 3.6×10^{-7} m/s^2 is over two orders of magnitude larger than the wind stress contribution of 10^{-9} m/s^2, suggesting that the uniformly distributed winds below 2 m/s do not significantly affect the shelf momentum balance.

Topographic features such as the HSV and FTS can modify the shelf flow by introducing along-shelf variability. In the low wind background current field, the flow velocity is enhanced at the midshelf just to the south of the HSV and FTS 2.4(a)). The surface along-shelf velocity for two cross-shelf transects is calculated from the low wind background mean field described above. One transect is just south of the HSV and the other transect is further south near the Tuckerton Endurance Line. The cross-shelf velocity profiles as a function of depth for the two transects are compared with the 2-D model result of *Lentz* (2008a) (Figure 2.4(b)). The linear 2-D model (green line) has a slope of -0.09 $cm\ s^{-1}\ m^{-1}$ and an intercept of -0.6 cm/s, within the range of uncertainty provided by *Lentz* (2008a). The different flow dependence on water depth

is noted for the two transects with different cross-shelf topography. The along-shelf flow across the northern HSV transect (blue), is significantly different from the linear 2-D model (green). The observed flow exhibits a non-monotonic dependence on the depth of the isobath with a maximum in along-shelf velocity observed at the midshelf just to the south of the HSV. The southern transect, on the other hand, has an along-shelf current speed that is nearly a linear function of depth out to the 70 m isobath (red). Offshore of the 70 m isobath, the linear relationship still holds but the flow speed's dependence on depth has a steeper slope. This increase in alongshelf speed seaward of the 70 m isboath is likely due to the effect of the shelf slope frontal jet meandering onto the outershelf near the edge of the CODAR coverage. The shelf-slope frontal jet is not included in the *Lentz* (2008a) model.

The direction and the general features associated with this background flow do not change with the seasons, although the magnitude of the flow in the seasonal low wind field can vary up to 3 cm/s compared to the multiyear mean. Specifically there is enhanced downshelf flow at the outershelf in the autumn and just south of the HSV in the winter. For the majority of the shelf and for most of the year, the variability in the low-wind background flow is less than $2cm/s$. The weak winds condition is not common on the shelf, occurring on average 8% of the time. Over the seasonal time scale, the weak wind condition is more frequent in the summer occurring 10% of the time and significantly less frequent in the winter occurring only 4% of the time. Over the interannual time scale, the annual average of the low wind condition ranges between 6% of the time and 12% of the time over a 20 year period from 1987 to 2007.

Before investigating the surface flow response to winds and stratification on the

NJ Shelf, we want to remove the effect of the topographically modulated pressure gradient driven background flow using the calculated low wind mean surface current as a representation of the surface response to the large scale alongshelf forcing. The multiyear averaged low wind mean is used as the background field because the observed seasonal variability of the low wind current is relatively small and the enhanced coverage gained by combining the limited amount of low-wind data is significant. The calculated background field is then subtracted from the surface current data in our Eulerian analysis of seasonal wind-driven circulation (Section 2.4.4, 2.4.5). This approach enables us to look more directly at the spatial and temporal structure of the flow response associated with the surface wind forcing from various directions and under different stratification regimes.

2.4.3 Stratification, Wind & Seasonal Flow

While many factors contribute to the variability of the surface currents, two significant forcing factors are stratification and wind (*Beardsley and Boicourt*, 1981; *Kohut et al.*, 2004; *Lentz*, 2001; *Dzwonkowski et al.*, 2008b). The NJ shelf undergoes an annual cycle ranging from intense stratification in the summer to mixed conditions in the winter (*Bigelow*, 1933; *Bigelow and Sears*, 1935; *Castelao et al.*, 2008b; *Schofield et al.*, 2008). The changes in the water column's density structure can affect the vertical transfer of momentum, which in turn can affect the current's response to wind forcing. Wind stress is highly variable on the shelf in the synoptic band (2-10 days) due to broadband atmospheric transients (*Beardsley and Boicourt*, 1981). Seasonal variability of stratification and wind forcing can have significant effect on the seasonal flow, which is characterized by calculating the mean surface current for each of the seasons for the

six years from 2002 to 2007.

Representative hydrographic sections from the Tuckerton Endurance Line (*Castelao et al.*, 2008b) for each of the four seasons are shown in Figure 2.5. The summer months are highly stratified, characterized by a strong thermocline at mid-depth. In the cooler, windy winters the water column is well-mixed. For the transition seasons, the water column is stratifying in the spring from seasonal heating and increased river runoff and de-stratifying in autumn due to seasonal cooling and storm-induced mixing. The four seasons are defined as in *Flagg et al.* (2006)'s climatological analysis of the outershelf currents, a reasonable choice based on our historic knowledge of the MAB (e.g. *Bigelow* (1933)), recent analysis of the seasonal variability in the NJ shelf hydrography (*Castelao et al.*, 2008b), and our own climatological analysis of winds from NOAA NDBC Buoy 44009 (1987 - 2007, outside Delaware Bay) (Figure 2.6 and 2.7).

Winter, from December to February, is characterized by a well-mixed water column (*Castelao et al.*, 2008b) and the prevalence of NW winds blowing across the shelf (*Mooers et al.*, 1976). A sample glider cross-shelf density transect during the month of January shows the typical winter time NJ Shelf density structure (Figure 2.5(a)). The 2-D histogram of wind speed and wind direction for 2002-2007 indicates that the frequency of NW winds was highest during the winter season, occurring on average 41 percent of the time (Figure 2.6(a)). Over the period from 1987 to 2007, the relative frequency of NW winds varies from 30% in 1998 to 53% in 2007 (Figure 2.7(a)). For all years except 1990 when SW winds were dominant, NW is the dominant wind direction for the winter mixed season. The wintertime mean surface flow has three notable characteristics (Figure 2.8(a)). First, in the region south of the HSV, the southward

flow is nearly spatially uniform and directed offshore and downshelf. The flow velocity is $\sim 6\ cm/s$ for most of the shelf except at the outershelf region. Second, along the outershelf seaward of the 80 m isobath at the shelfbreak, the surface flow speed increases to greater than 13 cm/s while the flow direction turns along-shelf. Third, in the region north of the HSV, the current velocity is very weak ($< 3\ cm/s$). Over most of the shelf, the surface flow over seasonal scales is wind-driven except for the area near the HSV and the shelfbreak where topographic steering effects become important and baroclinic forcing drives a shelf-slope frontal jet. Compared to the long term mean (Figure 2.3(a)), the wintertime flow has a significantly higher cross-shelf flow for most of the shelf except for the region near the HSV and just to the south where it was similar to the mean.

Spring, from March to May, is characterized by the transition from a well-mixed water column to a more stratified water column. During most years the highest freshwater river discharge onto the shelf also occurs during the spring season (*Chant et al.*, 2008). A sample glider cross-shelf transect from April shows a partially stratified water column with significantly more of the lower-density riverine water appearing on the shelf (Figure 2.5(b)). During spring, the wind pattern is less stable than either the stratified or the mixed season. The weakening NW winds give way to more frequent but lower energy along-shore NE and SW winds (Figure 2.6(b)), occurring on average 21 and 32 percent of the time, respectively. The spring wind pattern can vary significantly on the interannual time scale. NW winds can occur 8% (1991) to 28% (1997) of the time, NE winds can occur 10% (1997) to 38% (1987) of the time, while SW winds can occur 17% (1992) to 44% (1991) of the time (Figure 2.7(b)). The causes of such interannual variability are likely associated with variability in the large scale atmospheric

circulation pattern and the frequency of storms. NE winds tend to drive alongshelf downshelf flow. The 6-year climatology of seasonal flow on the shelf during the spring is directed mostly downshelf towards the southwest with a speed of 3 to 7 cm/s (Figure 2.8(b)). A large portion of the area to the south of the HSV has a velocity of less than 5 cm/s. Near the shelfbreak, offshore of the 100m isobath, the current velocity increases significantly to over 15 cm/s. The increased alongshore wind forcing combined with buoyancy forcing due to increased river discharge results in favorable conditions for along-shelf transport during the spring. Compared to the long term mean, springtime flow has weaker offshore flow, especially in the region south of the HSV and inshore of the 40 m isobath.

Summer, from June to August, is characterized by a highly stratified water column. As shown in the sample cross-shelf density section (Figure 2.5(d)), the stratified surface layer is 10 to 25 meters thick. The density difference between the surface and bottom layer could be as large as 6 kg/m^3, sometimes higher. The overall wind strength for the summer season is weaker than all the other seasons. The wind direction is predominately along-shore from the upwelling favorable SW, occurring 48 percent of the time (Figure 2.6(d)). This SW wind pattern varies little interannually ranging from 30% in 1998 to 55% in 1988 (Figure 2.7(d)). NE winds are the second most common direction during the summer, with occurrences ranging from 7% (1994) to 22% (1995) of the time, and averaging 15% of the time between 2002 and 2007. The climatology of mean surface currents for the summertime from 2002 to 2007 includes a continuous band of stronger flow on the shelf (Figure 2.8(d)), starting with the region just south of the Hudson Shelf Valley stretching from the innershelf to the outershelf with the flow directed mostly cross-shelf. This cross-shelf flow connects with faster offshore flows

seaward of the 60 m isobath, where the flow is directed more along-shelf with a velocity of 7-9 cm/s. The surrounding regions, in particular the region north of the HSV and the region in between the 40 and 60 m isobath to the south, has downshelf surface current speeds weaker than 5 cm/s, directed downshelf to the SW. Shoreward of the 40 m isobath, the current velocity drops to nearly zero. The increased offshore flow is qualitatively consistent with a SW wind driving a coastal upwelling system on the shelf. The summertime flow structure over the HSV and offshore is similar to that of the long term mean, but the flow at the innershelf has a weaker alongshelf component compared to the overall mean.

Autumn, from September to November, is characterized by frequent storms that break down the summer stratification. The cooling of the surface layer preconditions the water column for storm mixing. A cold and fresh surface layer tend to overlay a warm and salty bottom layer during autumn on the NJ Shelf. Eventually increased storm activity mixes away the remaining stratification. A sample density cross-shelf section from November shows that the stratification of the water column had already broken down at the innershelf and is reduced at the mid to outershelf (Figure 2.6(c)). During this time, the winds shift from the weaker SW winds of the summer (23% of the time between 2002 and 2007) to the stronger and more frequent NE and NW winds associated with passing fronts and storms occurring 24% and 25% of the time (between 2002 and 2007), respectively (Figure 2.6(c)). There is significant variability in their relative frequency over the interannual time scale. Over the twenty year time period from 1987 to 2007, the occurrence of autumn SW winds ranged from 13% (2004) to 35% (2001), the occurrence of NW winds ranged from 13% (1992) to 34% (2000), and the occurrence of NE winds ranged from 10% (1996) to 28% (1992 and 2004) (Figure 2.7(c)).

The frequent NE winds drive enegetic along-shelf and onshore flow. The seasonal mean surface current map shows three distinct flow regions (Figure 2.8(c)). North of the HSV, there is weak flow with speeds less than 3 cm/s. The mid to outer portion of the shelf south of the HSV includes a broad band of strong alongshore, downshelf flow with the highest seasonal mean velocity of any of the seasons, averaging 8-10 cm/s. The current at the innershelf region south of the HSV is weak with velocities less than 5 cm/s. Compared to the long-term mean, the autumn downshelf flow is significantly higher at the mid and outershelf in the region south of the HSV.

2.4.4 Wind-Driven Circulation

We next calculate the mean spatial response of the surface circulation on the NJ Shelf to wind forcing and seasonal changes. Using the low-wind mean as an estimate for the non-wind driven background component of the surface circulation, it is then subtracted from the conditionally averaged fields to obtain the wind-only component of the surface flow for different wind regimes. The response of the ocean surface to each wind regime for the different seasons with the background low-wind mean removed are shown in Figures 2.9-2.12. At a first glance, the surface flow is largely in the direction of the wind during the winter when the water column is well-mixed and more to the right of the wind during the summer when the water column is highly stratified. For the transition seasons of spring and autumn, the wind driven response of surface flow is in between the angular range of the winter and summer scenarios. To characterize the effect of wind forcing on the current variability for all the seasons, the spatially averaged RMS/Mean for each case of the wind-based conditionally averaged flow are computed and presented in Table 2.3. The total RMS/Mean for all seasons and all wind

directions is 3.3. In general the variability of the current compared to the mean is much lower for wind-driven flows with RMS/Mean ranging from 1.1 under NE winds to 1.8 under SW with the exception of SE winds (with a value of 3.5) because the flow is very weak under those conditions. In some cases such as under NE winds during winter and spring, the RMS/Mean is less than 1. This result confirms that wind forcing variability is the dominant source of subtidal temporal variability for the shelf surface flow.

The surface flow responses to winter wind forcing are shown in Figure 2.9. Winter is characterized by strong NW winds, which occur 41 percent of the time with a mean velocity of 9.1 m/s (0.13 N/m^2), followed by SW winds which occur 24 percent of the time with a mean velocity of 6.73 m/s (0.072 N/m^2). Under the cross-shore NW winds, the surface flow is cross-shelf in the offshore direction (Figure 2.9(a)). However, despite the strong wind forcing, the flow velocity over the HSV and the nearby region remain weak with mean current speeds of less than 5 cm/s. Nevertheless, winter can be a season of significant cross-shelf transport due to frequent NW winds driving cross-shelf flow. Southward of the offshore tip of the FTS, the flow velocity increases to 8 cm/s. The shelf-wide offshore flow south of the HSV has little cross-shelf variability, suggesting a depth independent wind-driven response of the unstratified water column. Under wintertime SW winds, the surface flow is essentially upshelf towards the NE with a speed of 8-14 cm/s (Figure 2.9(c)). An offshore veering is observed as the flow reaches the southern side of the FTS. For the two less common wind regimes, NE winds (13 percent of the time) drive along-shore, downshelf flow with speeds of 7-16 cm/s (Figure 2.9(b)), and SE winds (5 percent of the time) drive onshore, upshelf flow with speeds of 3-7 cm/s for most of the shelf (Figure 2.9(d)).

The surface flow responses to different spring wind forcing regimes are shown in

Figure 2.10. Spring is characterized by the weakening of NW winds and a corresponding increase in the frequency of NE and SW winds. NW winds, common in the early part of spring, occur 21 percent of the time with a mean wind speed of 7.2 m/s. Under such wind forcing, the surface flow is largely cross-shelf for the southern portion of the NJ Shelf. The flow is similar to what was observed during the winter but with an expanded low speed zone that includes the whole HSV and FTS area. The combination of the weakening of the cross-shore NW wind and shrinking area of the cross-shelf flow suggest less offshore transport during the spring. SW winds, more common in late spring, occur 32 percent of the time with a mean speed of 5.7 m/s (Figure 2.10(c)). It generates an along-shore upshelf flow pattern that is largely similar to that of the wintertime case. The alongshore NE winds, which occur 21 percent of the time with a mean velocity of 6.96 m/s, generate the most energetic flow response of the spring. The surface current speeds range from 8 cm/s near the HSV to over 20 cm/s near the Tuckerton Endurance Line (Figure 2.10(b)). Just south of the HSV, over the FTS region, the flow is mostly onshore. Further south near the Tuckerton Endurance Line, the flow turns alongshore at the innershelf (Figure 2.10(b)). The counterclockwise veering of the flow under NE winds is observed for much of the southern region approaching the innershelf from offshore.

The surface flow responses to different summer wind forcing regimes are shown in Figure 2.11. The summer stratified season is the least energetic of all the seasons. Nearly 48 percent of all winds are along-shore SW winds with a mean speed of 5.3 m/s. SW winds tend to drive upshelf flow at the inner shelf and cross-shelf offshore flow at the mid to outershelf (Figure 2.11(c)). The flow over the HSV is the weakest with a speed of 7 cm/s, while the flow at the innershelf and over the FTS south of the HSV

is the strongest with a speed of 10-12 cm/s. Of the three other wind regimes during the summer, NE winds, occurring 15 percent of the time with a mean speed of 5.5 m/s, drive a nearly onshore flow with a slight downshelf component (Figure 2.11(b)). NW winds, occurring 11 percent of the time with a mean speed of 4.57 m/s, drive a downshelf flow of 4 to 8 cm/s. SE winds, occurring 9 percent of the time with a mean speed of 4.4 m/s, interestingly stop nearly all wind-driven components of the surface flow on the shelf (Figure 2.11(d)).

The surface flow response to autumn wind forcing regimes are shown in Figure 2.12. Surface flow during autumn is the most energetic of all the seasons. With the arrival of autumn, decreasing surface temperature and increased storm frequency enhance the vertical mixing of the water column. The wind regime undergoes a transitional phase from weak SW winds to strong NE winds often generated by storms. Winds from all three principal directions, NW, SW, and NE, are significant contributors during the autumn, each account for 25, 23, and 24 percent of the total winds, respectively. The response of the shelf flow under NW winds is offshore and downshelf with a flow velocity of 5 to 9 cm/s south of the HSV (Figure 2.12(a)). Under SW winds the flow is offshore and upshelf, similar to the summer scenario but more intense with flows of 8 to 16 cm/s (Figure 2.12(c)). NE winds generate the most intense flow, mostly downshelf and onshore with velocities in excess of 10 cm/s for nearly the entire shelf south of the HSV with peak currents of over 18 cm/s near the Endurance Line (Figure 2.12(b)). Near the HSV, the flow is 6 to 10 cm/s. Lastly, under the onshore SE winds, the flow is weakly inshore and upshelf with a speed of 2 to 6 cm/s (Figure 2.12(d)).

The response of the surface currents to the different wind forcing regimes show clear seasonal differences. The surface flow is to the right of the wind during the summer

stratified season and largely in the direction of the wind during the winter mixed season. The spatial maps exhibit along-shelf shelf variability and weak cross-shelf variability. Flow near the Hudson Shelf Valley has a persistently weaker response to wind forcing compared to regions downshelf to the south. SW winds are most common for summer, and NW winds are most common for winter. All three major wind directions (SW, NW and NE) are significant during the transition seasons of spring and autumn. During the transition seasons, NE winds in particular generate strong downshelf and onshore flow, the most energetic surface current response to wind forcing observed on the NJ shelf.

2.4.5 Wind-Current Correlation

The 2-D maps of surface flow from the previous section show that surface currents have a strong seasonal variability in response to wind forcing. This is consistent with modeling results showing the wind-driven MAB shelf flow is strongly dependent on the stratification (*Keen and Glenn*, 1994). The structure of the surface and bottom boundary layers determine the vertical mixing of momentum, which is reflected observationally in the seasonal differences in the wind-current correlation angle. Weak winds and strong stratification (i.e. summer) result in separate surface and bottom layers across the shelf except at the coastal upwelling zone (*Keen and Glenn*, 1994). The strong summer stratification tends to constrain the surface mixed layer to the upper 10-12 meters, above the season pycnocline (*Castelao et al.*, 2008b). On the other hand, strong winds and moderate stratification (i.e. spring and autumn) can result in interacting boundary layers at the innershelf (*Glenn et al.*, 2008) and separate boundary layers over the outershelf. Finally strong winds and weak stratification (winter) can result in

interacting boundary layers across the entire shelf. One can estimate the depth of the surface Ekman layer (*Csanady*, 1976; *Lentz*, 2001) for an unstratified water column:

$$\delta_s = \frac{\kappa}{f}\sqrt{\frac{\tau^s}{\rho}}$$

where $u^* = \sqrt{\frac{\tau^s}{\rho}}$ is the shear velocity and $\kappa = 0.4$ is von Kàrmàn constant. Let f = 9*10^{-5} s^{-1} at latitude 39 N, and assume $\tau = 0.1$ N/m^2 (corresponding to 8 m/s wind at 5 meters above sea level), the surface Ekman layer depth is 43 m. If the wind stress increases to 0.35 N/m^2, as was occasionally seen on the NJ Shelf during the winter, the estimated surface Ekman layer would extend over 80 m. The bottom mixed layer typically has a height of less than 10 m during the stratified season but can also exceed 20 m on the MAB (*Perlin et al.*, 2005; *Lentz and Trowbridge*, 1991; *Glenn et al.*, 2008). Solutions to the classic Ekman problem using different vertical eddy viscosities exhibit significant differences in the wind-current angle depending on the structure of the vertical eddy viscosity (*Ekman*, 1905; *Madsen*, 1977; *Trowbridge and Lentz*, 1991).

It is therefore worthwhile to quantify the wind-current correlation as a function of time and space over the NJ Shelf. A small correlation angle would be consistent with an eddy viscosity profile of a water column with interacting boundary layers and a large angle would be consistent with a shallow surface Ekman layer and separate boundary layers. The monthly climatology of the complex cross-correlation between lowpassed wind velocity and subtidal surface current velocity are calculated for eight cross-shelf stations just south of the Tuckerton Endurance Line using the 6-year CODAR dataset and the NOAA wind dataset from NDBC buoy 44009 (Figure 2.13). For this analysis, the low-wind background mean is removed from the surface current velocities. The color

of each pixel indicates the angle of the complex correlation between wind and current. A correlation angle of zero (blue) signifies flow exactly in the direction of the wind and a correlation angle of 90 (red) signifies perpendicular flow to the right of the wind. The magnitude of the complex correlations range between 0.5 and 0.8 with the lower values seen at the outermost station near the 200 m isobath for this set of eight stations. For the NJ Shelf, the angle between the wind and the surface currents is larger during the stratified summer ($>$ 45 deg) and smaller during the unstratified winter ($<$ 20 deg) (Figure 2.13). In particular, during the summer months of June through August, the mid to outershelf stations (deeper than the 50m isobath) show a correlation angle of 60 to 70 degrees while the same stations during the winter months December through February show a correlation angle of 10 to 20 degrees. The inshore stations also show a seasonal difference but with less varability. At the inner most station on the 20 m isobath, for example, the wind-current correlation angle is less than 20 degrees for most months of the year except during the summer months when the angle increases to 35 degrees in July. Simple Ekman theory predicts a maximum deflection angle of 45 degrees between the wind and surface current when the vertical eddy viscosity is constant (*Ekman*, 1905). The fact that correlation angles of greater than 45 degrees are observed suggests that the non-Ekman component of the background downshelf flow is not completely removed. Processes such as the interaction of the wind and the shelf-slope frontal jet could be a contributing factor. The correlation angle increases from the innershelf to the midshelf near the 50 m isobath, and beyond that there is little cross-shelf variation. The transition seasons are more dynamic in nature. At each cross-shelf location, the wind-current correlation angles change rapidly during spring (increasing from April to May) and autumn (decreasing from October to November).

These results suggest that the seasonal change in stratification exerts a strong influence on the response of surface flow to wind forcing on the NJ Shelf.

To visualize the effect of wind-driven circulation in the context of along-shelf and cross-shelf transport, wind-current cross-correlations along the natural geographic axes of the shelf are also calculated (Figure 2.14). The along-shore and cross-shore axes on the NJ Shelf are rotated 35 degrees clockwise from True North. The cross-correlation between the winds and currents are calculated for the along(cross)-shore wind and along(cross)-shelf currents for each month of the year along the same cross-shelf transect south of the Endurance Line noted earlier. The along-shore winds are correlated with along-shelf currents for all months of the year shoreward of the 40 m isobath (Figure 2.14(a)). The shallow innershelf has an unstratified water column most months of the year. The overlapping bottom and surface Ekman layers would cause wind driven flow to be in the direction of the wind. The winds and currents are especially well correlated with each other (> 0.7) shoreward of the 50 m isobath during the spring and autumn months (Figure 2.14(a)). This could be due to the frequent occurrence of energetic along-shelf wind during the transition seasons which tend to drive along-shelf downshelf flow. Offshore of the 50 m isobath, the correlation decreases between the along-shore winds and the along-shelf currents. During the summer months of June, July and August, the correlation is less than 0.3, indicating the along-shore wind is not a significant factor driving along-shelf flow at the outershelf.

The along-shelf wind is highly correlated with cross-shelf current at the mid to outershelf from late spring to early autumn with a correlation coefficient of > 0.8 from May to September (Figure 2.14(b)). A linear fit between the summer along-shore winds and cross-shelf flow at the 60 m isobath is shown in Figure 2.15(a). The slope for the

summer fit is 0.0067 and it has a R^2 of 0.59. This is consistent with the observations of upwelling favorable wind from the SW driving surface flow cross-shelf (Figure 2.11(c)). Using a subset of the surface current data from 2003-2004, *Dzwonkowski et al.* (2008b) also finds strong summertime correlations between along-shore winds and the cross-shelf currents. Coastal upwelling due to along-shore winds on the shelf results in the offshore transport of the surface layer seaward of the upwelling region. Shoreward of the 30 m isobath, the correlation is weak, likely due to contributing factors within the coastal upwelling zone (*Glenn et al.*, 2004). During the unstratified periods there is a relatively weak correlation between the along-shore wind and cross-shelf current with a correlation coefficient of < 0.5 for October to March. This is not surprising since we know from earlier analysis that the along-shelf wind was not dominant and that the flow is in the direction of the wind during the winter season.

Cross-shelf wind and cross-shelf currents have strong correlations (> 0.7) during the late autumn and winter across the entire NJ Shelf (Figure 2.14(c)). Since the dominant winds during late autumn and winter are mainly cross-shore, strong cross-shelf flow is observed during these times (Figure 2.9(a)). Cross-shelf depth variation does not appear to affect the variability of the cross-shore flow offshore of the 20 m isobath. A linear fit between winter cross-shore winds and cross-shelf transport at the 60 m isobath is shown in Figure 2.15(b). The slope for the winter fit is 0.0096 and it has a R^2 of 0.50, indicating a stronger response of cross-shelf flow to winter wind forcing than summer wind forcing. During the summer stratified season, the correlation between cross-shore winds and cross-shelf current is significantly reduced due to upwelling favorable along-shore winds driving cross-shelf flow.

In summary, cross-shelf flow is driven by different wind patterns during the stratified summer and unstratified winter seasons. It happens that the alongshore wind is dominant during summer and cross-shore wind is dominant during winter. The large wind-current correlation angle at mid to outershelf during the summer is consistent with a shallow Ekman layer and separate boundary layers, with alongshore SW wind driving offshore flow. The small wind-current correlation angle shelf-wide during the winter is consistent with an eddy viscosity profile reflecting interacting boundary layers and cross-shore NW winds driving offshore flow. During the transition seasons of spring and autumn, boundary layer interactions are complicated by changing stratification and frequent storms. During this time along-shelf flow is mainly driven by along-shore winds, especially at the inner to mid shelf.

2.4.6 Interannual Variability

Both the magnitude and the sign of the seasonal along-shelf and cross-shelf surface flow can vary on the interannual time scale. The analysis in the previous sections showed that changing winds and changing water column stratification are major drivers of the seasonal and annual variability of the shelf flow. To examine the interannual variability, potential forcing functions including the Hudson River discharge (Figure 2.16a), NJ statewide average air temperatures (not shown), and along-shelf and cross-shelf winds from NDBC Buoy 44009 (Figure 2.16b) were seasonally averaged for each year. The along-shelf and cross-shelf current response are similarly averaged at several locations across the shelf. At each site, current vectors within a 10 km radius are averaged for each time step before being seasonally averaged. The 10 km radius was chosen to be consistent with the averaging radius used to construct CODAR vector field. Selected

seasonal time series at the innershelf (39.4 N, 73.9 W) and the outershelf (38.95 N, 73.3 W) sites along the Tuckerton Endurance Line (*Castelao et al.*, 2008b), as well as a midshelf (39.5N, 73.3W) location to the north of the line are plotted in Figure 2.16c and 2.16d. The innershelf site is located on the 30 m isobath near the inshore edge of the coverage area. The midshelf site is located right over the FTS near the 40 m isobath. The outershelf site is located in between the 60 and 70 m isobaths, inshore of the shelf-slope frontal jet. The sites are chosen to highlight the interannual variability of cross-shelf flow differences.

Both the summer stratified season (red) as well as the winter mixed season (blue) are characterized by consistently offshore flow across the entire shelf with low interannual variability (Figure 2.16c, d, e, solid lines). Despite the large injection of freshwater by the Hudson River during the summer of 2006, the shelf circulation as indicated by the time series in Figure 2.16 is similar to the other years. For the spring (green), the cross-shore flow also is usually offshore except for 2003. The anomalous spring of 2003 exhibited colder air temperatures (not shown), higher river discharge, and strong alongshore winds from the NE. It is the only spring with a strong onshore wind (green lines, Figure 2.16b), and it is the only spring in which a reversal of the cross-shelf flow to onshore at the mid and outershelf is observed. Cross-shelf flow during autumn (purple) is largest at midshelf and is offshore, with fluctuating weak flows observed at the inshore and offshore sites.

For the alongshore flow during the summer, despite the consistent upwelling favorable winds, the current is usually downshelf at the mid to outershelf (Figure 2.16d and e, red dashed line). The only flow reversal occurs in 2003 at the midshelf when the summer upwelling wind is strongest (Figure 2.16b, red dashed line). In contrast to the

mid and outershelf, the summer innershelf current oscillates around zero (Figure 2.16c), possibly due to the nearly equal influences of the wind-driven, upshelf transport and the diminishing shoreward effect of the large scale along-shelf pressure gradient. In winter, the pattern of alongshore currents on the innershelf (Figure 2.16c, blue dashed line) is highly correlated with the pattern of alongshore winds (Figure 2.16b, blue dashed line). A reversal in the winter alongshore current to upshelf at the innershelf location in 2002, 2006 and 2007 is observed when the alongshore NE winter winds weaken below 2 m/s. At the midshelf, the alongshore current reverses to upshelf in only winter 2002 and summer 2003. Spring alongshelf flow is persistently downshelf. The anomalous 2003 experienced the strongest downshelf flow at the innershelf site, consistent with a buoyant river plume driven by high river discharge, the only onshore spring winds, and strong downwelling favorable winds from the NE (Figure 2.16c). Alongshelf flow is strongest and downshelf in autumn, especially at the midshelf where 2004 and 2005 are especially intense.

2.4.7 Transport & Residence Time

Understanding the transport pathways and residence time of material is important for addressing many biogeochemical questions on continental shelves. The MAB is highly productive and its biological activity exhibits strong seasonal cycles (*Schofield et al.*, 2008). Analysis of Eulerian surface current data in the previous sections have shown that circulation on the shelf also has strong seasonal cycles driven by seasonal wind forcing and changing stratification. Given the potential influence of shelf circulation on biogeochemical activities, we want to examine the potential transport pathways and estimate the residence time on the NJ Shelf from a Lagrangian perspective. The large

spatial coverage area of the CODAR fields, the high temporal resolution, and the long observation duration allow us to capture the advective state of the ocean and use it in a numerical Lagrangian drifter study. To visualize the transport pathways, virtual drifters are deployed in the CODAR fields at various locations on the NJ Shelf. The Lagrangian virtual drifter study focuses on the Long Range CODAR data from June 2006 to May 2007. This time period has excellent data coverage and as the previous interannual study indicates, does not exhibit anomalous seasonal circulation patterns compared to the other years.

The effect of dispersion in the virtual drifter advection scheme associated the instrument uncertainty and the sub-grid scale variability is estimated using a Markovian random flight model (*Griffa*, 1996). Prior applications of this type of drifter dispersion model include the U. S. Coast Guard Search and Rescue (SAR) comparison study of CODAR virtual drifters and actual self-locating datum marker buoys (SLDMB) (*Ullman et al.*, 2006). The random flight method they used provided search areas that enclose the real drifter approximately 90% of the time in this same CODAR current field. A set of best fit parameters for the U and V components of the turbulent velocity dispersion on the NJ Shelf are derived by minimizing the least squared difference between the actual drifters and the virtual drifters. The same methodology and the same set of best fit turbulence parameters from Table 2 of *Ullman et al.* (2006) are used to estimate the combined instrument uncertainty and the sub-grid scale dispersion. The U component of the velocity dispersion σ_u is 11 cm/s and the V component σ_v is 12 cm/s, with the turbulent time scales $T_u = 3.3$ hours and $T_v = 3.1$ hours.

The integration of the drifter velocities is formulated using a first order scheme. The error associated with the first order integration is the highest for a circular flow

field such as that of an eddy. Persistent eddy fields on the shelf, however, are rare. We estimate the advective error for a typical situation and compare with the dispersion error associated with uncertainty in the velocity field. Assuming a current speed of 30 cm/s, a radius of curvature of 50 km as discussed before, and an integration step of 3 hours, the maximum advective error from using a first order integration scheme for each time step is 0.1 km. On the other hand, assuming a velocity dispersion of 11 cm/s, the random distance per time step of integration (3 hours) is 1.2 km. The numerical error introduced by using a first order advection scheme is an order of magnitude smaller than the uncertainty associated with sub-grid scale variability for typical flow conditions, justifying its usage.

Two sets of virtual drifter experiments are performed. The first set deploys virtual drifters at three inshore sites to determine the cross-shelf transport pathways and residence times during all four seasons. The amount of time it takes each of the drifters to reach the 60 m isobath is calculated. The three deployment sites are chosen to capture the cross-shelf transport for different parts of the NJ Shelf while maximizing the drifters exposure to the high data coverage areas. These locations are consistent with regions of offshore flow seen in the HF Radar data between 2003-2004 (*Dzwonkowski et al.*, 2008a). The northern release site (N) is located on the HSV at (73.66 W, 40.18 N), the central release site (C) is located 20 km offshore of Loveladies, NJ (73.85 W, 39.70 N), and the southern release site (S) is situated 30 km offshore of Tuckerton, NJ (74.00 W, 39.30 N). The sites are located 97 km, 82 km and 67 km from the 60 m isobath, respectively. One drifter is deployed every 3 hours at each location for 30 days and is then allowed to drift for up to 90 days. Occasional missing CODAR grid points are filled in with the mean current from each 90 day interval. Drifters are stopped

once they reach the boundary of the CODAR coverage or the 60 m isobath line. The mean travel time, the cross-shore speed, and the fraction of drifters reaching the 60 m isobath from their release locations are listed in Table 2.4. Example transport pathways for drifters released at Site C, offshore of Loveladies, are shown for the summer 2006 (Figure 2.17(d)) and the winter 2006 (Figure 2.17(a)).

For the study period from June 2006 to May 2007, drifters deployed at the innershelf that reached the outershelf 60 m isobath took 2 to 5 weeks, traveling at speeds of 19 to 50 km/week. Summer experienced the fastest cross-shelf flow and spring exhibited the slowest (Table 2.4). Summer time upwelling favorable winds and the winter offshore winds result in the persistent offshore advection of the surface drifters. The majority of the drifters deployed during the stratified summer and well-mixed winter reach the 60 m isobath boundary. During the transition seasons of spring and autumn, a significant fraction of the drifters that do not reach the 60 m isobath and instead exit through the inshore/downshelf pathway. A particularly interesting feature of summer drifters is that they are often advected upshelf along the innershelf before moving cross-shelf at the midshelf and eventually veer downshelf near the shelfbreak. This inverted U shaped pattern south of the HSV (Figure 2.17(d)) is a persistent circulation feature of summer 2006. The average cross-shelf speed of the drifters is 43 km/week, significantly faster than the average winter cross-shelf speed of 31 km/week. The average cross-shelf speed for the minor fraction of drifters released in spring 2007 and autumn 2006 that do make it across to the 60 m isobath are 21 km/week and 29 km/week, respectively. There is large scatter in the actual traversal time of individual drifters. Some of the virtual drifters can cross the shelf in a week whereas others can take over a month. The summer drifter paths show less spatial scatter compared to the paths of the winter

drifters.

The second set of drifter experiments focuses on illustrating the residence time and transport pathways during the transition seasons of spring and autumn. Spring and autumn mean fields are generally dominated by along-shelf flow on the NJ Shelf. Drifters are released at a site situated over the HSV (73.35 W, 40.00 N) for two seasons at the beginning of spring (March 2007) (Figure 2.17(b)) and the beginning of autumn (September 2006) (Figure 2.17(c)). The drifter deployment location is chosen to maximize their data exposure in the along-shelf direction. The spring drifters take an average of a month and half to travel the length of the NJ Shelf with relatively little scatter despite the month long release schedule (Figure 2.17(b)). The average along-shelf velocity for the spring drifters is approximately 25 km/week. Recall NE winds become more frequent during the spring time. When the wind is from the NE, the surface flow is predominantly downshelf and alongshore. For autumn, winds from the SW, NW and NE all occur about the same percentage of time although NE winds generate the most energetic flows. While the different wind conditions of autumn likely cause the drifters to follow more scattered paths, the drifters still exhibit a clear alongshore downshelf movement (Figure 2.17(c)). Drifters deployed during the month of September 2006, for example, show a variety of downshelf transport pathways, some exit the study region at the innershelf, some head down at midshelf while others are exported towards the shelfbreak. Despite the more scattered drift paths, however, the autumn drifters move at a significantly faster speed down the shelf, taking approximately 3-4 weeks at an average speed of 44 km/week, nearly twice as fast compared to the spring season. On average the alongshelf transport time scale for the transition seasons is the same as the cross-shelf transport time scale for the stratified and mixed seasons on the

NJ Shelf.

2.5 Discussion

Large scale background flow, local shelf topography, changes in stratification and wind forcing influence the spatial and temporal transport patterns on the NJ shelf. The surface flow under various wind and stratification regimes display both coherent large scale patterns as well as small scale variability. Shelf scale wind forcing and background flow determines the large scale patterns of along-shelf or cross-shelf transport while local topography modulates the direction and magnitude of the flow near the HSV/FTS region. The different forcing mechanisms come together such that during the transition seasons of spring and autumn, the surface transport on the shelf is primarily alongshore and downshelf while during the stratified summer and mixed winter seasons the surface transport on the shelf is primarily cross-shelf and offshore. Through the annual cycle the location of the downshelf transport shifts. During the transition seasons of the autumn and spring downshelf flow stretches across the entire shelf. During the winter and summer seasons, the downshelf flow is pushed offshore along the shelfbreak, fed by the flow of the inner and midshelf.

Such seasonal shift in circulation pattern could affect the rate of volume transport on the shelf. Previous studies of MAB watermasses showed that the volume of the shelf-water can vary seasonally with a magnitude on the order of the mean volume (*Manning*, 1991; *Mountain*, 2003). Shelf-water, defined to be water with salinity less than 34, reaches a maximum southwestward extent during the summer and retreats to a minimum volume during the winter (*Mountain*, 2003). We observed that the seasons of maximum and minimum shelfwater volume are characterized by mainly cross-shelf

transport, whereas seasons with the maximum change in the shelfwater volume are characterized by mainly alongshelf transport. The seasonal cycle of shelfwater volume was attributed to a change in the influx of the Scotian Shelf Water (*Manning*, 1991). A study by *Lentz* (2008b) using moored current meter data from the central MAB found that the magnitude of the seasonal variability of the alongshelf depth-averaged flow to be comparable to the mean, on the order of 4-6 cm/s. He attributed such variability to wind forcing, river discharge and the seasonal cycle of the cross-shelf density gradient over the shelf. We note that during the transition seasons of spring and autumn, when the maximum change in the shelf-water volume in the central MAB occurs, alongshore NE winds also become more common (Figure 2.10(b), 2.12(b)) and they appear to drive strong alongshelf surface flow and transport (Figure 2.8(b), 2.8(c), 2.17(b), 2.17(c)). During the summer stratified season and the winter mixed season, the NJ Shelf switches from an along-shelf flow regime to a cross-shelf flow regime. The cross-shelf surface flow, evident in both the seasonal mean fields (Figure 2.8(a), 2.8(d)) and the Lagrangian drifter maps (Figure 2.17(a), 2.17(d)), suggests a surface export from the shelf which must be balanced by a return onshore flow at depth as is the case with the innershelf (*Fewings et al.*, 2008). Such cross-shelf circulation patterns would imply that cross-shore shelf-slope exchange is enhanced during the winter and summer periods.

Over the interannual time scale, the seasonal mean along-shelf and cross-shelf flow for each year closely follows the six year mean from 2002 to 2007. No long term trends in the transport were observed at various cross-shelf locations. However, there are anomalous seasons for some of the years. For example, the spring of 2003 had higher Hudson River discharge, colder air temperature, more frequent NE winds and bigger

downshelf innershelf flow than the other years. This was a particularly stormy spring that could have delayed the onset of seasonal stratification and the timing of the spring bloom. The summer of 2006 had very high seasonal Hudson River discharge but the flow velocity at the inner, mid and outershelf are not significantly different from the other years. Shifts in the seasonal wind pattern over the longer time scale, such as those associated with the Atlantic Multi-decadal Oscillation (AMO) (*Delworth and Mann*, 2000; *Kerr*, 2000), could affect the seasonal shelf circulation as well as the biological response. A shift in the phase of the AMO from negative to positive took place in the mid-1990s (*Schofield et al.*, 2008). Analysis of the decadal pattern in wind variability and changes in biological productivity have shown that the negative phase of the AMO is associated with weaker winter winds and higher productivity whereas positive phase of the AMO is associated with stronger winter winds and lower productivity (*Schofield et al.*, 2008). Cross-shelf flow is significantly correlated with cross-shore and along-shore wind forcing at the midshelf during winter and summer respectively (Figure 2.14). We therefore expect that during the years when the seasonal winter wind forcing is weak, there will be a weaker cross-shelf surface transport over the NJ Shelf. On the decadal time scale, we expect to see stronger wintertime cross-shelf transport during the present positive phase of the AMO and weaker wintertime cross-shelf transport during the negative phase of the AMO.

The different flow patterns for each of the seasons on the NJ Shelf are likely to have important implications for physical transport dependent biological processes such as shelf primary production (*Schofield et al.*, 2008; *Xu et al.*, 2009) and recruitment dynamics of key shelf fish species (*Nelson et al.*, 1977; *Werner et al.*, 1997; *Hare et al.*, 1999; *Quinlan et al.*, 1999).

2.6 Summary

Here we study the spatial and temporal variability of the surface flow on the New Jersey Shelf over a six year period from 2002 to 2007. The mean surface flow on the NJ Shelf is equatorward and offshore towards the south. The flow is significantly affected by bottom topography, stratification and wind forcing on the monthly to annual time scales. A band of higher velocity cross-shelf flow exists in the mean field just south of the Hudson Shelf Valley, indicating that the valley exerts a dynamical influence on the surface flow at the longest time scales. Furthermore, the HSV acts as a dynamical boundary between flow to the north and flow to the south. Divergent flow is observed over the HSV and to the north whereas convergent flow is observed just to the south. The shelf undergoes large changes in stratification from well-mixed during the winter to highly stratified during the summer. The response of the surface flow is characterized for the dominant wind conditions of the different seasons. The angle between wind stress and surface current is larger when the water column is more stratified and it exceeds Ekman theory at the mid to outershelf. The angle is small (< 25 degrees) when the water column is well-mixed. On the seasonal time scale, the surface flow oscillates between being along-shelf dominated during the transition seasons of spring and autumn and cross-shelf dominated during the stratified and well-mixed seasons of winter and summer. Cross-correlation of winds and currents along a cross-shelf transect south of the Tuckerton Endurance Line show that the winter cross-shelf flow is highly correlated with cross-shore winds dominated by the NW winds, and the summer cross-shelf flow is highly correlated with along-shore winds dominated by the SW winds. Flows during the transition seasons are mainly along-shelf and they are correlated with the along-shore NE winds. From a Lagrangian perspective, the summer and winter

drifters move predominantly cross-shelf. They make their way across the shelf over the period of 2 to 5 weeks. Spring drifters travel mainly alongshore and take 4-7 weeks to travel the alongshore distance of the NJ Shelf. Autumn drifters move and scatter on the shelf rapidly due to the energetic surface flow often driven by storms; their paths can scatter over the whole shelf and the drifters can exit the NJ Shelf via a variety of pathways at the inner, mid and outershelf in a month or less. Physical transport can affect shelf biology over temporal scales from days to decades. Changes in wind strength associated with decadal shift in climate pattern can drive changes in the cross-shelf and along-shelf transport which can potentially affect shelf primary production and recruitment dynamics of key MAB fish species.

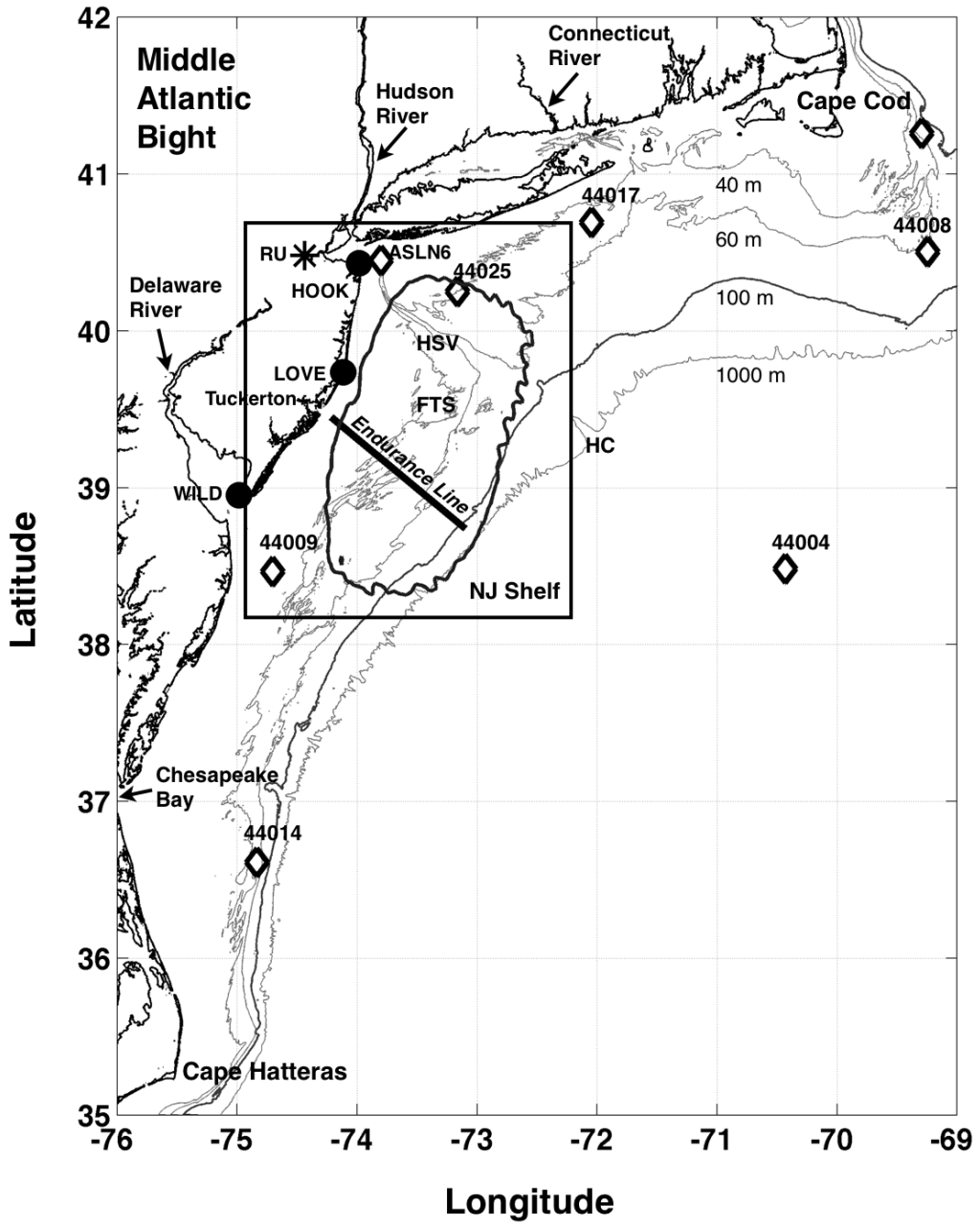

Figure 2.1: Middle Atlantic Bight from Cape Hatteras up to Cape Cod. The 40, 60, 100 and 1000 meter isobaths are marked. HSV: Hudson Shelf Valley, HC: Hudson Canyon, FTS: Fortune Tiger Shore, RU: Rutgers University, HOOK: Sandy Hook CODAR site, LOVE: Loveladies CODAR site, WILD: Wildwood CODAR site. 50% CODAR coverage area for the NJ Shelf is outlined. NOAA NDBC buoys are marked as diamonds and are labelled.

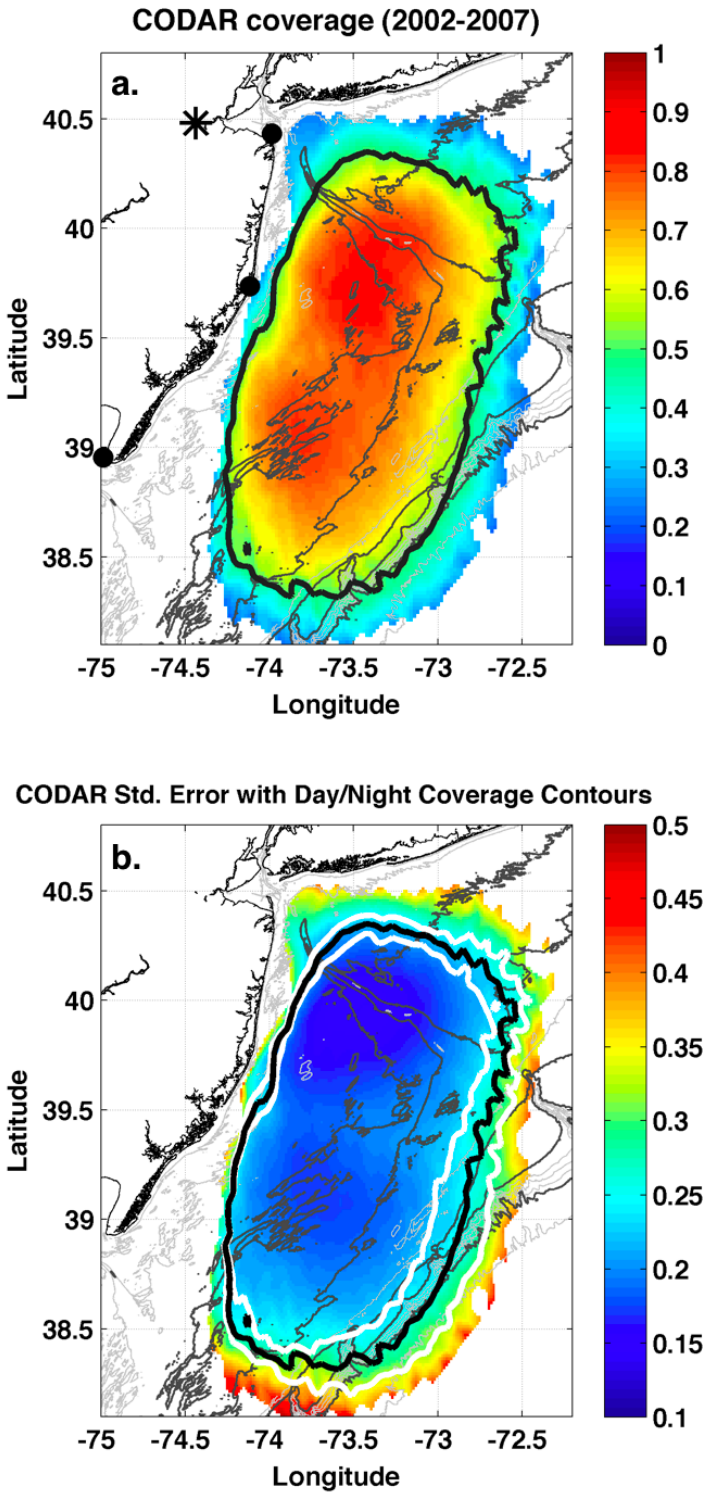

Figure 2.2: (a) Long Range CODAR data coverage for the NJ Shelf from 2002 - 2007. The 50% contour is drawn in black. (b) The standard error of the mean current (in cm/s) with day (outer) and night (inner) coverage contours (white).

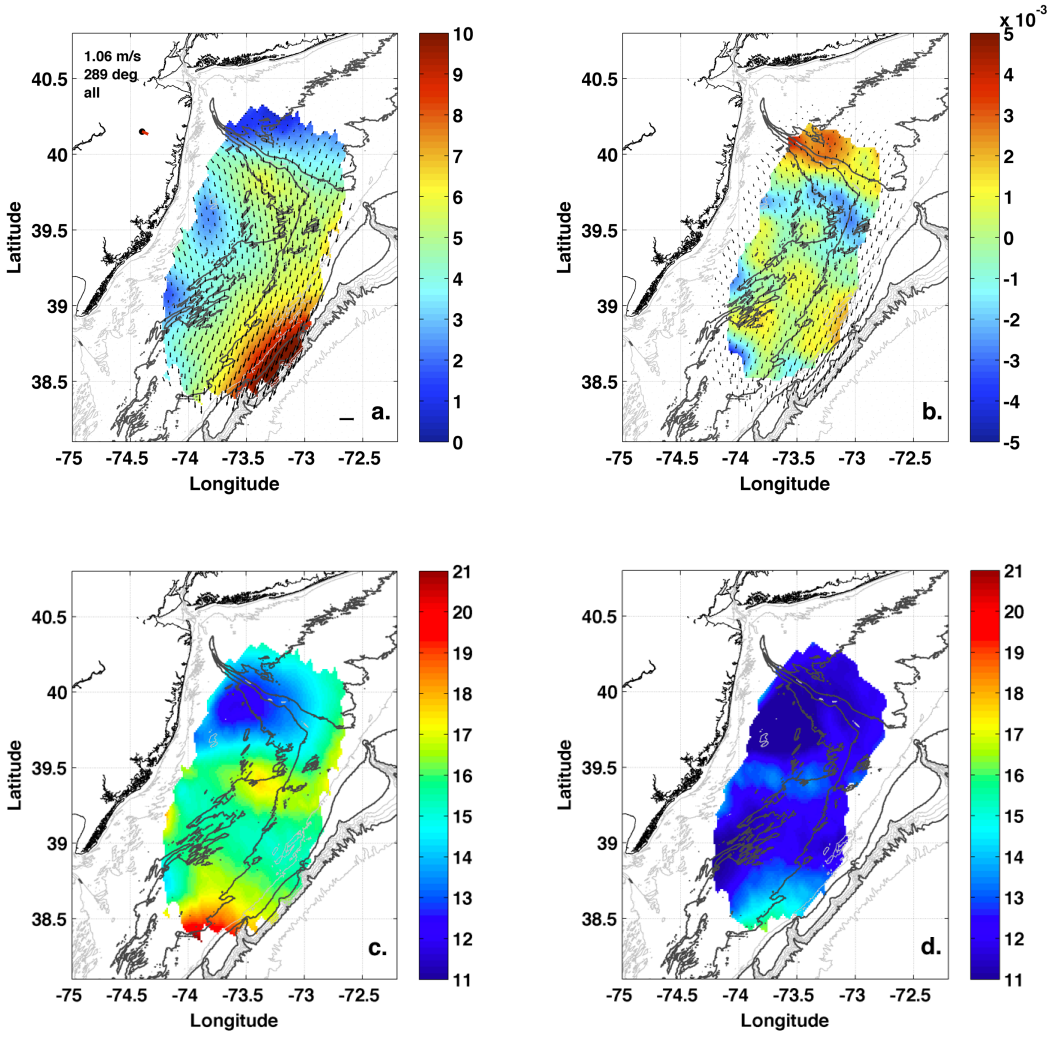

Figure 2.3: (a) Mean surface current for NJ Shelf (2002-2007) in cm/s. Average wind speed (m/s) and direction (degrees from True North) measured by NOAA NDBC Buoy 44009 is given. (b) Divergence map of the CODAR mean surface current (2002-2007) in $1/hr$. (c) R.M.S. of the detided surface current from 2002-2007. Colorbar indicates current speed in cm/s. (d) R.M.S. current speed for weak wind conditions when winds were less than 2 m/s.

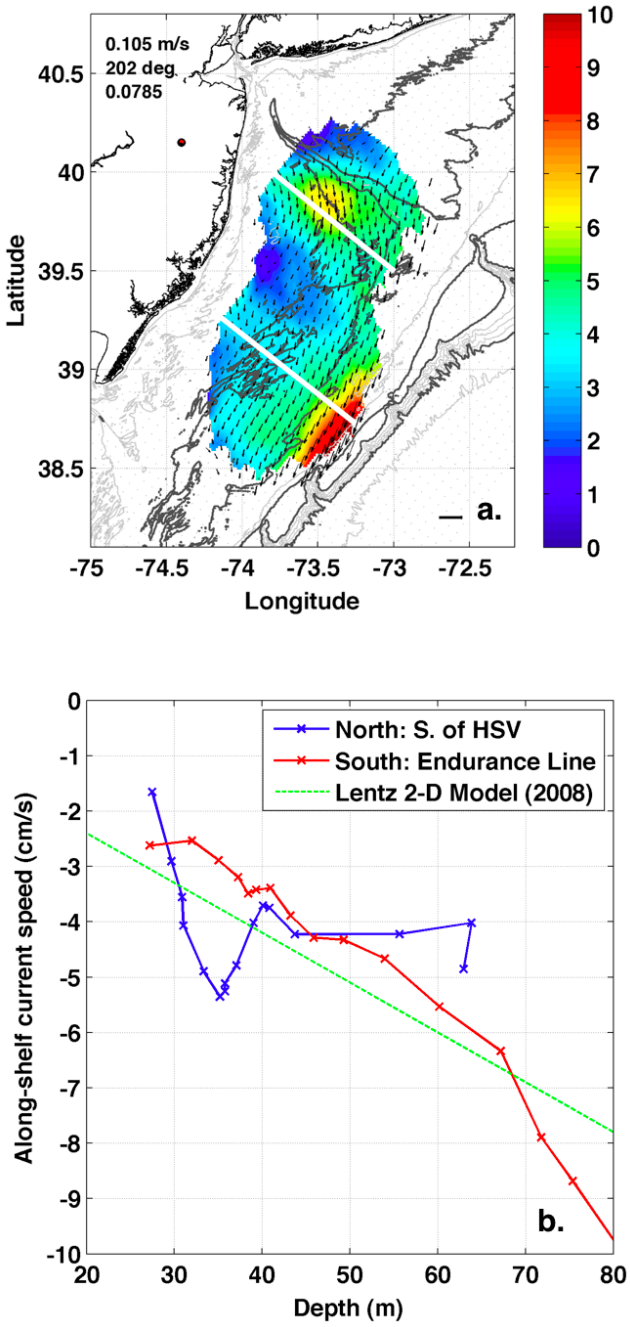

Figure 2.4: (a) Mean surface current field for weak wind conditions ($<$ 2 m/s) for 2002-2007 in cm/s. The mean wind speed, direction and fraction of the total time are listed. (b) Comparison of alongshelf velocity for a cross-shelf section just south of HSV (blue) and another south of the Tuckerton Endurance Line (red). The depth-averaged alongshelf flow velocity given by a 2-D shelf model is shown in green.

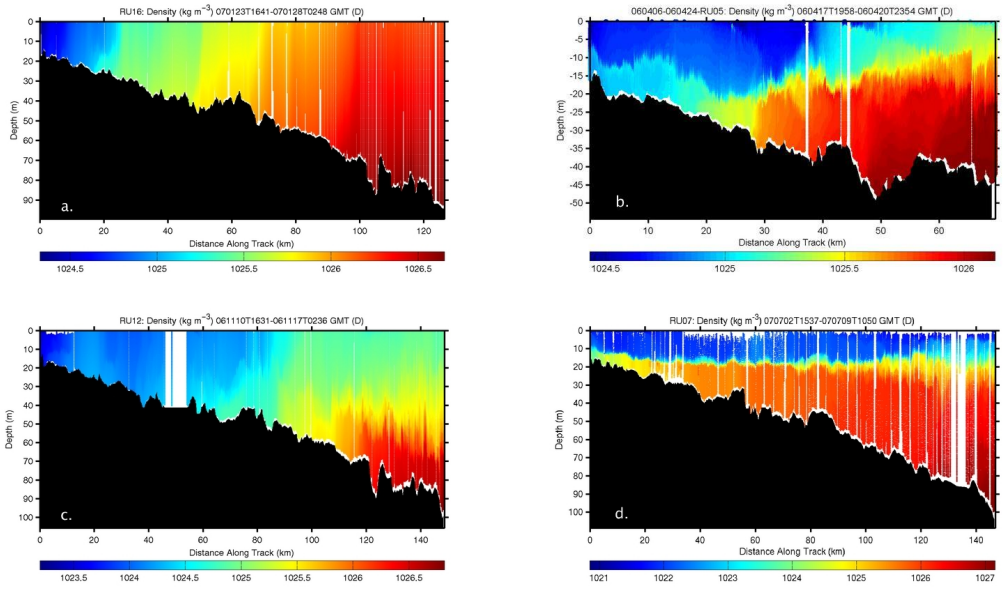

Figure 2.5: NJ Shelf Seasonal Density Sections along the Tuckerton Endurance Line (kg/m^3): (a) Unstratified Winter (December - February) (b) Stratifying Spring (March - May) (c) De-stratifying Autumn (September - November) (d) Stratified Summer (June - August)

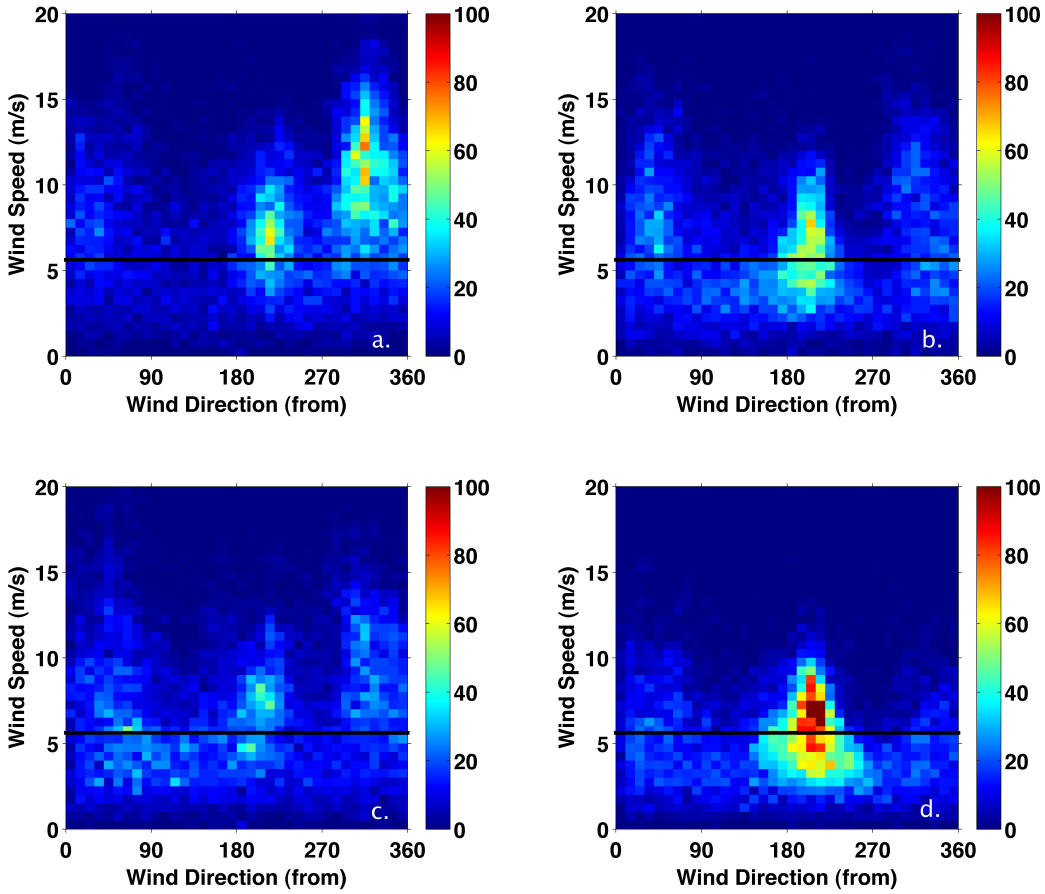

Figure 2.6: Histogram of hourly winds by season with colorbar indicating number of occurrences. The black line on each figure represents a wind stress of 0.05 N/m^2: (a) Winter (December - February) (b) Spring (March - May) (c) Autumn (September - November) (d) Summer (June - August)

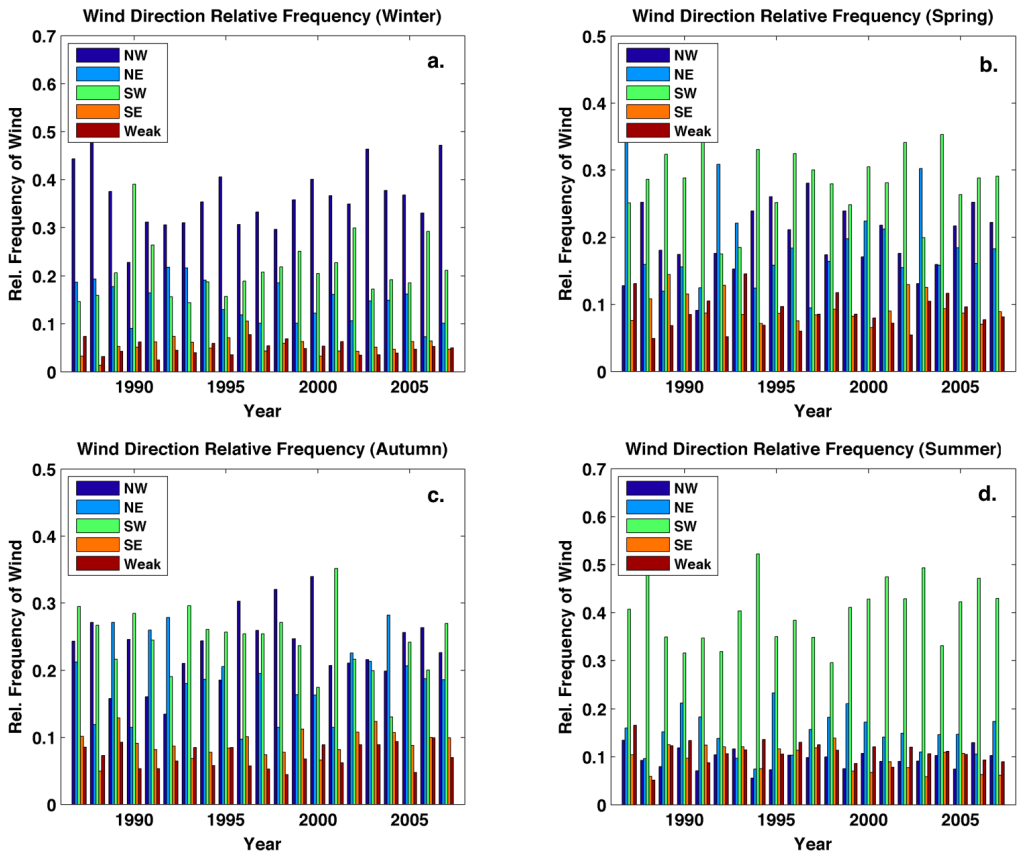

Figure 2.7: Interannual variability of the relative frequency of NW, NE, SW, SE and weak (less than 2 m/s) winds for NOAA NDBC Buoy 44009. (a) Winter (December - February) (b) Spring (March - May) (c) Autumn (September - November) (d) Summer (June - August)

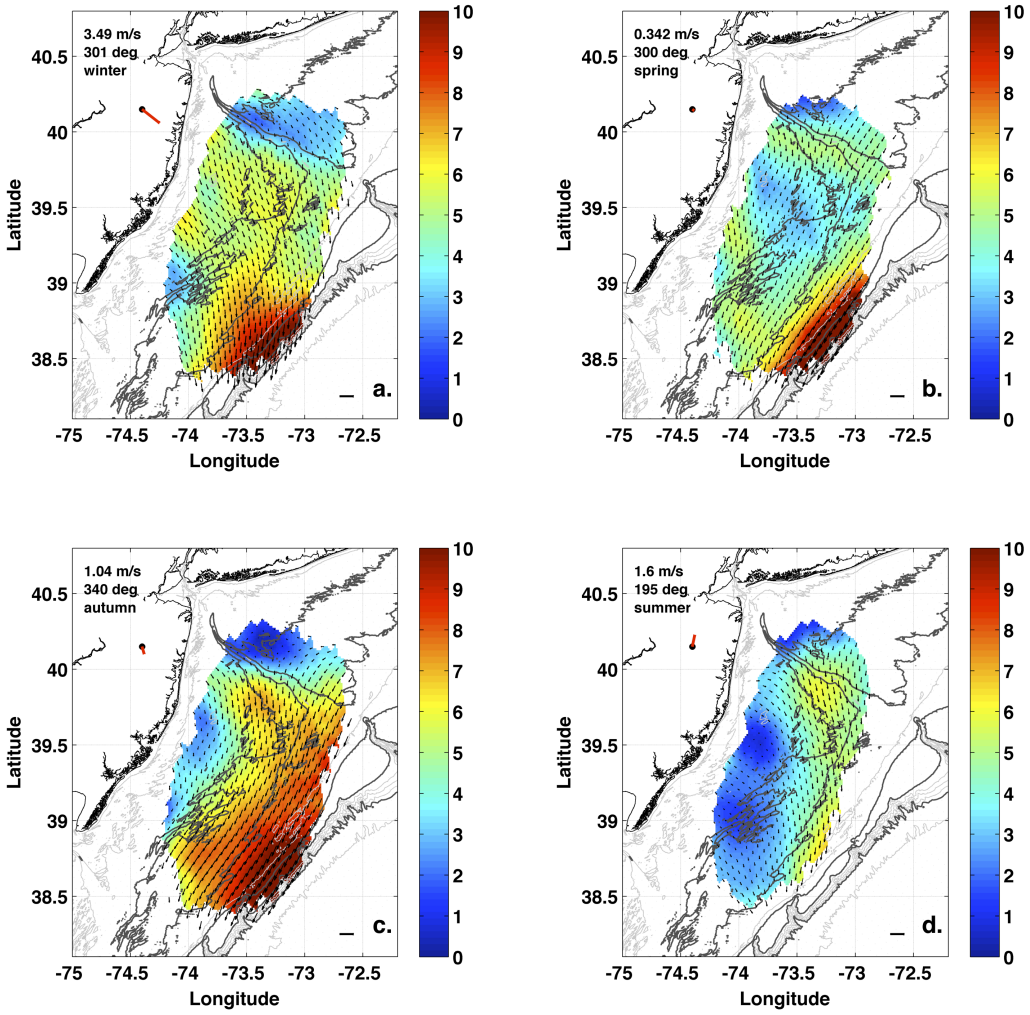

Figure 2.8: Seasonal Surface current on the NJ Shelf (cm/s): (a) Winter (December - February) (b) Spring (March - May) (c) Autumn (September - November) (d) Summer (June - August)

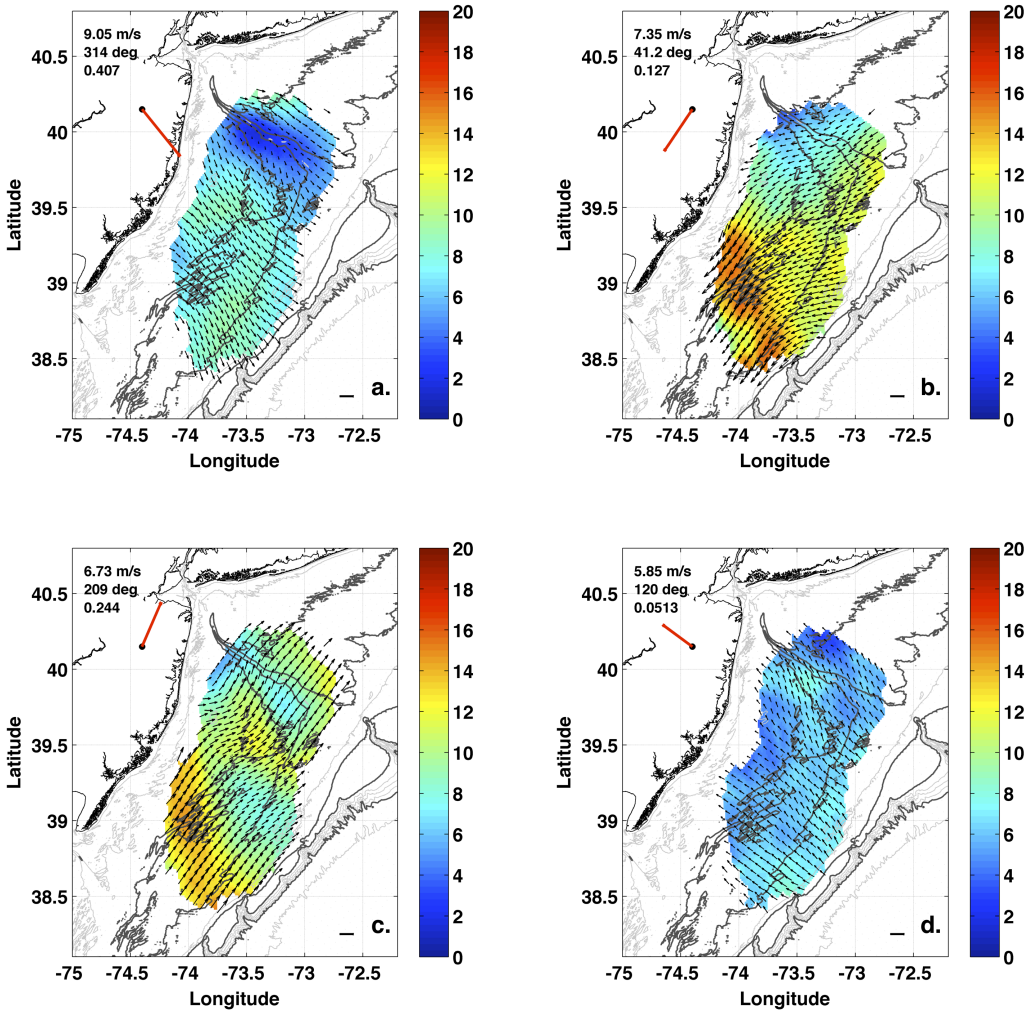

Figure 2.9: Winter mean current based on wind (cm/s): (a) Northwest winds (b) Northeast winds (c) Southwest winds (d) Southeast winds

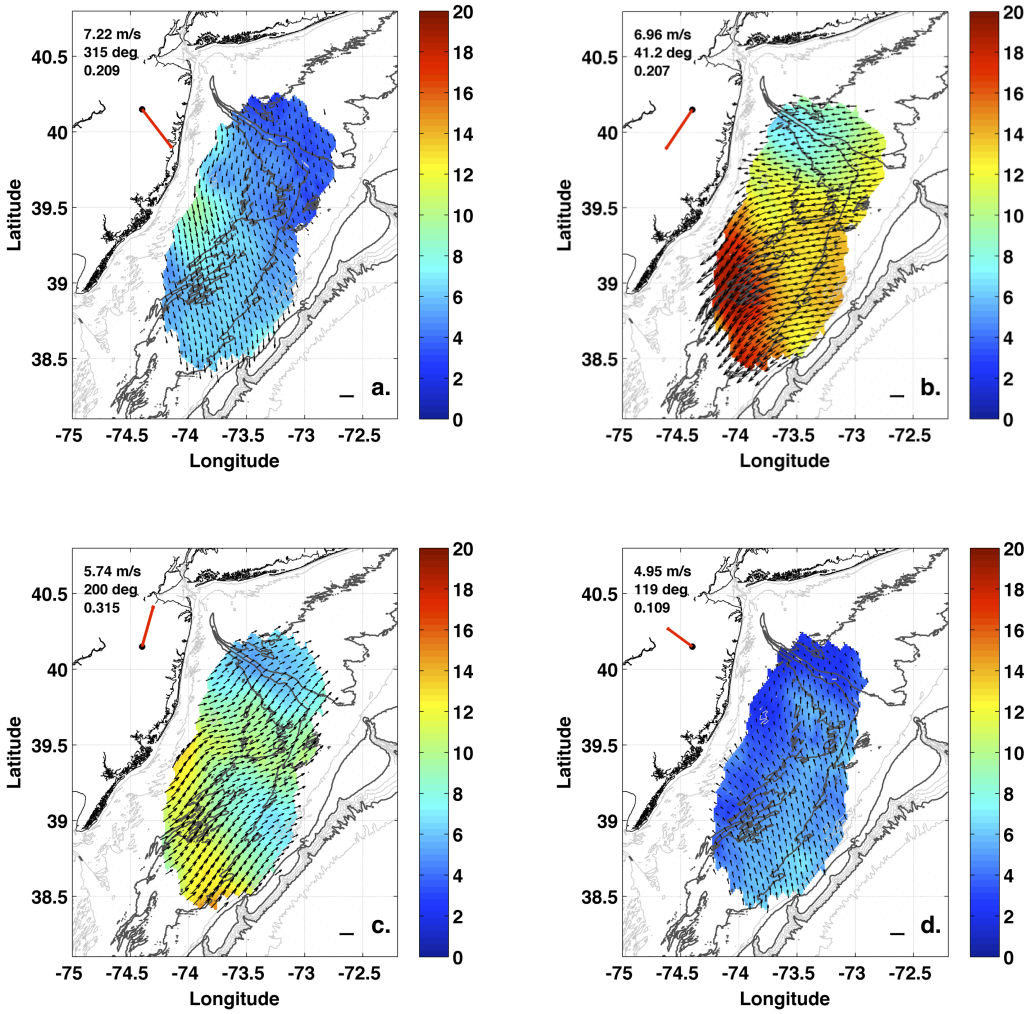

Figure 2.10: Spring mean current based on wind (cm/s): (a) Northwest winds (b) Northeast winds (c) Southwest winds (d) Southeast winds

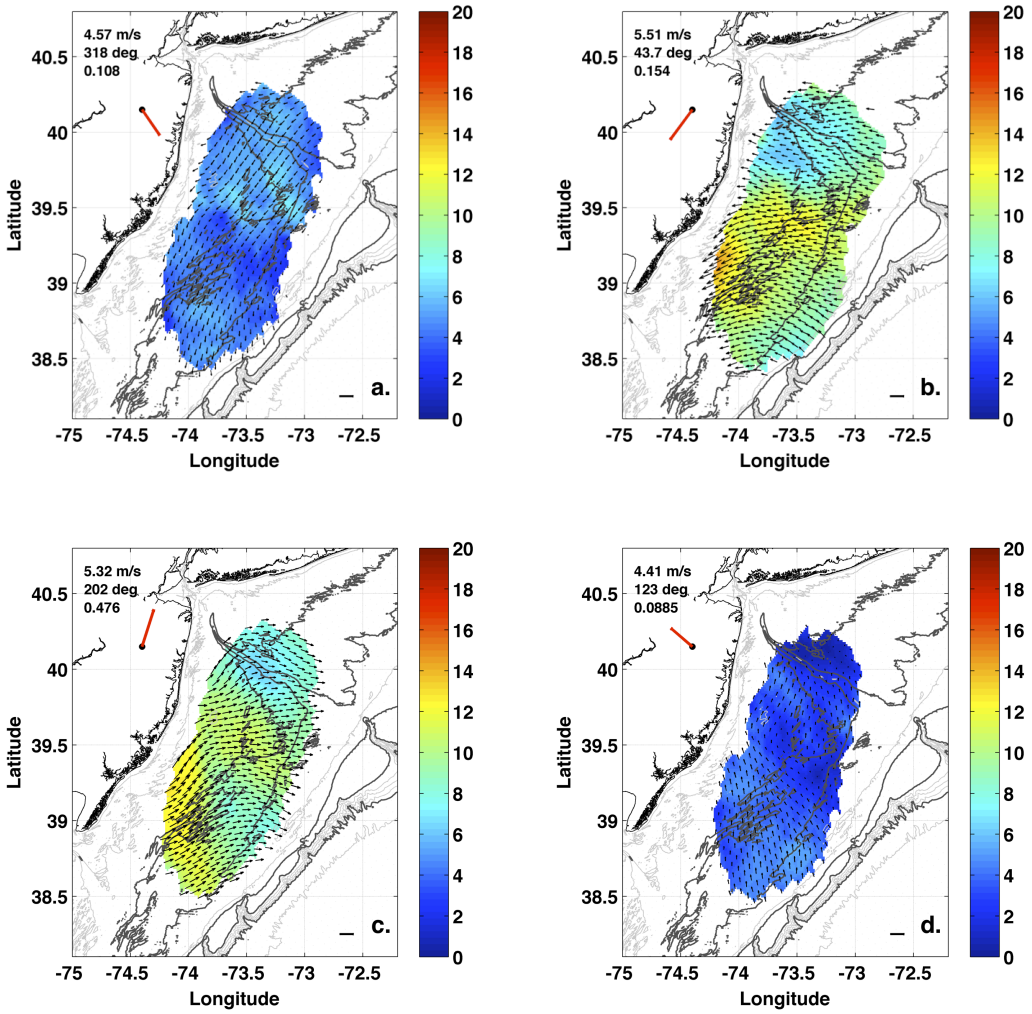

Figure 2.11: Summer mean current based on wind (cm/s): (a) Northwest winds (b) Northeast winds (c) Southwest winds (d) Southeast winds

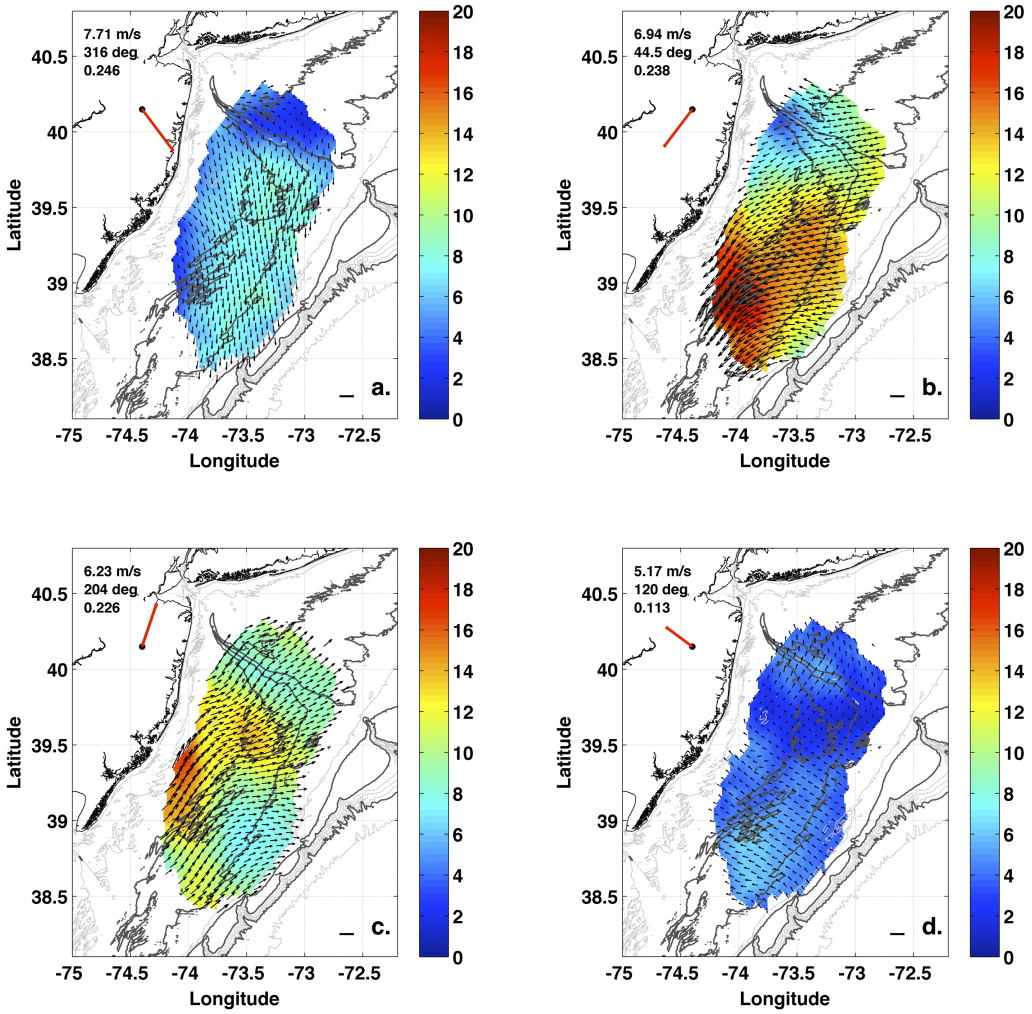

Figure 2.12: Autumn mean current based on wind (cm/s): (a) Northwest winds (b) Northeast winds (c) Southwest winds (d) Southeast winds

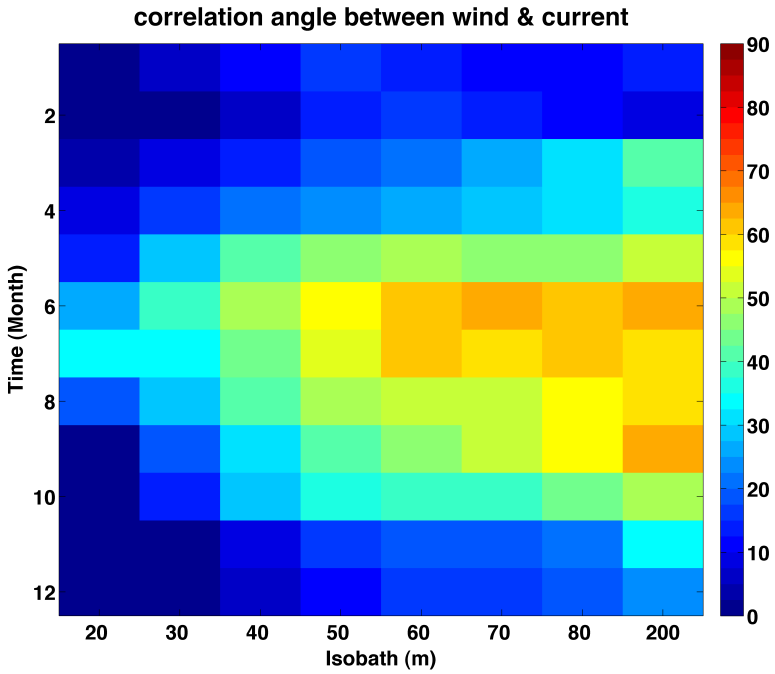

Figure 2.13: Correlation angle between wind and current along a cross-shelf transect just south of the Tuckerton Endurance Line (2002-2007).

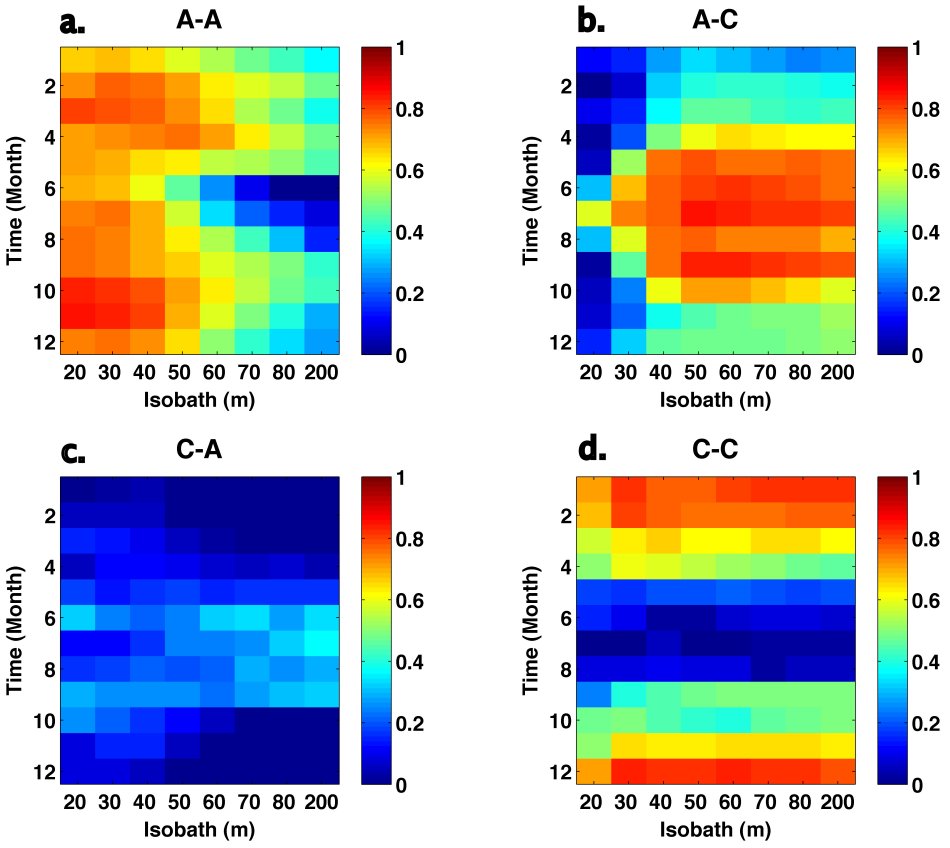

Figure 2.14: Cross-correlation along geographic axes between wind and current (2002-2007): (a) Along-shore winds and along-shelf current, (b) Along-shore winds and cross-shelf current, (c) Cross-shore winds and along-shelf current, (d) Cross-shore winds and cross-shelf current.

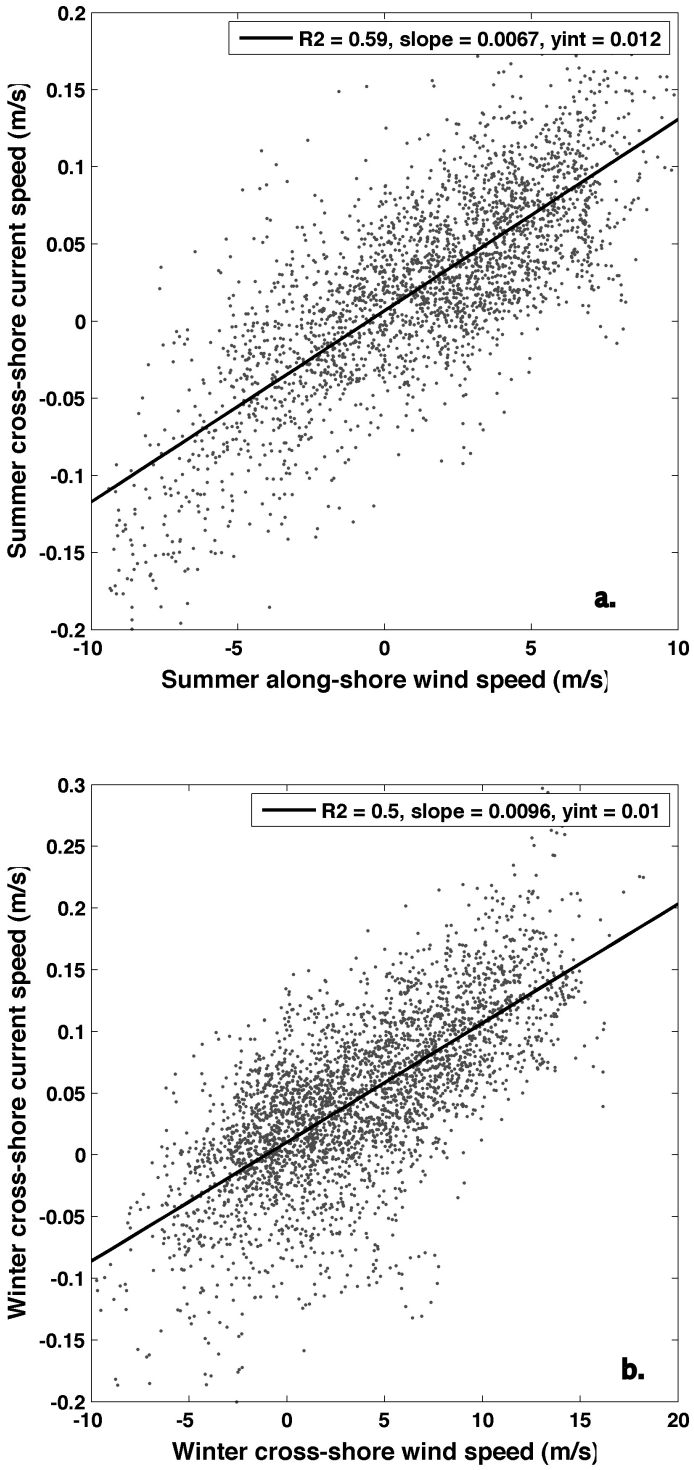

Figure 2.15: Wind-Current speed correlation at a 50 m isobath site: (a) Summer correlation between along-shore wind speed and cross-shore current speed. (b) Winter correlation between cross-shore wind speed and cross-shore current speed.

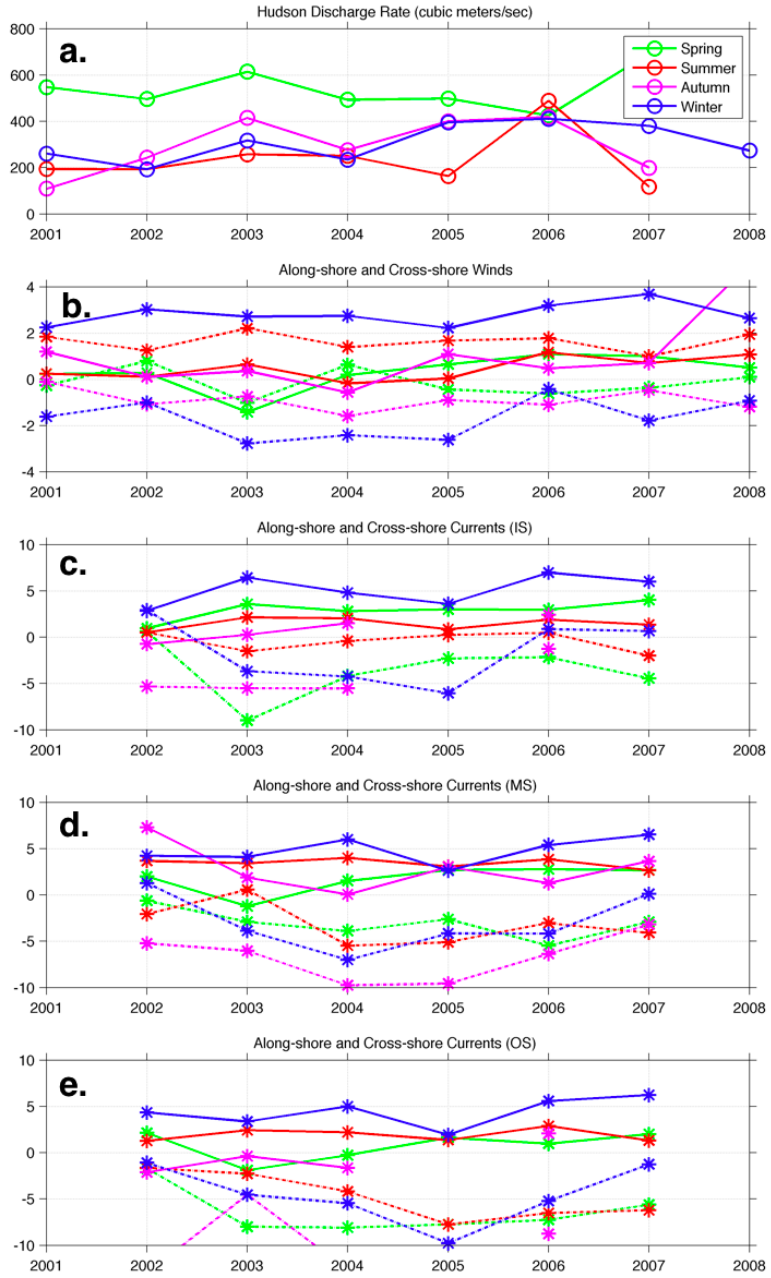

Figure 2.16: (a) Seasonal time series of Hudson River Discharge, (b) along-shelf and cross-shelf winds, (c) mean along-shelf and cross-shelf surface current at the innershelf, (d) midshelf and (e) outershelf. Solid lines are cross-shore (positive offshore) and dashed lines are along-shore (positive upshelf). Red is summer, blue is winter, green is spring, purple is autumn.

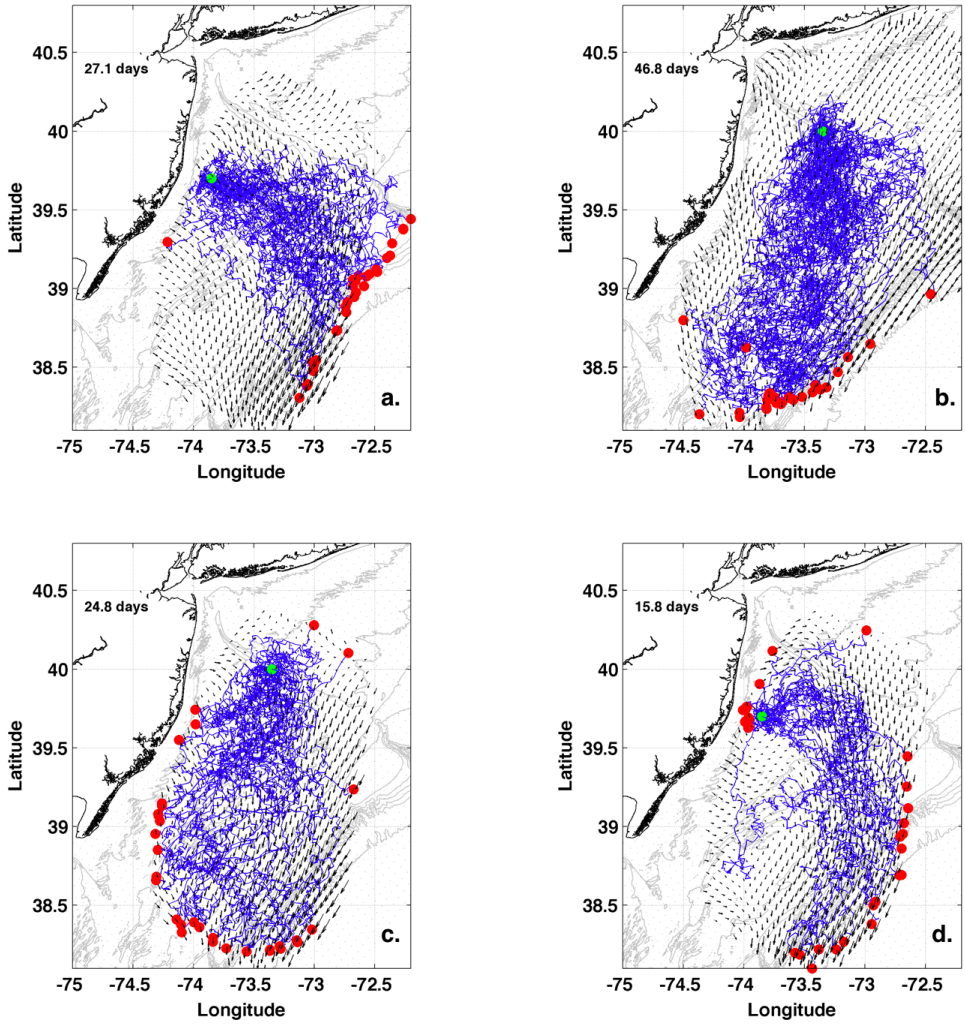

Figure 2.17: Virtual drifter transport study, green dot is deployment location, red dots are end locations. Mean transport times are printed. (a) Winter: December 2006 (b) Spring: March 2007 (c) Autumn: September 2006 (d) Summer: June 2006

Table 2.1: NDBC Buoy Wind Cross-correlation Magnitudes

Wind XCORR	ASLN6	44025	44009	44017	44004
ASLN6	1.00	0.82	0.72	0.84	0.56
44025		1.00	0.80	0.82	0.64
44009			1.00	0.79	0.70
44017				1.00	0.51
44004					1.00

Table 2.2: NDBC Buoy Wind Cross-correlation time lags (hours)

Wind t-lag (days)	ASLN6	44025	44009	44017	44004
ASLN6	0	-1	1	-3	-5
44025		0	2	-2	-4
44009			0	-4	-6
44017				0	-2
44004					0

Table 2.3: Relative Variability of detided CODAR currents: R.M.S. / Mean

RMS/Mean	Summer	Winter	Spring	Autumn	All
All Dir.	4.9	2.6	3.0	3.0	3.3
NW	1.9	1.4	1.4	1.6	1.6
NE	1.3	0.9	0.9	1.1	1.1
SW	1.7	1.7	1.8	1.8	1.8
SE	6.8	1.8	3.7	3.0	3.5

Table 2.4: Cross-shelf drifter time (days), speed (km/wk) and fraction reaching 60 m isobath

Drifter Time	Jun 06	Sep 06	Dec 06	Mar 07	Dist to 60m
Site N	13.6	30.7	23.9	36.1	97
Site C	13.3	20.5	17.4	24.8	82
Site S	12.9	13.1	14.9	27.6	67
Drifter Speed	Jun 06	Sep 06	Dec 06	Mar 07	Dist to 60m
Site N	49.9	22.1	28.4	18.8	97
Site C	43.2	28.0	33.0	23.1	82
Site S	36.4	35.8	31.5	21.4	67
Fraction to 60m	Jun 06	Sep 06	Dec 06	Mar 07	Dist to 60m
Site N	0.27	0.09	0.73	0.39	97
Site C	0.68	0.17	0.99	0.71	82
Site S	0.77	0.25	1.00	0.45	67

Chapter 3

Characterizing summer-time shelf-slope exchange processes on the New Jersey Shelf

3.1 Introduction

The outer continental shelf is a region where multiple watermasses can come together and interact in a relatively narrow and often highly energetic part of the ocean. The interaction of the different watermasses affects not only the physical dynamics but also influences the biogeochemical activities of the outershelf/shelfbreak region. For major portions of the Mid-Atlantic Bight (MAB), the shelf-slope front (SSF) is approximately on the scale of 20 to 30 km wide with its foot centered near the 80 m isobath (*Flagg et al.*, 2006; *Linder and Gawarkiewicz*, 1998; *Linder et al.*, 2004). The major watermasses present in this region are riverine water, shelf bottom water, warm core ring (WCR) / slope eddy water, and intermediate depth slope water (*Bigelow*, 1933; *Bigelow and Sears*, 1935; *Wright and Parker*, 1976). How do these watermasses come together, what is the structure of this interface, how does this interface vary in space and time, and what processes drive the transport/exchange across this interface are the guiding questions of this study. Specifically, this work will address how the various forcing mechanisms acting on the watermasses present at the outer continental shelf can affect different parts of the water column and the intra-seasonal evolution of the SSF. The

study site is located in the central portion of the Mid-Atlantic Bight (MAB) on the New Jersey Shelf (NJ Shelf), south of the Hudson Shelf Valley (HSV).

The major estuaries along the east coast of the United States discharge significant amounts of fresh riverine water into the MAB. In particular, during the spring discharge season, the Hudson River estuary can have a peak discharge rate of over 8000 m^3/s (*Chant et al.*, 2008) onto the NJ Shelf. The freshwater can exit via one of the several along-shore or cross-shore transport pathways across the shelf (*Gong et al.*, 2006; *Zhang et al.*, 2009). The high discharge in the spring helps to setup the seasonal stratification of the shelf. Large discharge events in late spring and/or summer can lead to the formation of an extensive region of river-influenced surface water which can be transported out past the shelfbreak into the slope sea. The transport of the fresh surface water is largely driven by winds, the background flow and local topography. Both modeling (*Zhang et al.*, 2009) and observational (*Castelao et al.*, 2008b) studies have shown that the HSV enhances the cross-shelf transport of fresh riverine water in the region just to the south of the shelf valley. This type of cross-shelf flow pattern is persistent in the annual mean current field. Offshore winds enhance the cross-shelf flow during the winter mixed season while upwelling favorable winds enhance the cross-shelf flow during the summer stratified season (*Gong et al.*, 2010).

In the summertime, beneath the MAB seasonal pycnocline, lies the remnant of winter-cooled water traditionally labelled the 'cold pool' (*Mooers et al.*, 1979). In the central portion of the MAB, this watermass is characterized by a temperature that is typically less than 10 °C in mid-summer during August (*Houghton et al.*, 1982). The width of the cold pool is on the order of 40 km and the thickness is on the order of 20 to 40 m. The core of the cold pool is typically centered between the 60 and 70

m isobaths and the body of water extends from Cape Cod down to Cape Hatteras (*Houghton et al.*, 1982; *Flagg et al.*, 2002). The spatial and temporal variabilities of the cold pool below the pycnocline and river-influenced water above the pycnocline result in intra-seasonal variability of the seasonal stratification on the shelf. Variability in the seasonal stratification can affect mesoscale processes such as cross-shelf transport (*Lentz*, 2001; *Gong et al.*, 2010) and sub-mesoscale processes such as the propagation of non-linear internal waves (NLIW) on the shelf (*Shroyer*, 2010).

Slope water is often present on the outer continental shelf in the form of the various types of intrusions. Intrusions of slope water onto the shelf have long been recognized as potentially important mechanisms of shelf-slope exchange of heat, salt, nutrients, and fish larvae (*Boicourt and Hacker*, 1976; *Churchill et al.*, 2003; *Lentz*, 2003; *Hare et al.*, 2002). While shelf/slope intrusions have been investigated for decades, the spatial structure, temporal variability, and their role on shelf/slope exchange processes remain poorly understood partly because of the difficulty in sampling their variable structure. *Bigelow and Sears* (1935) first documented mid-depth 'reversals of salinity' in hydrographic data collected during a series of hydrographic cruises on the MAB between 1919 and 1933, and they noted that 'they are short-lived, or in a state of constant alteration'. These events are often termed 'S-max intrusions' or 'salinity intrusions', and climatological analysis shows that intrusions mainly occur during the summer stratified season at a depth of 40 m to the surface with a tendency to be centered near the seasonal pycnocline (*Lentz*, 2003). Using a salinity of 34 as the definition of the boundary between the shelf and slope water (*Houghton and Marra*, 1983; *Manning*, 1991), termed the 'shelf-slope front' (SSF), one can trace the cross-shelf extent of the salinity intrusions under different forcing conditions. The canonical cross-shelf

configuration of different summertime watermasses on the MAB is shown in Figure 4b of *Fairbanks* (1982). On the seasonal time scale, salinity intrusions along the pycnocline which significantly distort the SSF, are a prominent feature. The advection of warm and salty offshore water shoreward along isopycnals across the summertime thermohaline SSF has been the proposed mechanism to generate the salinity intrusions, while double-diffusive mixing of the warm and salty slope water with cool and fresh bottom shelf water has been hypothesized as the decay mechanism. (*Houghton and Marra*, 1983). The interaction of shelf watermasses with slope watermasses determines the structure and variability of the SSF. Understanding the kinematics and the dynamics of the intrusions on the shelf is key to understanding the behavior of the SSF.

Based on observational and modeling studies, various forcing mechanisms such as baroclinic pressure gradients (*Posmentier and Houghton*, 1981; *Gordon and Aikman III*, 1981), wind forcing (*Churchill*, 1985; *Flagg et al.*, 1994), double diffusion (*Voorhis et al.*, 1976), warm-core rings (*Gawarkiewicz et al.*, 1996b; *Churchill et al.*, 2003), and geostrophic adjustment (*Gawarkiewicz et al., in prep.*) have been proposed as generating mechanism for the salinity intrusions on the shelf. For example, using a set of high-resolution Conductivity-Temperature Depth (CTD) data with 3.7 km separation, *Burrage and Garvine* (1988) studied feature propagation and concluded that the intrusions advect along-shelf due to along-shelf pressure gradient. More recently, *Lentz* (2003) used a historical CTD database to observe the large-scale patterns in the along-shelf distribution of salinity intrusions finding an increasing prominence of intrusions on the MAB down-shelf of Georges Bank. This is consistent with a simple double diffusive based decay model and the decay timescale was estimated to be >90 days assuming constant intrusion generation along the shelf. In contrast, analysis of

mooring data on Georges Bank revealed intrusions that were potentially much more variable with a generation and decay timescale of a few days or less (see Figure 13 of *Churchill et al.* (2003)). This variability was related to wind forcing events and the passage of frontal meanders and eddies at the shelfbreak.

Secondary circulation processes, such as bottom boundary layer (BBL) detachment, have been shown to play a key role in the development and maintenance of the shelf-slope front (*Gawarkiewicz and Chapman*, 1992; *Chapman and Lentz*, 1994). The location of the SSF can affect the behavior of salinity intrusions and the transport of biogeochemical tracers at the outershelf. Idealized modeling studies of secondary circulation over a sloping continental shelf provide two possible mechanisms of BBL detachment, assisting the formation of the shelf-slope front. The first is associated with the convergence of cross-shelf buoyancy advection near the shelfbreak, leading to BBL detachment and frontogenesis (*Gawarkiewicz and Chapman*, 1992). The second is associated with balancing the Ekman driven offshore advection of buoyancy with the onshore advection of density at the shelf density front (*Chapman and Lentz*, 1994). Strong upwelling and downwelling associated with surface and bottom convergence at the SSF also have been found in both observations and model outputs (*Gawarkiewicz et al.*, 2001; *Gawarkiewicz and Chapman*, 1992; *Chapman and Lentz*, 1994). Upwelling associated with BBL detachment could bring salty slope water and nutrients from the bottom layer to the upper water column. The BBL detachment process can be detected using simple cross-shelf hydrographic CTD sections by tracking temperature changes along certain isopycnals (*Pickart*, 2000). Local minima in the contours of accumulated temperature change were shown to follow the detached BBL's. This technique has been applied to study the seasonal behavior of BBL detachment near the SSF using

select MAB cross-shelf hydrographic sections from the PRIMER experiments (*Linder et al.*, 2004). That study found that the detached BBL extends higher in the water column during the winter than the summer due to the presence of seasonal pycnocline which can inhibit vertical circulation. The same technique of BBL detachment detection is applied to a subset of the SW06 glider dataset to study summertime secondary circulation on the NJ Shelf (*Gong and Glenn*, submitted). Their study showed that secondary circulation associated with BBL detachment was spatially coherent on the 10 km alongshelf scale and occurred simultaneously in multiple cross-shelf regions.

Most observational studies of the SSF, in its various names and forms (i.e. the shelfbreak front, coastal density front), have been either synoptic or climatological in nature. While these observations have been helpful in developing a seasonal view of the SSF and dynamical theories for the mean state of the SSF, they provide limited information on the spatial and temporal variability of the SSF in response to environmental forcing. The sub-mesoscale to mesoscale (5-50 km, hours to weeks) regime of the shelf-slope region remains highly undersampled both spatially and temporally. The intra-seasonal variability of the SSF and the associated secondary circulation has not yet been documented observationally. The dataset used here offers an unique multi-dimensional view for the SSF for nearly the whole summer season, allowing the temporal variability of the SSF to be characterized on subtidal to intra-seasonal timescales. In this paper, we focus on characterizing the spatial and temporal variability of the SSF and understanding the effect of the changing environmental forcing on the structure of the SSF over the stratified summer season on the New Jersey Shelf.

The experimental setup, the observational platforms and the data processing are discussed in Section 4.2. The mean summertime hydrography and circulation for the

SW06 region are characterized in Section 3.3.1, and the main environmental forcing factors and major forcing events on the NJ Shelf are characterized in Section 3.3.2. In Section 3.3.3 the oceanographic response to environmental forcing on the intraseasonal timescale is presented. It is followed by characterization of the different types of salinity intrusions, 3-D structure of the SSF, and a salt budget analysis of the outer NJ Shelf in Section 3.3.4. The influence of shelf-slope frontal eddies on the subtidal variability of the shelf hydrography and flow are examined in Section 3.3.5. The movement of the SSF, the associated secondary circulation, and its effect on sub-pycnocline intrusions are studied in Section 3.3.8. Finally in Section 3.3.7, the intraseasonal change of shelf stratification as a result of the changing hydrography and the potential connection of stratification with nonlinear internal wave activity are discussed.

3.2 Data and Methods

3.2.1 Shallow Water 2006 Joint Experiment

This study uses the extensive oceanographic dataset from the Shallow Water 2006 Joint Experiment sponsored by the Office of Naval Research. The observational platforms selected here include underwater gliders (hydrography), oceanographic moorings (winds, currents, hydrography) and satellites (sea surface temperature). The glider flight tracks and oceanographic mooring locations are shown in Figure 3.1. The central mooring array, indicated by SW30, is located approximately 70 km south of the head of the Hudson Canyon near latitude 39N, longitude 73W. The sampling platforms have different capabilities in terms of resolution and coverage in space and time. The gliders have excellent spatial hydrographic coverage in the vertical and the cross-shelf directions but coarse temporal resolution. The moorings provide high temporal resolution measurements of

current and hydrography in both the cross-shelf and along-shelf directions but coarse spatial resolution. Finally the satellite Sea Surface Temperature (SST) data have far field information such as offshore eddies/rings that can potentially influence the study area but no sub-surface information. The multiple data platforms complement each other and together they provide a more complete 4-D view of the SW06 study region. The intra-seasonal variability of shelf hydrography were characterized using gliders deployed from July through September. The analysis of moorings and SST data focuses on the mid to late summer time period from July 31 to September 9, 2006. One major event that marked the end of summer and transition to autumn was the passage of Tropical Storm Ernesto in early September. The structures of the water column before and after the storm were very different. Based on the timing of the storm, three periods of interest are defined: pre-storm (August 1 - August 31), during-storm (August 31 - September 2, 1600) and post-storm (September 2, 1600 to September 9, 0900). Most of the analyses in this paper will focus on the pre-storm period. All times are referenced to Coordinated Universal Time (UTC).

3.2.2 Gliders

A fleet of Webb Slocum Electric Gliders were deployed from 14 June 2006 to 02 October 2006 at the outer New Jersey shelf. During the experiment, 356 glider days (one glider day is defined as one glider flying for one day) were flown covering a total distance of 6683 km. Eight gliders in 17 deployments collected a total of 51933 CTD casts. These gliders typically fly with a vertical velocity of about 12.5 cm/s and a horizontal velocity of about 28 cm/s. Each complete yo (one set of up and down casts) took approximately 25 minutes in 100 m water. The gliders had an endurance of 3 to 6 weeks depending

on the sensors mounted on the glider. The total SW06 glider deployment area was approximately 100 km (along-shelf) by 100 km (cross-shelf). The majority of the hydrographic sampling was focused on the outer 45 km of the NJ Shelf between the 60 m and the 100 m isobath along six cross-shelf lines (Figure 3.1). This core sampling box was approximately 70 km (along-shelf) and 40 km (cross-shelf). Sampling resolution was 0.25 m in the vertical, 300 m in the cross-shelf, and 15 km in the along-shelf, and spanned an area covering over 4000 km^2. The number of gliders deployed at a given time varied during the experiment. The first glider was deployed in June and recovered in July. Starting 19 July 2006, which marked the official beginning of the SW06 experiment, at least two gliders occupied the SW06 glider lines. All six lines were occupied for most of August into September.

Each glider carried a basic set of hydrographic instruments including a Seabird CTD (un-pumped) and a pressure sensor. Slocum gliders were not equipped with pumped CTD's back in 2006. All the SW06 glider CTD data are processed using the data pipeline developed by (*Kerfoot et al.*, 2010). Thermal-inertia of the conductivity sensor was an issue for all glider CTDs, pumped or un-pumped, especially when sampling across the sharp thermocline of the summer. In SW06, the uncorrected mismatch between the upcast and downcast salinity measurement were as large as 2 near the thermocline. The SW06 glider CTD data were corrected using an algorithm based on one originally developed for shipboard CTD sampling (*Lueck*, 1990; *Morison et al.*, 1994). Each pair of up and down temperature and salinity casts were fitted to a conductivity correction model which contains four tunable parameters governing the temperature shift relative to the pressure, the conductivity shift relative to pressure at constant

temperature, the amplitude of the correction, and a time constant of the thermal inertia of the conductivity sensor. The parameters were functions of flow speed through the CTD sensor, thus the un-pumped CTDs had the additional calibration challenge of correcting for non-uniform flow through the sensor. Furthermore, some of the gliders used in SW06 had data timing issues due to inaccurate reporting of the time lag between the CTD sensor and the science computer, and the lack of timestamps for some measurements. Both timing issues were be as large as a few seconds and seemed to occur randomly. An engineering fix to the data timing problem was not available at the time of the experiment, thus during data processing, a smoothing function was applied to the glider time and the times from each cast was referenced with the more regular pressure measurements. Data with missing or repetitive timestamps were rejected. The timing issue limited the accuracy of the gliders time to a few seconds. The four tunable parameters of the conductivity correction model were fitted for a couple characteristic glider sections during the SW06 deployment and their values were applied to the entire fleet of gliders for the whole SW06 experiment. Furthermore hydrostatic stability of the water column was enforced by minimally adjusting salinity so that density inversions were removed.

This best of effort corrected glider CTD downcasts showed significant improvement versus uncorrected profiles as seen in the improved matching of up and down casts (see Figure 3.2). The correction step discussed above removed the majority but not all of the mis-match between up and down casts of the uncorrected profiles, especially in the pycnocline region. After the correction, the salinity anomalies are in the same direction and have the same sign for both up and downcasts. The salinity error for most

of the corrected casts of an un-pumped CTD is on the order of 0.3 or less. Occasionally however, the corrected casts can still have salinity error greater than 0.5. Gliders with pumped CTD's are currently being tested (as of 2009), and early test results have shown significant improvement in the thermal inertia lag issue with uncorrected up and down casts showing error of less than 0.2 in most cases (*Kerfoot et al.*, 2010).

3.2.3 Moorings

The SW06 mooring array was one cross-shelf line from the 60 m isobath out to the 460 m isobath and one alongshelf line along the 80 m isobath. Together they formed an inverted 'T' at the outershelf with the top of the 'T' in the cross-shelf direction and the longer stem of the 'T' in the along-shelf direction (Figure 3.1). The center was located just a few kilometers west of 39N, 73W. The cross-shelf moorings were SW29 (60 m), SW30 (center mooring, 80 m), SW42 (160 m) and SW43 (460 m). The alongshelf moorings (from SW to NE) were SW30, SW32 and SW33. The moorings were all deployed on or before July 31, 2006 and recovered after September 7, 2006. Each mooring was instrumented with an ADCP, except for SW42 and SW43, which had two each. SW29, SW30, SW32, and SW33 also had Conductivity-Temperature sensors. The location of each mooring and the depths of the CT sensors are listed in WHOI Technical Report 2007-04 (*Newhall et al.*, 2007). Both the current and the hydrographic mooring data were hourly averaged in this study. Low-pass filtering was performed using Hamming filter with a 33 hour window. At latitude of 39N, the inertial period is 19 hours. Inertial bandpass filtering used a 14.5 to 21 hour window. The wavelet analysis used the Matlab software was developed by *Torrence and Compo* (1998).

Two Air-Sea Interaction Spar (ASIS) wind buoys from the University of Miami

were deployed along the main cross-shelf mooring line (*Graber et al.*, 2000). Buoy SW57 'Yankee' was deployed at 39.0191 N, 73.0535 W on July 30, 2006 inside the central mooring cluster at the 80 m isobath. Buoy SW58 'Romeo' was deployed further shoreward at 39.0739 N, 73.1640 W on August 1, 2006. Wind analysis presented in this study used SW57 Yankee due to its proximity to the central mooring array as well as having two additional days of deployment at the beginning of the experiment. Buoy wind data was reported in half hourly intervals and interpolated to hourly intervals using a cubic interpolation scheme. Low-pass filtering was performed in a similar fashion as the current data mentioned above using the same filter window width of 33 hours.

Both the wind buoy data and the mooring current data are rotated to align with the geographic orientation of the along-shelf and cross-shelf axes at the SW06 central mooring site. The along-shelf orientation of the 80 m isobath at the SW06 site is approximately 34 degrees clockwise of True North. All wind and current velocity data are rotated so that the cross-shelf offshore (onshore) direction is the positive (negative) x direction with speed in that direction indicated by u, and the along-shelf upshelf (downshelf) direction is the positive (negative) y direction with speed in that direction indicated by v.

3.3 Results

3.3.1 Mean and Subtidal Variability

The mean summertime flow and hydrography for the SW06 study region are shown in Figure 3.1 and 3.3. The mean cross-shelf hydrographic sections include glider data from July 1, 2006 to September 1, 2006. The mean depth-averaged currents (upper 100 m of the water column) and surface wind vectors include mooring data from August 1,

2006 to September 1, 2006. Data from the time periods during and after the passage of Tropical Storm Ernesto (September 1 to October 2, 2006) are not included in the mean flow calculation. The subtidal variability of the averaged glider sections for the innner 4 transects are calculated for the month of July, August, and September.

Mean Flow

The mean depth-averaged flow at the outershelf/shelfbreak region was mainly along-shelf towards the southwest with speeds ranging from 6.0 cm/s to 9.8 cm/s (Figure 3.1). The northern most mooring (SW33) and the deep moorings at 160 and 460 m (SW42 and SW43) had flows with a discernible onshore cross-shelf component. The alongshelf flow between the 60 m isobath and the $>$ 160 m shelfbreak isobaths was weakly convergent at the SW06 study location. The depth-averaged cross-shelf speed for August at both SW42 and SW43 were 2.5 cm/s onshore. On the other hand, the midshelf mooring (SW29) and the outershelf mooring (SW30) show flow with discernable offshore component. The depth-averaged cross-shelf speed for August at SW29 was 1.2 cm/s offshore. The cross-shelf flow between the midshelf mooring (SW29) and the deep moorings (SW42 and SW43) was convergent. The value of the divergence was $\partial u/\partial x = -8.5 \times 10^{-7}\ 1/s$. Compared to the Shelfbreak PRIMER observation of flow convergence on the New England Shelf, this value was approximately an order of magnitude less. The total divergence, $\nabla_h \cdot \vec{v}$, including both the cross-shelf and along-shelf flow components, was $-1.5 \times 10^{-6}\ 1/s$. Furthermore the mean depth-averaged flow had both along-shelf and cross-shelf flow shear centered around the central mooring (SW30). Using current data from SW29, SW33, and SW43, which surrounded SW30, the mean vorticity of the flow at SW30 for August was estimated to be $\nabla \times \vec{v} = 2.2 \times 10^{-6}\ 1/s$.

Analysis is Section 3.3.8 will show that the flow vorticity is very different for different parts of the water column (i.e. pycnocline versus near bottom), and that the instantaneous vorticity value (detided) can be an order of magnitude higher than the mean value. Energetic events such storms and eddies, which can induce significant flow shear at the shelfbreak, appeared to coincide with observations high flow vorticity.

Mean Wind

The wind velocity during August oscillated between upwelling favorable winds from the southwest and downwelling favorable winds from the northeast. The mean wind speed, as measured by ASIS buoy 'Yankee', was 0.4 m/s from the southwest at an angle of 220 deg from True North (vector indicated by grey line originating from the star in Figure 3.1). For the same time period, at NOAA NDBC buoy 44009 (38.464 N 74.702 W), the mean wind was 1.0 m/s, also from the southwest at an angle of 205 deg (not shown).

Mean Hydrography

The mean glider temperature, salinity, and spiciness cross-shelf sections as well as the standard deviations of each of the variables for the months of July and August, 2006 are shown in Figure 3.3. Spiciness, which is only a function of temperature and salinity, was useful for studying watermass interactions near the shelfbreak because it can help differentiate between watermasses with similar densities (*Flament*, 2002). The depth of the pycnocline was located between 15 and 20 m with an average $N^2 = 0.002\ 1/s^2$ at the midshelf point and $0.003\ 1/s^2$ at the outershelf. On most portions of the shelf, except near the offshore edge, the pycnocline separated the warm surface shelf water from the cold bottom shelf water. The surface shelf water had a mean temperature of

24 to 26 °C and a salinity of generally less than 32. Below the pycnocline, residing in the bottom layer of the shelf, was the MAB cold pool situated near the 60 m isobath. The cold pool was characterized by water with temperature less than 10 °C, with a salinity between 32.5 and 33.5. Cross-shelf glider section showed that it could extend 20 km seaward of the 60 m isobath at depths just below the pycnocline. The cold pool generally did not extend past the 80 m isobath, although separate parcels of cold pool water were sometimes found further offshore. Seaward of the 80 m isobath, the influence of the warmer and saltier slope water were clearly seen in temperature, salinity, and spiciness. A significant amount of salty slope water is observed on the outershelf in the form of bottom intrusions. Slope water intruding onto the outershelf contributed to a general increase in temperature, salinity and spiciness. The different types of intrusions will be discussed in detail in section 3.3.4.

Subtidal Variability

The main source of sub-tidal hydrographic variability on the stratified outershelf was in the thermocline and near the surface. The variability was greatest near the shelf-break due to the complex interaction of the shelf and slope watermasses. The study of baroclinic instability in the shelfbreak region had shown that stratification and shelf-break topography are key factors in sustaining unstable frontal waves (*Gawarkiewicz*, 1991). Using characteristic summertime parameters for the New England shelf, modes of unstable waves with a wavelength of 25 km, cross-shelf scale of 7-8 km, and e-folding time scale of 4-8 days was obtained in a 3 layer shelfbreak model (*Gawarkiewicz*, 1991). The passage of these frontal waves in the SW06 region could introduce hydrographic variability that would be observable in the glider cross-shelf sections. During the two

months sampling for July and August 2006, the average standard deviation of the cross-shelf temperature was between 3 and 5.5 °C in the thermocline region (Figure 3.3(b)). The variability was highest on the offshore side. This was consistent with temperature standard deviation observed during the Shelfbreak PRIMER experiment (*Linder et al.*, 2006). And an EOF analysis of the PRIMER cross-shelf temperature showed that the amplitude of Mode 1, which account for 43% of the variance, is maximal in the same offshore region (*Linder et al.*, 2006).

High values of standard deviation in the cross-shelf section of salinity was mainly concentrated in the surface mixed layer, with values as high as 1.6 near the shelfbreak (Figure 3.3(d)). The cross-shelf extent of the high salinity variability (> 1) was approximately 5-10 km shoreward of the 100 m isobath. The mean position of the offshore boundary of the fresh surface layer ($S < 32$) extends a few kilometers further offshore into the high salinity variability region, but still shoreward of the 100 m isobath. The observed pattern of salinity variability was consistent with the physical scale of cross-shelf variability due to surfaced-trapped frontal waves (*Gawarkiewicz*, 1991) and with the magnitude of salinity variability due to frontal meandering (*Linder et al.*, 2006). The relatively low value of salinity standard deviation below the pycnocline suggests that the movement of the SSF due to either bottom-trapped frontal waves or wind forcing played a relatively minor role in cross-frontal heat and salt exchange compared to the surface cross-shelf flux. Similar to salinity, variability in spiciness was also concentrated on the pycnocline near the shelfbreak (Figure 3.3(f)). It will be shown later in section 3.3.5 that spicy water was associated with offshore forcing of the slope eddies. The variability in spiciness was primarily due to the passage of eddies through the study region.

3.3.2 Seasonal Forcings and Variability

Hudson River Discharge

A significant upstream source of freshwater entering the SW06 study region was river discharge from the Hudson River watershed. The timing and the amount of the discharge strongly affected stratification on the shelf. The total discharge rate of the Hudson River watershed was estimated to be twice the combined measured discharge rate measured at Fort Edwards and Cohoes (*Chant et al.*, 2008). The daily discharge rate for the Hudson River is shown in Figure 3.4. The solid line indicates discharge rate for 2006 and and the dotted line is the daily discharge climatology for the past 90 years. Climatology indicates that most of the river discharge occurs in the spring with a peak in April. Summer is typically the low discharge season. However, for 2006, there was a large discharge event just before July, reaching a peak discharge rate of 7000 m^3/s. This was the fifth highest peak discharge on recorded history for the Hudson River and the highest for July. The total freshwater volume output to the NJ Shelf from June 20 to July 20 by the Hudson was 4.1×10^9 m^3, enough to fill a 100 km by 100 km section of the shelf with freshwater 0.41 meters deep. *Castelao et al.* (2008b) demonstrated a surface transport pathway leading from the innershelf to the outershelf operating during the same time period. This pathway carried the discharge water directly into the SW06 study area, creating very low salinity surface layer water with salinity less than 30 observed in the upper 10 meters of the water column for much of July and into mid-August. The fresh lens of surface water led to the development of strong stratification with a density difference in excess of 7 kg/m^3 in late July and early August.

Surface Heating

The New Jersey Shelf experiences seasonal heating and cooling of the surface mixed layer with temperature ranging from 5 °C in winter to 25 °C in summer on the monthly time scale (Figure 3.5b). During the winter, the mixed layer spans the whole water column with little or no vertical stratification. Combined with low solar insolation and surface air temperature, the entire water column is cold. In the summer, a strongly stratified surface mixed layer forms due to high spring time river discharge, more intense seasonal solar heating, and lower number of storm mixing events. The warm surface mixed layer is significantly warmer than the cold pool below the seasonal pycnocline that have a temperature of 10 °C or colder in August. Over the interannual time scale, monthly SST time series at the SW06 site (the black dot in Figure 3.5) shows winter minimum temperature variability between 5 to 9 °C and summer maximum temperature can vary between 21 to 25 °C (Figure 3.5b). Averaged over the summer season (June-August), the SST for summer 2006 was the highest on record for the past decade (Figure 3.5c). The warm surface temperatures combined with low salinity due to high river discharge, resulted in 2006 summer being one of the most stratified in the recent decade.

A summer 30 day composite SST map (July 30 - August 28) for the MAB region in 2006 shows the distribution of warm and cold surface watermasses (Figure 3.5a). For major portions of the MAB, except at the very northern tip near Georges Bank, the temperature was above 23 °C. SST on the shelf was nearly uniform except at the innershelf which showed slightly lower temperature. The lack of surface temperature gradient between the shelf and slope water near the shelfbreak indicated that the surface manifestation of the SSF would primarily be due to the salinity difference of the

watermasses.

Winds

Summer winds on the NJ Shelf are typically from the southwest, while autumn winds were both stronger and more varied in direction (*Gong et al.*, 2010). Wind data from both the ASIS buoy 'Yankee', located at the experiment site, as well as the NOAA NDBC buoy 44009, located to the southwest closer to the Delaware Bay, indicated that a transition from the summer like regime to the more autumn like regime took place during course of the experiment. The transition was sharply marked by a major storm (Tropical Storm Ernesto) passing through the study region at the very beginning of September. Before the storm, wind conditions during July and August 2006 were typical of summer in the MAB. The magnitude of the mean wind velocity vector at buoy Yankee (from 7/31/2006 to 8/31/2006) was 0.761 m/s from the southwest, 229 deg clockwise from True North (vector directed from star in Figure 3.1). This was consistent with a mean summertime upwelling favorable winds. The mean wind speed during the passage of Tropical Storm Ernesto (from 8/31/2006 to 9/2/2006 1600 GMT), on the other hand, was 14.4 m/s from the east, 83 deg clockwise from True North. This was a common wind direction on the shelf during the passage of a tropical storm or Nor'easter on the New Jersey Shelf. After Ernesto (from 9/2/2006 1600 GMT to 9/9/2006 0930 GMT), the mean wind speed was 1.26 m/s from the NW, 327 deg clockwise from True North. This was characteristic of autumn conditions when winds from NE and NW become more common. The monthly wind histograms for July, August and September at NOAA NDBC Buoy 44009 are shown in Figure 3.6a - 3.6c. For July, winds from the southwest dominated, occurring nearly 50% of the time, and the mean along-shelf

wind stress is 0.032 N/m^2, directed towards the northeast. For August, winds from the southwest became less dominant with more frequent episodes of northeasterly winds, and the mean along-shelf wind stress was 0.009 N/m^2, directed towards the northeast. When September arrived, winds from all the major directions (NW, NE, SW) were common. The mean along-shelf wind stress for September was -0.012 N/m^2, directed towards the southwest.

Offshore forcing

A variety of offshore forcings of either local or distant origin can facilitate the transport of heat and salt across the continental shelfbreak. The possible mechanisms for driving the cross-frontal exchange on the MAB include: (1) Warm Core Rings (WCR) on the scale of $100-300$ km (*Morgan and Bishop*, 1977), which originate from the Gulf Stream, (2) cyclonic and anticyclonic shelfbreak eddies or ringlets on the periphery of a WCR, on the scale of $40-50$ km (*Pingree*, 1979; *Kennelly et al.*, 1985; *Houghton et al.*, 1986; *Garvine et al.*, 1988), and (3) shelf-slope frontal waves on the scale of $20-40$ km (*Gawarkiewicz*, 1991), which can grow from frontal instability. A large WCR with a diameter of approximately 300 km developed south of Georges Bank in April 2006. This ring was never completely detached from the Gulf Stream and slowly propagated northeastward until it was re-absorbed by the Gulf Stream south of the Grand Banks in early August 2006. During the time period from April to August, the northern edge of the WCR often came in contact with the shelfbreak. Wave like instabilities along the shelfbreak appeared to be associated with the WCR contact. These large frontal waves undulate with a wavelength of 50 to 100 km. The alongshelf scale of the frontal disturbance was over 350 km extending from the southern side of Grand

Banks to southwest of the head of the Hudson Canyon. Using satellite observations, *Ramp et al.* (1983) showed that flow shear between the shelfbreak jet and a WCR could generate frontal waves with a wavelength of 23 km and growth time scale of less than 18 hours, which is significantly smaller than the observed undulation here. Baroclinic instability could be a candidate for generating these larger scale frontal disturbances on longer time scales (*Fratantoni and Pickart*, 2003). In addition to the large WCR and its direct influence on the shelf-slope front, smaller eddies with a length-scale of 50 *km* carrying WCR type water were observed moving southwestward along the MAB shelfbreak during SW06. These could be similar to the shelfbreak eddies as observed by *Garvine et al.* (1988), or they could also be ringlets advected around a previously well-sampled WCR with a similar size scale as the shelfbreak eddies (*Kennelly et al.*, 1985). As is usual, the available satellite sea surface temperature could identify the horizontal geometry of the eddies but could not provide data about the eddies' sub-surface properties. Due to the uncertainty in identifying the origin of these eddy-like features, they will all be labelled as 'slope water eddies' in this study, with the understanding that these eddies carrying WCR type water could have come from a larger WCR or of a local origin carrying shelfwater. Two of the slope water eddies passed through the SW06 study area in August, and during each eddy's passage, intrusions of salty slope water were observed at the depth of the pycnocline. These intrusions will be investigated in detail in Section 3.3.4. The first eddy came around August 6-11, the second eddy came in August 21 - 28.

3.3.3 Oceanographic Response on the Intraseasonal Timescale

Foot of the SSF and Outershelf Salt Variability

The monthly mean cross-shelf sections of Temperature, Salinity, and Density for July, August and September 2006 are shown in Figure 3.6. The transects are created by averaging the inner four glider transects (3 to the north of the main cross-shelf mooring line, 1 to the south, see box in Figure 3.1) and binning the cross-shelf casts at 1 km resolution.

The location of the foot of the SSF marks the extent of the cross-shelf excursion of slope water onto the shelf bottom layer. Subtidal variability in the surface wind stress is known to affect the structure of the SSF (*Fratantoni and Pickart*, 2003). Glider transects along the SW06 main cross-shelf mooring line were used to calculate its location (Figure 3.6). Individual glider transect measurements of the near bottom cross-shelf location of the front (using salinity of 34.5) as a function of the subtidal along-shelf wind stress is shown in Figure 3.7(a). The correlation between the wind and the frontal location is 0.65. The slope is 347 $m/(N/m^2)$ and the intercept is -86.7 m. The monthly mean locations of the foot of the front for July, August, and September were estimated to be at 71 m, 77 m, and the 83 m isobath, and they are also plotted as a function of the monthly mean wind stress in Figure 3.7(a) (stars). The slope calculated using the monthly data is 295 $m/(N/m^2)$. It is within the 95% confidence interval of the slope calculated using individual transect data.

Boicourt and Hacker (1976) proposed a simple 1-D model for the cross-shelf salt balance. In this model, the cross-isobath advection of salt from the offshore was balanced by the temporal change in near bottom salinity (inside the bottom Ekman

layer). The cross-isobath transport was assumed to be due to bottom Ekman forcing generated by the along-shelf flow. The bottom stress was assumed to be proportional to the alongshelf wind stress. The cross-shelf salt balance can be expressed as:

$$\frac{\partial S}{\partial t} \approx -u\frac{\partial S}{\partial x} \tag{3.1}$$

Note that in this rotated reference frame, x is the cross-shelf direction and u is the cross-shelf velocity. *Lentz* (2001) tested this simple model using a year long mooring data from the Coastal Optics and Mixing experiment. He found that the balance between the left and right sides of Equation 3.1 basically held for the bottom 10 m with a correlation of 0.64. Furthermore, the along-shelf wind stress was found to be correlated with the cross-shelf salinity with a correlation coefficient of 0.49. Unfortunately a direct comparison of the results of the two experiments cannot be made because the near bottom current measurements from the mooring ADCP's during SW06 were very sparse. For the cross-shelf moorings there were no current measurements within 10 m of the bottom. Therefore the salinity balance for the 'bottom portion' of the water column was tested by examining the contribution of both the along-shelf and the cross-shelf advection to the salinity variability at the central site (SW30). Low-passed (33 hour filter) salinity and velocity measurements in the lower 30 m of the water column at SW29 (60 m isobath, inshore), SW30 (80 m isobath, central), and SW32 (80 m, upshelf) were used.

Salinity time rate of change in the bottom 30 m of the water column at the central mooring was well correlated with along-shelf advection of salt (correlation of 0.8 at the 99% confidence level). The advective term led the time rate of change term

by 10 hours (Figure 3.7(b)). Somewhat surprisingly, the salinity change however was not correlated with the cross-shelf advection of salt. The along-shelf wind stress was correlated with the depth-averaged current below the pycnocline (correlation coefficient between 0.63 and 0.68) at the 99% confidence level for all three moorings on the 80 m isobaths (SW30, SW32, and SW33 from south to north). The along-shelf wind stress was also weakly correlated with the 'near bottom' cross-shelf current with a correlation coefficient of 0.43. This is consistent with the values reported by *Lentz* (2001) on the New England Shelf. The strongest cross-shelf current was observed during Tropical Storm Ernesto. The effect of the storm on the outershelf surface salt budget will be discussed in Section 3.3.6. The variability of the sub-pycnocline salinity suggests that both along-shelf advection and cross-shelf advection are important in the sub-pycnocline salt balance. The strong correlation between along-shelf wind stress and along-shelf current suggest that summertime upwelling favorable winds plays an key role in modulating the along-shelf flow on the outer MAB shelf. The fact that $\partial S/\partial t$ was not correlated with $u\ \partial S/\partial x$ in the water column interior below the pycnocline does not mean that the 1-D cross-shelf salt balance model of *Boicourt and Hacker* (1976) cannot be applied to this portion of the shelf for this particular time period. The model was designed to be applied to the bottom Ekman layer, which is not sampled effectively here. An event-based analysis of the temporal variability of outershelf currents and hydrography will be presented in Section 3.3.5.

Hydrographic Response of Shelfwater Masses

The depth of the pycnocline increases during the course of the summer. In July (Figure 3.6j, the pycnocline is at a mean depth of 15 meters, increasing to 18 meters in August

(Figure 3.6k) and 25 meters in September (Figure 3.6l). The surface mixed layer is warmest and freshest during July and August with temperatures of 24-25 °C (Figure 3.6d and 3.6e). The high summertime discharge of the Hudson River, combined with persistent upwelling favorable winds during 2006, result in fresh river water being advected cross-shelf along an offshore transport pathway just south of the HSV (*Castelao et al.*, 2008b). The surface freshwater extends past the 100 m isobath into the slope sea in July and early August and lowers the outershelf surface salinity to 30-32 (Figure 3.6g and 3.6h) for much of the summer. Salinity intrusions driven by slope water eddies delivered a significant amount of salty offshore water to the upper water column of the outershelf. When Tropical Storm Ernesto passed through the outer-shelf in September, it drove significant shoreward flow and intense mixing in the surface layer, which erased the mean vertical salinity gradient for much of the outershelf and increased the surface salinity at the midshelf between the 55 m and the 80 m isobaths by 2 in early September (Figure 3.6i). It also led to significant cooling of the surface layer temperature to 20-22 °C and deepening of the depth of surface mixed layer to 25 meters. The resulting surface density change from both cooling and salting is approximately 2 kg/m^3, which decreased the density difference between the surface and bottom layers from 4-5 kg/m^3 to 1.5-2 kg/m^2 in early autumn.

The intra-seasonal change in the watermass types as well as their cross-shelf extent can be visualized in Temperature-Salinity space. Using glider CTD data binned into three isobath depths (60m, 80m and 100m) based on the location of each individual cast, we construct T-S diagram for each of the three isobath depths (Figure 3.8). Density and spiciness contours are overlaid on each plot and the color of the dots represent the time of each measurement. Several of the shelf and slope watermasses identified by

Wright and Parker (1976) can be seen. One can also identify intra-seasonal patterns in the watermass properties. First, except for a gradual warming, the T-S properties of the bottom shelf water changed little throughout the whole summer season into early autumn, despite the energetic forcing of the storm passage. The salinity held steady between 32.5 and 33.5 while the temperature ranged between 8-12°C. The relative constancy in the properties of the bottom shelf water implies that there was very weak mixing of heat and salt across the seasonal pycnocline from above and across the SSF from offshore during the stratified summer season. The density of the bottom shelf water was essentially constant in time between 1025 kg/m^3 and 1026 kg/m^3. Second, the bottom slope water, having salinity between 35 to 36 and temperature between 12 and 16°C, was seen at the 80 and 100 m isobaths before the storm (Figure 3.8c, e), but only at the 100 m isobath after the storm (Figure 3.8f). The disappearance of the salty offshore water at the 80 m isobath after the storm was consistent with the offshore movement of the SSF in early autumn due to more frequent downwelling favorable winds. Third, the surface watermass shows dramatic change from fresh and hot riverine water before Tropical Storm Ernesto's passage to warm and salty slope water after the storm. The surface temperature dropped from 24-28°C to 20-22°C and the salinity increased from 30-32 to 32-34. The density of the surface layer increased from 1019 kg/m^3 in mid August to over 1023 kg/m^3 in late September. Finally, salinity intrusions at mid-water column are only observed at the 80 and 100 m isobath before the storm, whereas after the storm, salinity intrusion can be seen even at the 60 m isobath as indicated by the spicy water with density of 1024 kg/m^3 (Figure 3.8b, d, f). Watermasses with salinities of 35.5 or higher in this region tend to originate in the Gulf Stream (*Gawarkiewicz, per. comm.*). Here it was seen throughout August and

September, the high salinities of these watermasses suggest a non-local origin. The dramatic difference in hydrography on the shelf before and after the storm indicate a change in the dynamical mechanisms governing the SSF. The potential mechanisms of cross-shelfbreak exchange during the pre-storm period are discussed in Section 3.3.5.

3.3.4 Spatial Structure

Salinity Intrusion Classification

Salinity intrusions from the slope onto the shelf are a persistent summertime feature at the outershelf. The intensity, extent and the type of the intrusions can vary greatly depending on the stability of the thermohaline front, and other onshore and offshore forcing mechanisms (*Houghton and Marra*, 1983; *Gawarkiewicz et al.*, 1996a; *Churchill et al.*, 2003; *Kuzmina et al.*, 2005). Four types of intrusions are identified based on their location in the water column as well as their Density-Spiciness properties. Salinity intrusions with salinity less than 34, however, are not considered. Shoreward of the SSF, marked by the salinity 34 contour, the water column essentially has a simply stratified two-layered structure with fresh shelf water overlaying saltier shelf water (Figure 3.8a). Seaward of the SSF, complex slope water intrusions form multilayered salinity structures. The salty slope water can be seen at all depths of the water column, often with strong horizontal salinity gradient at the surface, pycnocline and at depth (Figure 3.9). The intrusions on the shelf are usually separated in space. The saltiest of the intrusions are typically seen at the pycnocline (marked in green in Figure 3.9a). A second batch of intrusions near the bottom of the pycnocline appears much further inshore (marked in red in Figure 3.9a). Below and above the pycnocline lays the bottom and surface intrusions.

The salinity cross-section plotted in Density-Spiciness space shows the differences in watermass properties among the different types of intrusions (Figure 3.9(b)). Bottom intrusions, the most common type and the largest contributor to the outershelf salt budget, have densities of greater than 1026.2 kg/m^3 and a spiciness between 0.5 and 3 (Figure 3.9(b), black ellipse). Recall that the foot of the SSF, which represents the shoreward extent of the bottom intrusions, is correlated with the alongshelf wind stress. This means that alongshelf windstress can affect the delivery of salt from the slope onto the shelf at depth. Above bottom intrusions reside the sub-pycnocline intrusions, which have densities between 1024.5 and 1026.2 kg/m^3 with spiciness between 1 and 3.2. They are also defined to reside at least 10 m below the surface as the seasonal pycnocline is rarely shallower than 10 m on the shelf (Figure 3.9(a), red ellipse). The presence and distribution of these sub-pycnocline intrusions are likely driven by secondary circulation at the SSF. *Gong and Glenn* (submitted) studied the structure of the SSF during the highly stratified SW06 time period in mid August and concluded that processes such as BBL detachment can be a driver of sub-pycnocline intrusions. The implications of secondary circulation and a double frontal interface at the shelf-slope front will be discussed in Section 3.3.8. Pycnocline intrusions are defined as watermasses having densities between 1022 and 1025.7 kg/m^3, spiciness greater than or equal to 3.4, and residing 10 m below the surface (Figure 3.9, green region). Its appearance on the shelf is correlated with the proximity of slope water eddies which will be discussed in Section 3.3.5. A surface intrusion is defined as having a density of less than or equal to 1024 kg/m^3, with no shelf water ($S < 34$) in the upper 5 m of the water column, and it has not already been classified as a pycnocline intrusion (Figure 3.9, blue region). The extent of the surface intrusions is determined by both the freshwater discharged onto

the shelf as well as possible offshore forcing such as eddies and rings. All four types of intrusions were defined to be exclusive of the other (i.e. one parcel of water can only be classified as one of the four types). As the example section in Density-Spiciness space indicates (Figure 3.9(b)), the bottom intrusions (black) and the sub-pycnocline intrusions (red) are closely connected to each other while the surface intrusions (blue) and pycnocline intrusions (green) are closely connected with each other. In the following section we will look at the 3-D structure of the slope water intrusions in more detail and estimate the cross-shelf and along-shelf scales of variability.

Spatial structure of the Cold Pool and Salinity Intrusions

The spatial distribution of the different intrusion watermasses on the outershelf had both along-shelf and cross-shelf variability. The 3-D salinity structure for the SW06 sampling volume for early and late August 2006 before the passage of Tropical Storm Ernesto are shown in Figure 3.10. The sampling volume covered 70 km in the alongshelf direction, 45 km in the cross-shelf direction and the depths varied from 60 m to 100 m. The gliders flew approximately in formation and were separated 10-15 km from each other in the along-shelf direction. Each cross-shelf sweep by the glider fleet took 2-3 days. The transects are numbered 1-6 from top to bottom (early August sampling is missing transect 6). The cross-shelf mooring line ran between transects 4 and 5.

The surface layer was noticeably fresher in early August and the fresh layer extends all the way to the shelfbreak in all six sections. In late August, the fresh surface layer began to retreat shoreward and surface intrusions were seen in the offshore edge of transects 3-5. The cold pool water had an intermediate salinity value of 32.5 to

33.5. It is represented by green color in the 3-D salinity field. Two interesting phenomenon regarding the cold pool were observed in the early August sampling. First, as one moves offshore along a section, the cold pool was 'lifted' above the bottom by salinity intrusions coming in along the bottom. Second, parcels of the cold pool were seen separated from the main body by saltier slope water elevated from the bottom. As an example, an elevated salinity structure near the middle of the cross-shelf transect divided the cold pool into two bodies in transect 3 of the early August sweep (Figure 3.10a). The offshore portion of the cold pool was completely detached from the bottom. Such hydrographic features were initially reported by *Houghton and Marra* (1983) and were interpreted as detached pieces of the cold pool. A later study by *Garvine et al.* (1988) suggested that 'backward' breaking shelf-slope frontal waves or shelfbreak eddies on the 20-40 km scale can create 3-D cold pool structures that would appear to have detached bodies in a 2-D cross-shelf view. 3-D reconstruction here using the glider data shows that the detached cold pool body in transect 3 was approximately coherent for an along-shelf distance of 10-15 km (comparing to transect 2 to the north and transect 4 to the south). By design, the hydrographic structure offshore of the 100 m isobath was not sampled by the gliders during SW06. While the depth-averaged current derived from the gliders did not indicate any eddy-like structure nearby, satellite SST did indicate a warm-core slope water eddy passing by on August 6. Unfortunately, cloudy conditions prevented successive satellite coverage of the eddy before it moved out of the study area. Based on the available data, it was difficult to determine whether the observed structure of the cold pool was due to the influence of a slope water eddy, but it was clear from the observed salinity distribution that large amounts of slope water had moved shoreward in the form of bottom intrusions while at the same time a significant

portion of the cold pool water moved offshore.

Arguably the cold pool retreated further shoreward in late August 2006 due to the strong presence of slope water throughout the mid water column, as evident in transects 3, 4, and 5 at the offshore end (Figure 3.10b). The sharp transition from the fresher surface shelf water to the surface slope water near the 85 m isobath was dramatic as the salinity difference of nearly 4 and the density difference of 1.5 kg/m^3 were seen within a 2 km distance in the cross-shelf direction. Below the surface layer, the pycnocline intrusions in transects 3 and 4 were very salty, with salinity values near 36. The pycnocline and sub-pycnocline intrusions were not visually distinct in these two middle sections of Figure 3.10b, but could be separated and identified based on the classification in Density-Spiciness space discussed earlier. The sub-pycnocline intrusions appeared to extend a significant distance inshore riding below the pycnocline. Unlike the middle section, the northern glider sections showed clear separation of the pycnocline and sub-pycnocline intrusions in TS space as well as the physical space.

The sub-pycnocline intrusions exhibited some unique spatial characteristics. They often took the form of shoreward extending arms that appear to be rooted in the bottom intrusions. The salt arm reached upward all the way to the lower portion of the pycnocline (Figure 3.9(a)). If the sub-pycnocline and bottom intrusion structures were indeed connected, then this implies isopycnal and diapycnal mixing possibly related to SSF secondary shelf circulation. The salinity structures were coherent in the along-shelf direction for up to 20 km. This could clearly be seen in the glider sections completed during the last week of August (Figure 3.10(b)) as the spatial structure of the northern two sections were very different than the cross-shelf structure of the central two sections.

Isolated patches of sub-pycnocline intrusions were seen significantly inshore of the shelf-slope front. These patches could have a cross-shelf extent of up to 20 km and a thickness of 15 meters. They could appear and disappear within 4 days, the amount of time it takes a glider to do a round trip along its transect. Given their rapid variability and no identifiable cross-shelf process driving such variability, the possibility that these features were advected along-shelf into the SW06 sampling space will be investigated below.

Sub-pycnocline intrusions in general were found inshore of the pycnocline intrusions. The sub-pycnocline intrusions, were often located physically higher in the water column due to tilting of the pycnocline near the shelfbreak. The pycnocline and sub-pycnocline intrusions were more separated in spiciness space than in density space as seen in Figure 3.9(b). The shoreward extent of the pycnocline intrusions were coincident with the offshore edge of the fresh surface shelf water, where the pycnocline isopycnals tended to tighten significantly. The shoreward extent of the sub-pycnocline intrusions could be 10 or more kilometers further onshore, and it interfaced with the offshore boundary of the cold pool.

The slopewater intrusions dominated the cross-shelf and the along-shelf variability in the salinity field. Although mid-water column intrusions were observed in both time periods, they were much more extensive in late August, existing in multiple layers from surface to bottom. The cross-shelf extent of the salinity intrusions were 15-25 km, although individual salinity structure was on the order 5-10 km. Looking at the data section by section, one could observe that coherent salinity structures existed in multiple transects, usually two to three transects, but no more than that. This suggests a natural alongshelf scale of 10-25 km, consistent with estimates by *Gawarkiewicz et al. [2010].*

Alongshelf Propagation Speed

Estimates of the alongshelf propagation speed in this region of the shelf were made using four different methods. There is a clear time lag between the intrusion features near the pycnocline seen in the central mooring SW30 and the mooring just to the north SW32. Cross-correlation analysis of salinity time series between the two moorings at 20 m gives a correlation coefficient of 0.7 and a lag of 19 hours, with SW32 to the north leading SW30 at the central mooring site. The separation between the two mooring is 10 km which means salinity intrusions propagate through the two mooring sites from northeast to southwest with an average speed of 15 cm/s. The direct time-averaged depth-integrated velocity estimate for August 2006 at SW30, on the other hand, gave an alongshelf speed of 7.6 cm/s. The discrepancy between the two calculated values is likely due to the velocity difference at 20 m versus that averaged over the whole water column.

A different estimate of the alongshelf propagation speed can be obtained using the calculation of the depth-averaged velocity from the gliders. As the gliders were flying 6 hour missions, a velocity vector could be estimated every 6 hours by integrating over both space and time. This estimate was based on measuring the difference between its expected and actual location at each surfacing. The mean speed estimate ranged from 7 to 13 cm/s. Although there was large variability in the individual glider velocity vectors, they were all directed towards the SW or the SSW. Finally, by tracking the movement of a particular hydrographic feature through the glider sections, a Lagrangian estimate of the propagation velocity could be obtained. An intrusion was observed in early August that extended 8 km inshore of the 100 m isobath. The feature was approximately 10 meters thick, and situated below the thermocline at 25 meters

depth (not shown). It appeared to have propagated downshelf to the southwest when it disappeared from the northern glider section and appeared in the southern glider sections 4 days later. The two glider transects were separated by 30-40 km. Assuming along-shelf propagation of the intrusion feature, the propagation speed was estimated between 8-12 cm/s, which was consistent with the depth-averaged current velocity of 7-13 cm/s estimated from glider navigation for that mission. The moorings correlation estimate at 20 m was slightly faster than but still consistent with estimates made using other methods. Using 7-13 cm/s as the expected range of propagation speeds for slope water intrusions through the SW06 sampling area (70 km x 45 km), it would have taken an average of 7 to 10 days for a feature to traverse through the SW06 sampling area completely from the northeast to the southwest.

3.3.5 Temporal Variability of flow and hydrography

Subtidal flow events and inertial variability

The interaction of the different watermasses near the SSF and the 3-D structure of the salinity intrusions, discussed in Section 3.3.3 and 3.3.4, varied on time scales from semidiurnal to bi-weekly. Such variabilities were driven by a combination of tidal, wind, and offshore eddy forcing. An overview of the temporal variability of the outershelf hydrography and currents is shown in Figure 3.11, illustrating the major periods of activity (highlighted in grey). Subtidal current measurements (33 hour low-passed) from mid and outershelf moorings (SW29 at 60 m isobath and SW30 at 80 m isobath) indicated four notable flow events during the month of August listed here: (1) Aug 4 - 10, a slope water eddy resided in the study area and pycnocline intrusions were observed, (2) Aug 16 - 20, strong baroclinic tide and sub-pycnocline intrusions were observed, (3)

Aug 23 - 28, another slope water eddy and associated intrusions were observed, and (4) Aug 31 - Sep 3, Tropical Storm Ernesto moved through the study area. Each of these flow events coincide with distinct changes in the outershelf hydrography (Figure 3.11a-c). All the events share the common characteristics of strong downshelf flow at the shelf moorings (Figure 3.11d), onshore flow at the shelfbreak moorings (SW42 and SW43), deepened thermocline (Figure 3.11a), and some type of intrusion activity taking place (Figure 3.11b,g). Furthermore, for all the events except for one case (Aug 23 - 28), the downshelf flow events were co-incident with downwelling favorable winds from the northeast (Figure 3.11e). The cross-correlation between low-passed alongshelf wind at ASIS buoy 'Yankee' and low-passed alongshelf current at SW30 was 0.63 with a time lag of 4 hours. This suggests that upwelling favorable winds from the southwest tend to pause and weaken the downshelf transport while downwelling favorable winds from the northeast enhance the downshelf transport.

During the third event period (Aug 23-28), when the slope water eddy was near, a very strong onshore cross-shelf flow in the surface layer and near the pynocline was observed at the offshore moorings (Figure 3.12(a)). This brought salty water from offshore onto the shelf. At the same time, strong near-inertial motion near the pynocline at the central mooring site was also observed (Figure 3.12(b)). Wavelet decomposition of winds at 'Yankee' buoy and near surface currents at SW30 showed that both winds and currents were oscillating at an inertial frequency of 17-19 hours in both the alongshore and cross-shore directions (not shown). At no other times in August were such strong near-inertial motions observed. The shoreward subtidal flow and strong inertial motion were concentrated near the pycnocline, where salinity intrusions were taking place. The combined subtidal and inertial motion could lead to enhanced onshore

transport of heat and salt through additional double diffusive mixing as the pycnocline intrusions are transported further shoreward than usual. Inertial current speeds of up to 20 cm/s were observed during this time. This is comparable to observation off Chile, which revealed strong near-inertial flows with speeds of 20 cm/s near the shelfbreak (*Sobarzo et al.*, 2007). Wavelet analysis of both winds and currents suggested that inertial motion is associated with a both inertial wind forcing (not shown) as well as the presence of an slope water eddy nearby as indicated by satellite SST taken during this time (Figure 3.13h). The inertial wind forcing and eddy presence appear to be coincidental.

Slope-water eddies and intrusion events

Offshore forcing from slope water eddies could drive salinity intrusions onto the shelf. As mentioned in the previous section, two slope water eddies passed through the SW06 study area. The first eddy transit was from Aug 4 to Aug 10 and the second one was from August 22 to August 28. The two eddies could be seen in a series of SST observations over the outershelf (Figure 3.13a,h). The radius of each eddy was approximately 50 km. Other finer structures such as tips and filaments on the length scale of 10 - 20 km were also seen (Figure 3.13a,e). This size scale translates to the separation of 2-3 glider transects and it was also similar to the scales of alongshelf hydrographic correlation as measured by the SW06 moorings. The boundaries marking the edge of the two eddies were highly distinct at the surface with a characteristic temperature difference of 2°C within 15 km or less (Figure 3.13c,d). The shape of the eddy is not circular or smooth, especially its southwest quadrant which formed a nearly 90 degree corner at the shelfbreak. In between the passage of two eddies, SST images showed cooler shelf

water occupying the surface layer in the SW06 study region (Figure 3.13c,d). The propagation speed of the second eddy was calculated by tracking the movement of the eye of the eddy (Figure 3.13d,f,h). The mean speed of the eddy core varied from $11 cm/s$ (between Aug 15 and 21) to 9 cm/s (between Aug 21 and 25), translating towards the southwest during both periods. Although similar in size to the shelfbreak eddies (*Garvine et al.*, 1988), hydrographic evidence suggests that both eddies were decaying WCR's despite their relatively small size ($\sim 50\ km$). The pycnocline intrusions likely induced by the eddies had temperatures of over 20°C and salinity of over 35.5 at the 100 m isobath. This is typical of WCR type water (*Gawarkiewicz, per. comm.*). Tropical Storm Ernesto at the beginning of September reset the shelfbreak and erased any surface manifestation of the slope water eddy during the time period immediately after the storm (Figure 3.13i).

The subsurface response of the shelf to the offshore forcing of the eddies as well as inshore forcing of shelf watermasses was captured by a series of glider sweeps along the SW06 cross-shelf mooring line (Figure 3.14, 3.15, and 3.16). The glider sections illustrate the evolution of the cross-shelf hydrographic structure of the water column during August. Spiciness was used as an indicator of surface and pycnocline salinity intrusions. The surface water was the warmest and freshest at the beginning of August (6-12) with a temperature of 26 °C or higher and salinity as low as 30 (Figure 3.14a,b and 3.15a,b). SST imagery during this time indicated that there was a slope water eddy near the study site that presumably brought intense pycnocline intrusions onto the shelf. This was observed in the glider salinity and spiciness sections (Figure 3.16a,b). The intrusion was nearly twenty meters thick, with a salinity of over 35.5 and a spiciness of over 5. It came in 12 km shoreward of the 100 m isobath, just shy of the 80 m isobath

mooring, thus its signature was not detected in the hydrographic measurements of the central mooring (SW30) shown in Figure 3.11b. A bottom intrusion was observed across nearly the whole outershelf during this time, extending to shoreward of the 70 m isobath. Cross-shelf and along-shelf (mooring) currents averaged over the 24 hour period prior to the closest glider passage are overlaid on top of the hydrographic sections shown in Figure 3.14 and 3.15. The cross-shelf component of the flow at the shelfbreak moorings (SW42 and SW43) showed shoreward flow with speeds up to 20 cm/s during the intrusion development (Figure 3.15a) and seaward flow during the intrusion retreat (Figure 3.15b). The along-shelf component of flow showed persistent downshelf flow (33 hour low-passed) with speeds of 10 to 20 cm/s at the mid-shelf (SW29 at 60 m isobath) and outer-shelf (SW30 at 80 m isobath) moorings (Figure 3.11d). These observations show that the advection of the pycnocline intrusion were in both the along-shelf and cross-shelf directions.

After the passage of the first eddy, the salty slope water retreated from the shelf and cooler shelf water moved into the SW06 region as seen in the SST (Figure 3.13c. During this time (Aug 12-16), the surface temperature was 24°C and salinity was 31 (Figure 3.14c,d) and 3.15c,d). Non-bottom intrusions nearly disappeared. The maximum spiciness in the water column was 3 or less (Figure 3.16c,d). Both along-shelf and cross-shelf flow on the shelf were relatively weak. Approaching the second period of activity (Aug 16-20) as mentioned in Section 3.3.5, slope water below the pycnocline moved inshore while the core of the cold pool moved offshore, forming a convergent zone near the 80 m isobath where the SSF reside (Figure 3.14e). Stratification across the whole outershelf region also increased. A vertical density difference of 4 kg/m^3 within less than 5 meters of depth was observed. Both the temperature and salinity sections

showed a complicated SSF configuration with significant of sub-pycnocline intrusions observed offshore of the SSF (Figure 3.14e, 3.15e). A detailed study of the SSF at the outershelf revealed two interfaces with upwelling and downwelling tendencies on opposing sides of the front (*Gong and Glenn*, submitted).

The second slope water eddy approaching the SW06 region towards the end of August brought extensive intrusions with complex salinity structure throughout the water column (Figure 3.13g,h). Compared to intrusions due to the first eddy, the second eddy resulted in much more intense sub-pycnocline intrusions that extended much further inshore, up to 27 km shoreward of the 100 m isobath (Figure 3.15g,h). Spicy water (> 3) was seen extending shoreward past the 70 m isobath (Figure 3.16g). The currents at the shelfbreak moorings (SW42 and SW43) were mainly cross-shelf directed inshore during the intrusion development, which can be seen in both the cross-shelf sections (Figure 3.14g) as well as the top-down view of the progressive vector diagram during this time (Figure 3.17(h)). Flow at the mid and outershelf moorings was mainly along-shelf towards the downshelf direction.

Interestingly, while the temperature section during the intrusion event showed top-down mixing of heat at certain locations (Figure 3.14g), the salinity section during the same time period suggest bottom-up delivery of salt at short cross-shelf distances away (Figure 3.15g). A modeling study by *Chapman and Lentz* (1994) showed that vertical circulation cells can develop on opposing sides of a shelf density front. If such secondary circulation patterns developed between the bottom and the pycnocline, it could be a mechanism for producing both upwelling and downwelling as suggested in the hydrographic observations. This possibility is explored in detail in *Gong and Glenn* (submitted).

The balance between the inshore influence of river discharge and the offshore forcing of the slope water eddies could affect the salt budget on the outershelf. Although pycnocline intrusions were clearly observed in both cases when the two eddies passed through the study region in the beginning and the end of August, surface intrusions were not detected during the first eddy and the surface shelf freshwater extended past the 100 m isobath. This may be attributed to the high summertime river discharge, which prevented surface intrusions from crossing onto the shelf. In the second case, the fresh riverine water likely had been advected to the southwest and the shoreward advancing eddy field led to significant salinity intrusions throughout the water column.

Location of the SSF

There was significant variability in the location of the SSF about its monthly mean position. Mooring data indicate that the cross-shelf location of the shelf-slope frontal jet varies on the time scale of 1 to 2 weeks. Its position is mainly affected by alongshelf wind forcing and the presence of slope water eddies. The cross-shelf location of the shelf-slope frontal jet is estimated through comparison of the depth-averaged currents across the cross-shelf mooring array (Figure 3.17). The three moorings were located at the 60 m isobath (SW29), the 80 m isobath (SW30), and the shelfbreak (SW42/SW43), respectively. The site with the fastest three-day averaged along-shelf flow compared to the other two sites would mean the SSF was near. Progressive vectors diagrams are helpful in visualizing the advection at the mooring sites as a result of the currents.

Early in August, a slope water eddy occupied the outershelf SW06 region, pushing the SSF shoreward of the 80 m isobath (Figure 3.17(a) and 3.17(b)). This is shown by the fast alongshelf flow at the 60 and 80 m moorings (SW29 and SW30) and by the

alongshelf flow reversal at the 160 and 460 m moorings (SW42 and SW43). In the cross-shelf direction, the near surface flows at the shelfbreak moorings were directed onshore. Approaching the middle of August, both the slope water eddy and the frontal jet moved offshore, as indicated by the more rapid flow speed observed at the outershelf 160 and 460 m moorings (Figure 3.17(d). Starting the second half of August, the frontal jet appears to move shoreward once more. A filament of the approaching eddy was likely already influencing the SSF during this time. Strong along-isobath downshelf flow is observed across the whole outershelf region (Figure 3.17(e)). Hydrographic analysis of temperature cross-shelf sections during this time period suggests that the SSF had two interfaces separated by approximately 15 km (*Gong and Glenn*, submitted). Later in August (21-27), the SSF continued to move shoreward likely pushed by a large slope water eddy moving onshore (Figure 3.13h, 3.17(g) 3.17(h)). The frontal jet stayed on the shelf until Tropical Storm Ernesto pushed it offshore in early September. The oscillating cross-shelf movement of the frontal jet, interacting with the salty slope water supplied by the slope water eddy, could help to create the complex multiple layered intrusion structures seen in late August at the outerhself (Figure 3.10(b)).

3.3.6 Outershelf Salt Budget

Three-dimensional coverage by multiple gliders allow an estimate of the salt budget for the SW06 sampling volume. The relative contribution of different types of salty slope water intrusions are calculated for a five-day period from August 24 to August 29 when the slope water intrusion onto the shelf is at a maximum. When Tropical Storm Ernesto approached, northeasterly wind advected a significant amount of the intrusions in the layers below the pycnocline offshore while driving the surface layer onshore with

cross-shelf velocity in excess of 15 cm/s. The mean surface and bottom layer salinities along the main cross-shelf mooring line before and after the passage of Tropical Storm Ernesto on September 2 are calculated using glider data. A rough estimate of the salt balance using offshore moorings current data is also calculated.

Before Tropical Storm Ernesto

The outer-shelf hydrography before the storm was characteristic of the late summer condition on the MAB. The sampling volume included the five northern glider lines covering the area between the 60 meter isobath and the 100 meter isobath. The bottom topography was approximately linearly sloping for all the sections, and all the glider sections were assumed to have the same cross-shelf geometry with the same bottom slope. This assumption introduced a 10% uncertainty in the sampling volume estimate. The horizontal area of the sampling volume extends 72 km in the along-shelf direction and 40 km in the cross-shelf direction with the center of the sampling box located at 39.2N, 73.04W. The cross-sectional area for each glider section was calculated to be $80m*40km = 3.2\ km^2$. The five glider cross-shelf transects were roughly equally spaced in the along-shelf. For the following salt budget calculation, each glider section was assumed to represent one-fifth of the total sampling volume. The relative contribution of each type of watermass in the SW06 sampling volume is calculated using the following formula: $R = \sum_i WaterMassArea_i/(5 * TotArea)$, where R is the relative fraction for each type of intrusion, $WaterMassArea_i$ is the cross-sectional area of the watermass of interest for each glider section (summed for all 5 sections), and $TotArea$ is the total cross-sectional area of each glider section.

Slope water ($S \geq 34$) contributed about 28 to 36 percent of the salinity in the

sampling volume. The relative fraction of each type of intrusion was calculated for two consecutive transects in late August. Surface intrusions accounted for 2-7% of the salinity of the sampling volume, pycnocline intrusions accounted for 13-17% of the salinity, sub-pycnocline intrusions accounted for a similar amount as pycnocline intrusions, and bottom intrusions accounted for 54-61% of the salinity. Pycnocline intrusions were the saltiest with a mean salinity of 34.86. Together, the four intrusion types accounted for approximately 90% of all the slope water on the outershelf by volume.

After Tropical Storm Ernesto

The arrival of Tropical Storm Ernesto at the beginning of September entrained much of the salt brought onto the shelf through mixing of the intrusions with shelf water. As a result, the halocline between the surface and bottom layers was essentially mixed away resulting in a significantly weakened pycnocline supported by only thermal stratification (Figure 3.14i).

The glider section along the main mooring transect right after the storm illustrates the effect of the storm on the surface salinity (Figure 3.15i). Compared to the time period right before the storm, the salinity of the surface layer between -42 km (57 m isobath) and -22 km (70 m isobath) increased from approximately 31.5 to 33.5, and the depth of the surface layer increased from approximately 15 m to 25 m. The cross-shelf current showed very strong shoreward flow in the surface layer. A simple 2-D salt budget calculation can show whether the cross-shelf transport of salt from offshore can

balance the salinity change observed at the mid-shelf:

$$S_f V_f - S_i V_i = S_{slope} T \Delta t \tag{3.2}$$

where S_i and S_f are the salinity of the mid-shelf surface layer before and after the storm, and V_i and V_f are the volume of the surface layer before and after the storm. S_{slope} is the salinity of the slope water being advected shoreward, T is the cross-shelf volume transport and Δt is the storm duration. Let $S_i = 31.5$, $S_f = 33.5$, $S_{slope} = 34.5$, and the cross-shelf width be 20 km. Let the depth of the surface layer be 15 m and 25 m for before and after the storm, respectively. For an unit along-shelf segment, the volume transport over a 24 hour period was 1.64 m^3/s. Assuming an averaged surface layer depth of 20 m, this translates to a cross-shelf velocity of 8.2 cm/s. Cross-shelf velocity measurements at the moorings showed that flow at the 60 m and shelfbreak moorings were over 10 cm/s, easily supporting the transport necessary to drive the observed change in surface salinity.

3.3.7 Outershelf Stratification

Stratification on the NJ Shelf during summer 2006 was primarily influenced by two factors: (1) freshwater discharged from the Hudson that was transported to the outershelf and (2) the intensity and frequency of pycnocline and surface intrusions, which is closely associated with slope water eddies. The first half of August was a more stratified time period with very fresh and warm surface layer across the outershelf. During this time, the arrival of a slope water eddy, which generated an intense but limited scale pycnocline intrusion, had the greatest effect on stratification near the shelfbreak.

With the departure of the slope water eddy and the persistence of surface freshwater in the study region in mid August, stratification reached a maximum around August 19 (Figure 3.19b). The pycnocline showed oscillations of 10-15 meters on semi-diurnal tidal frequency (Figure 3.19a). Coincidentally the internal tide also reached maximum strength as evidenced by the semidiurnal tidal oscillation of the pycnocline which can be seen in the wavelet decomposition of the SW30 mooring density calculated at 20 m (Figure 3.19a). This is also the time period of maximal non-linear internal wave energy coming onshore (*Shroyer*, 2010). When the second slope water eddy moved into the study region on Aug 24, it produced significant surface, pynocline and subpycnocline intrusions which weakened the strength of the pycnocline. Both internal tidal energy and NLIW energy decreased as well.

3.3.8 Shelf Secondary Circulation

Secondary circulation can take place in the vicinity of the SSF due to flow convergence in different portions of the water column. Previous studies have demonstrated flow convergence both at depth due to bottom boundary layer detachment (*Gawarkiewicz and Chapman*, 1992; *Pickart*, 2000) or near surface convergence due to SSF-eddy interaction (*Gawarkiewicz et al.*, 2001). In both cases the secondary circulation associated with the flow convergence can lead to upwelling and downwelling circulation cells in the vicinity of the SSF.

The method of accumulated temperature change (ATC) for detecting BBL detachment was applied to the SW06 glider hydrographic sections. The goal was to see whether the locations of BBL detachments were consistent with the location of the SSF. A modeling study of the shelf-slope front had shown upwelling flow on the shoreward

side of the front due to BBL convergence and downwelling on the seaward side of the front due to BBL divergence (*Chapman and Lentz*, 1994). Several glider salinity sections with density (white, 1026 kg/m^3) and ATC (black) contours overlaid are shown in Figure 3.18. The observed rise in the minimum ATC contour was nearly always shoreward of the SSF located between the 70 m and the 80 m isobaths, consistent with upwelling flow shoreward of the front. In some cases, the ATC contours suggest multiple regions of BBL detachment (Figure 3.18e,f). Using the high resolution glider temperature data, *Gong and Glenn* (submitted) explored the multiple SSF interface scenario using the ATC method as well as through visualization of the vertical temperature gradient. These visualization methods suggest that the BBL detachment might have been taking place at multiple locations on the outer NJ Shelf during the summer 2006. Furthermore, frontal upwelling and downwelling, in combination with diapycnal mixing as observed by *Barth et al.* (1998), could enhance the delivery of salt into the water column interior in the form of sub-pycnocline intrusions. The shoreward movement of the SSF and the associated secondary circulation may be the driver of the lifted salinity structure seen in the middle glider transects of Figure 3.10(a).

The shelf-slope frontal jet, through its interaction with slope water eddies, could generate strong horizontally sheared flow at the shelfbreak. Convergent flow surrounding the frontal jet can modify the fluid's relative vorticity sufficiently to affect the total absolute vorticity. The conservation of potential vorticity then requires either compression or expansion of the isopynals, leading to ageostrophic secondary circulation (*Pollard and Regier*, 1992). Observation of bathymetrically steered convergent flow on the New England Shelf showed that flow convergence both near the surface and bottom on the order of 10^{-5} s^{-1} leading to near bottom upwelling of 2 m/day and mid-water

column upwelling of nearly 10 m/day (*Fratantoni et al.*, 2001).

Unfortunately, the three SW06 cross-shelf moorings did not resolve the cross-sectional flow structure of the jet. Based on past climatological studies and our interpretation of the velocity data from the moorings, we could still reasonably assume that the jet likely resided somewhere between the 60 m isobath and the shelfbreak mooring at the 460 m isobath. Based on this assumption, the divergence and relative vorticity of the flow were calculated for the layer of fluid near the pycnocline (Figure 3.19c) and near the bottom (Figure 3.19d) centered on the central mooring (SW30). Most interestingly, the most convergent flows observed near the pycnocline, as indicated by the solid line, were at times of the two eddy transits (8/6 and 8/26), with a value of $0.6 \times 10^{-5}\ s^{-1}$ for both times. This was comparable the value of $0.9 \times 10^{-5}\ s^{-1}$ reported by *Fratantoni et al.* (2001) when downwelling near the shelfbreak jet was observed during the winter. The observations here support the idea that convergent flow during times of eddy passage can induce ageostrophic secondary circulation in stratified water column near the pyncocline. Furthermore, there was a gradual increase in the relative vorticity in the lower water column in late August, peaking at the time of Tropical Storm Ernesto's passage in early September with a maximum value of $2 \times 10^{-5}\ s^{-1}$. This is consistent with the introduction of positive vorticity into the water column due to a cyclonic system.

3.4 Discussion and Summary

Scientists have long studied how the different watermasses come together at the MAB shelf-slope boundary forming the shelf-slope front (SSF) during the different times of the year (*Bigelow*, 1933; *Wright and Parker*, 1976; *Linder and Gawarkiewicz*, 1998).

One of the longterm research objectives had been to explain the structure and variability of the SSF in relation to the different forcing mechanisms acting in the shelfbreak region. Better understanding of the causes of the SSF variability enables more accurate characterization of the cross-shelf-slope transport and mixing of materials such as nutrients, pollutants, and dissolved/particulate organic matter. This study's aim was to quantify the oceanographic response to key forcing mechanisms such as wind, river discharge, slope water eddies, and passing storms during the stratified summer season. This study did not address how upstream and boundary forcing factors would affect the watermass interaction at the outershelf of the MAB. These include variability in the shelf flow supplying the cold pool, meandering of the shelfbreak jet/frontal waves, tidal forcings, and mixing effect of nonlinear internal waves. An extensive field program lasting from mid summer into early autumn in 2006, through the application of a new generation of oceanographic tools such as gliders in combination with traditional tools such as moorings and satellites, enabled a detailed characterization of the 3-D oceanographic state and how it varied in time. The key results are as follow:

(1) The structure and location of the shelf-slope front (SSF) varied on tidal to intra-seasonal time scales due to the combined forcing of seasonal heating, wind stress, river discharge, slope water eddies, and storms.

(2) Different forcing mechanisms affected the different parts of the water column. Along-shelf wind stress affected the location of the foot of the front, river discharge and slope eddies affect the cross-shelf extent of surface and pycnocline intrusions, and secondary circulation near the SSF can affect the delivery of heat and salt into the water column interior.

(3) The observed slope water intrusions were 3-D hydrographic structures that

varied in time. Along-shelf features were coherent on the 10-30 km scale, and cross-shelf features were coherent on the 5-20 km scale. Both along-shelf and cross-shelf advection were important in driving intrusion into and out of the SW06 study region. Subtidal temporal variability was predominantly forced by wind and offshore forcing.

(4) Outershelf stratification was correlated with the intensity of nonlinear internal wave activity. Strong shelf stratification coincided with a period of strong internal tides, which likely induced an increase in nonlinear internal wave activity on the NJ shelf during August 17-19, 2006.

Despite the varied forcing on the outershelf, salty intrusions of slope water are observed throughout the summer of 2006. Each type of intrusion, however, is sensitive to different types of forcing such as winds, offshore eddies, and movement of the cold pool. The offshore portion of the cold pool exhibited rich a 4-D structure. While the cold pool's Temperature-Salinity and its centroid location was close to the climatological mean, it was far from a stationary body of water and it appeared to interact with the bottom and mid-water column salinity intrusions on the time scale of 1-3 days and spatial scale of less than 20 km during the course of the study.

The overall cross-shelf extent of an intrusion event could extend over 25 km with multiple intrusion structures appearing at the same time. The cross-shelf extent of an individual intrusion structure was on the order of 10-15 km. The largest intrusion event in late summer (August 23-28) was observed in multiple glider lines stretching 70 km in the alongshelf direction. Although the along-shelf extent of the intrusion can be large, coherent spatial structures were only observed over the 10-20 km length scale. A variety of offshore forcing mechanisms such as frontal waves, WCR's, and shelfbreak eddies can lead to enhanced salinity intrusion events. The location of the

shelfbreak jet appears to vary on the time scale of one to two weeks. While this was approximately coincidental with the duration separating the arrival of the two slope water eddies, it was also the natural growth rate time scale for unstable frontal waves at the shelfbreak (*Gawarkiewicz*, 1991). Both processes in theory can contribute to some of the observed hydrographic and current variabilities. In fact, detailed synoptic hydrographic sampling of the outershelf and shelfbreak region during the second eddy period (Aug 23-28) have shown that a large frontal wave was interacting with the slope water eddy (*Gawarkiewicz, per. comm.*).

The intrusion water on the central MAB shelf was classified into four types: surface, pycnocline, sub-pycnocline, and bottom intrusions. This classification was useful because the variability in each of the types could be studied in association with different sets of forcing mechanisms. Taken together, the physical distribution of the different types of intrusions could affect the outershelf salt budget and cause subtidal variability in the seasonal stratification. For an outershelf volume bounded by the 55 and 100 m isobaths, slope water accounted for approximately 30 percent of the outershelf watermass by volume. Bottom intrusions were the most common and their cross-shelf extent were correlated with the along-shelf wind stress. Strong upwelling favorable winds tended to push the fresh surface shelfwater further offshore and pull the salty slope water onshore. The bottom intrusions also contributed to the majority of the outershelf salt budget. Pycnocline and surface intrusions appeared to be associated with nearby slope water eddies, as the appearance of two eddies in the August 2006 were matched with two significant pycnocline intrusion events. The surface and pycnocline intrusions observed here were warm and very salty ($S > 35$), carrying the characteristic of Gulf Stream water. They tended to directly weaken the strength of the pycnocline

at the offshore end of the shelf's seasonal pycnocline.

Compared to pycnocline intrusions, sub-pycnocline intrusions were further inshore and generally less spicy. Sub-pycnocline intrusions were potentially related to secondary circulation processes at the shelfbreak, such as BBL detachment at the foot of SSF. Studies using dye releases (*Houghton and Visbeck*, 1998) and suspended sediments (*Barth et al.*, 1998) provided observational evidence for BBL detachment. *Linder et al.* (2004) applied *Pickart* (2000)'s method and studied the seasonal behavior of BBL detachment on the MAB and found that seasonal stratification strongly limited the vertical extent of the detached BBL. Tests for BBL detachment were performed on SW06 glider data using the ATC method. In most cases, BBL detachment was seen occurring shoreward of the SSF as predicted by the idealized modeling study of *Chapman and Lentz* (1994). The location of the SSF oscillated in the cross-shelf direction with a characteristic time scale of several days. The movement of the front also appeared to be correlated with the slope water eddies which tended to push the SSF shoreward.

It should be noted that the detachment of the BBL is normally explained as an along-isopycnal mixing process but the signature of the observed sub-pycnocline intrusion suggests diapycnal mixing as well. Previous summer time observations by *Barth et al.* (2004) on the MAB showed that a similar salinity structure connecting below-pycnocline intrusions and bottom intrusions (see their Figure 3b). They observed significant diapycnal velocity during brief episodic periods of less than 2 hours and derived diapycnal thermal diffusivity of $1.2 \times 10^{-2}\ m^2/s$ suggesting that diapycnal mixing maybe playing a key role in forming the observed cross-isopycnal hydrographic structure of the observed intrusions in SW06.

Outershelf stratification was influenced by a combination of factors with upstream

forcing acting from both the innershelf as well as offshore. Fresh river discharge from the innershelf as well as intense summer heating helped to setup strong stratification whereas slope water eddies weakened the stratification by driving pycnocline intrusions onshore. The peak period of stratification during summer 2006 occurred Aug 18-19 when a fresh surface layer and salty intrusions below the pycnocline sets up a density change of 4 kg/m^3 observed in less than 2 m in the vertical. During the non-linear internal wave component of the SW06 experiment, maximal nonlinear internal wave activity (August 18-20) (*Shroyer*, 2010) coincided with this period of maximal stratification. Interestingly, the nonlinear internal wave activity was highest when offshore forcing (due to eddies and storm) was the weakest.

Pycnocline intrusions associated with eddies and rings were the most likely candidate for transporting offshore constituents onto the continental shelf. Furthermore, major energetic mixing events such as hurricanes and nor'easter could help to entrain the salt and other constituents from the slope onto the shelf. The amount of salt advected laterally shoreward by a passing storm was enough to account of the salinity increase in the upper water column.

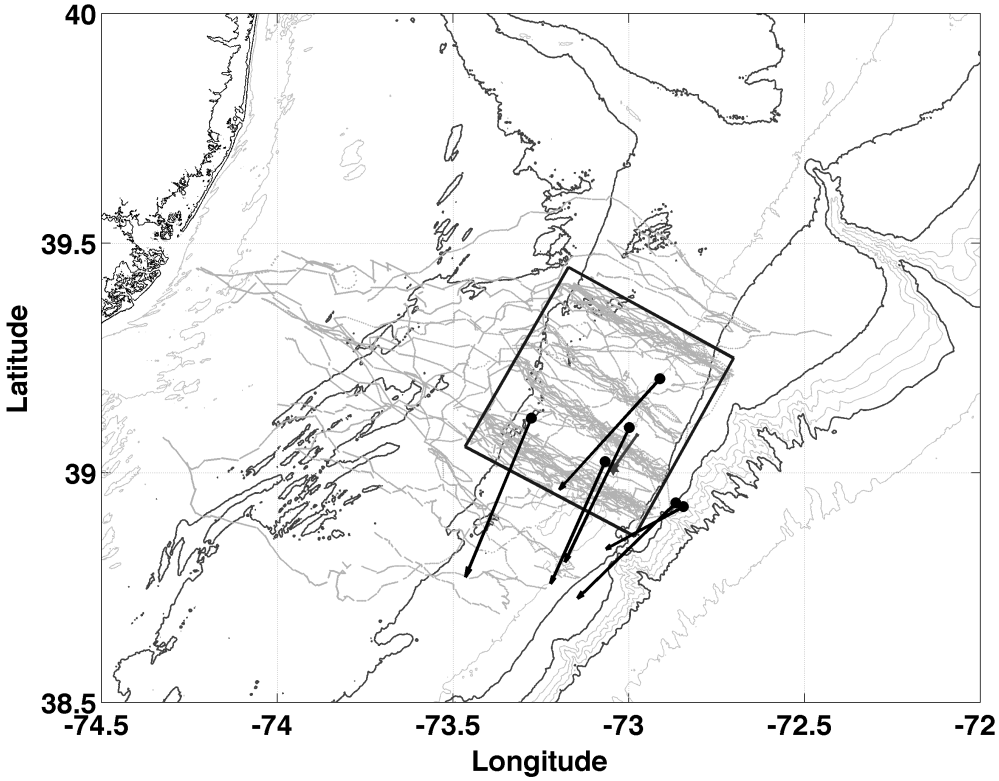

Figure 3.1: Map of the SW06 study region on the New Jersey Shelf. The light grey lines are the glider tracks for all the SW06 deployments from July 19 to October 2, 2006. The black box is the core sampling area for the gliders. It consists of four repeated glider transects occupied by multiple gliders during this time period. The black dots are the physical oceanographic moorings instrumented with CT and/or ADCP. From left to right: SW29 (60 m isobath), SW30 (80 m isobath), SW32 (80 m), SW33 (80 m), SW42 (170 m), SW43 (460 m). The black arrows originating from each mooring site are the time mean depth-averaged currents from August 1 to September 1, 2006. The star near SW30 represents the ASIS wind buoy and the vector originating from it is the mean wind vector during the same time period.

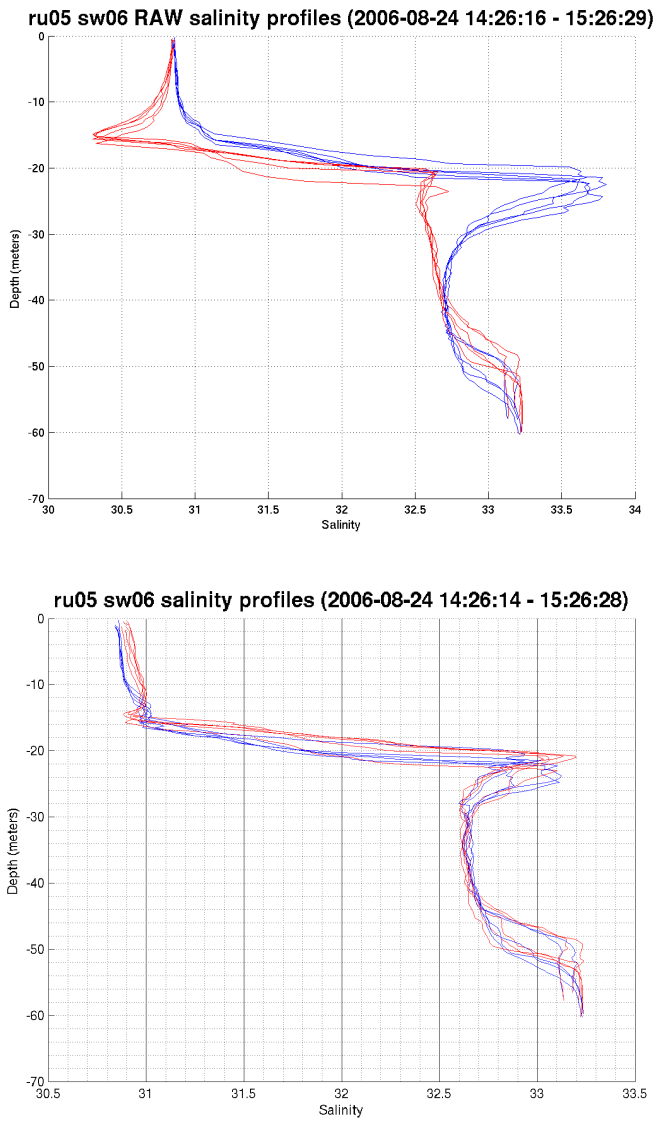

Figure 3.2: Comparison of glider CTD salinity for an example set of up and down casts before and after thermal-lag correction. (a) Uncorrected upcasts (red) and downcast (blue) for a segment of a RU05 August deployment. (b) Corrected upcasts (red) and downcast (blue) for the same segment.

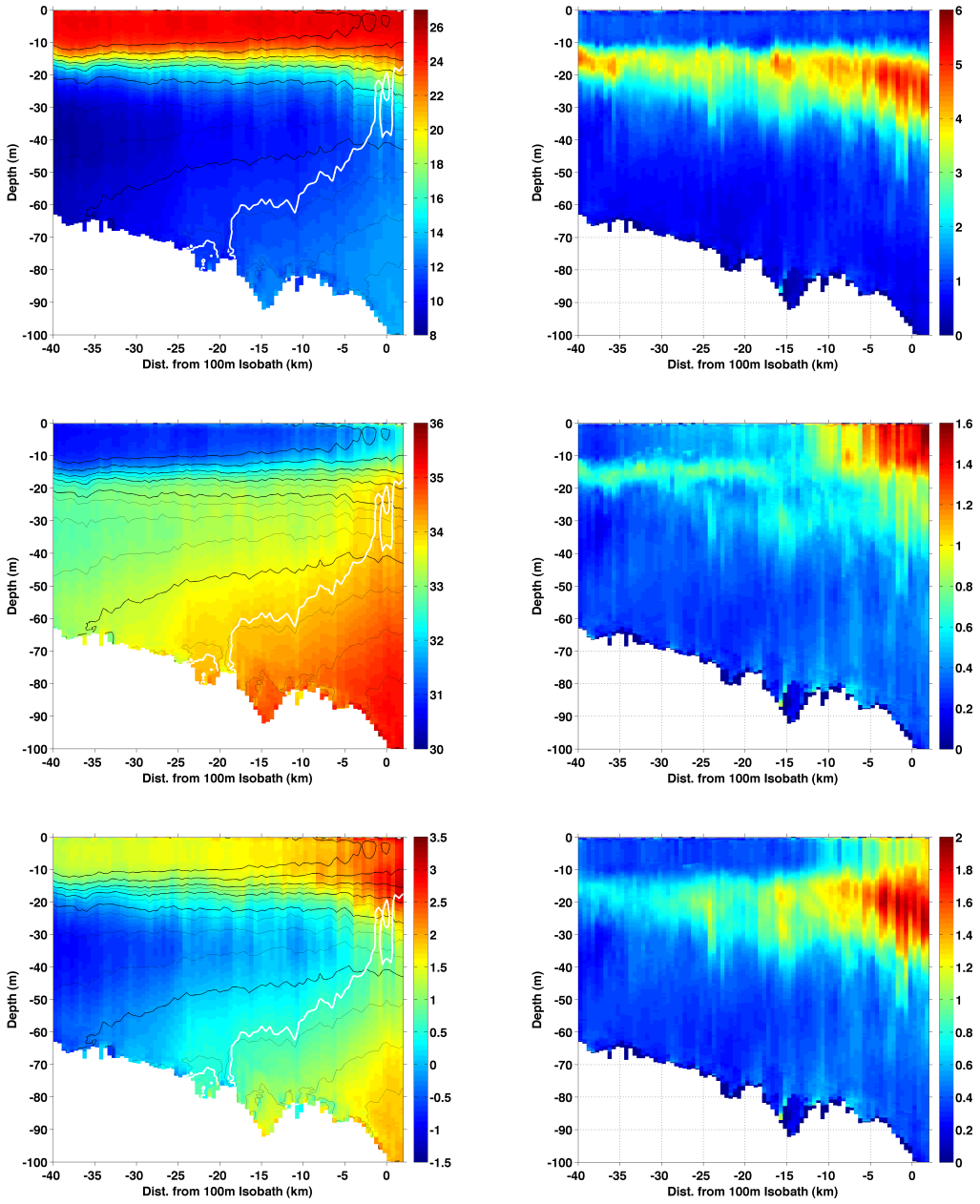

Figure 3.3: Summer mean hydrography and variability for July to August 2006. The black contour lines are density contours and the white contour line is salinity of 34. (a) Temperature. (b) Temperature standard deviation. (c) Salinity. (d) Salinity standard deviation. (e) Spiciness. (f) Spiciness standard deviation.

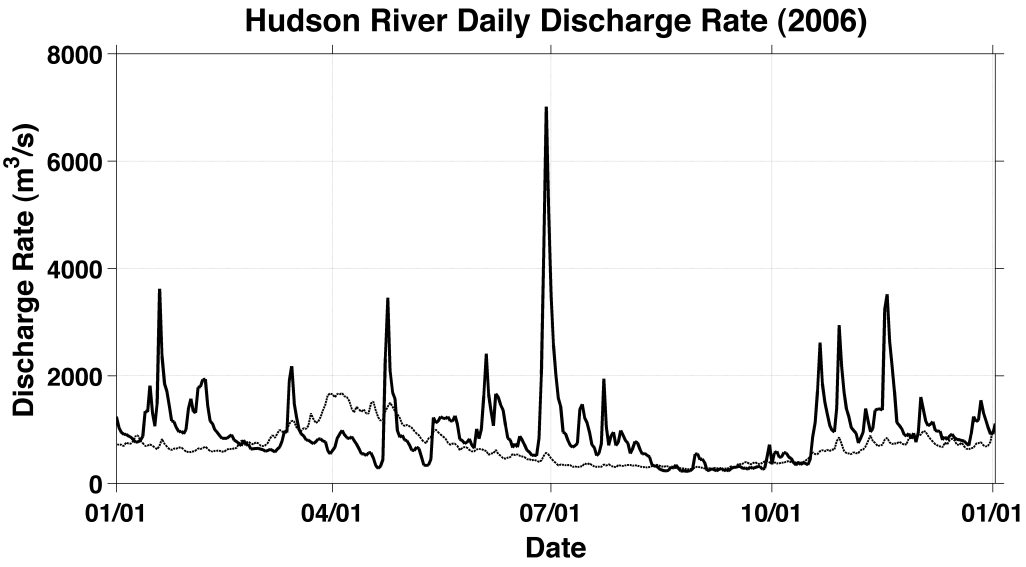

Figure 3.4: Hudson River daily discharge rate (twice the sum of Fort Edwards and Cohoes). The black line is the daily discharge rate for 2006 and the dotted line is the daily climatological discharge rate averaged from 1918 to 2009. For most years, peak discharge occurs in spring from March to May. 2006 was an exception with maximum discharge occuring during summer. The peak 2006 discharge rate was 5th highest in 90 years.

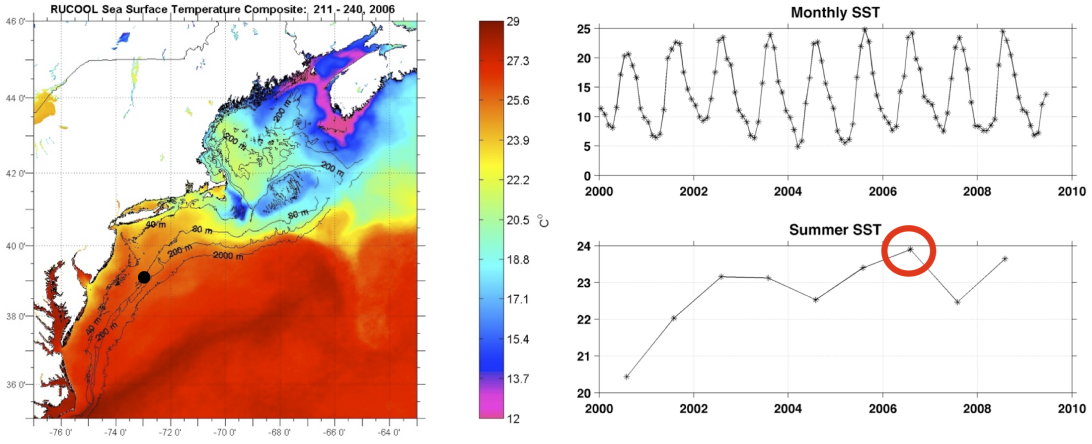

Figure 3.5: (a) Mean Sea Surface Temperature map of the Mid-Atlantic Bight and northern regions for July 30 to August 28, 2006. The black dot indicates the SW06 study region. (b) Monthly SST at the SW06 site from 2000 to 2009. (c) Mean summer SST for 2002 to 2008 at the SW06 site.

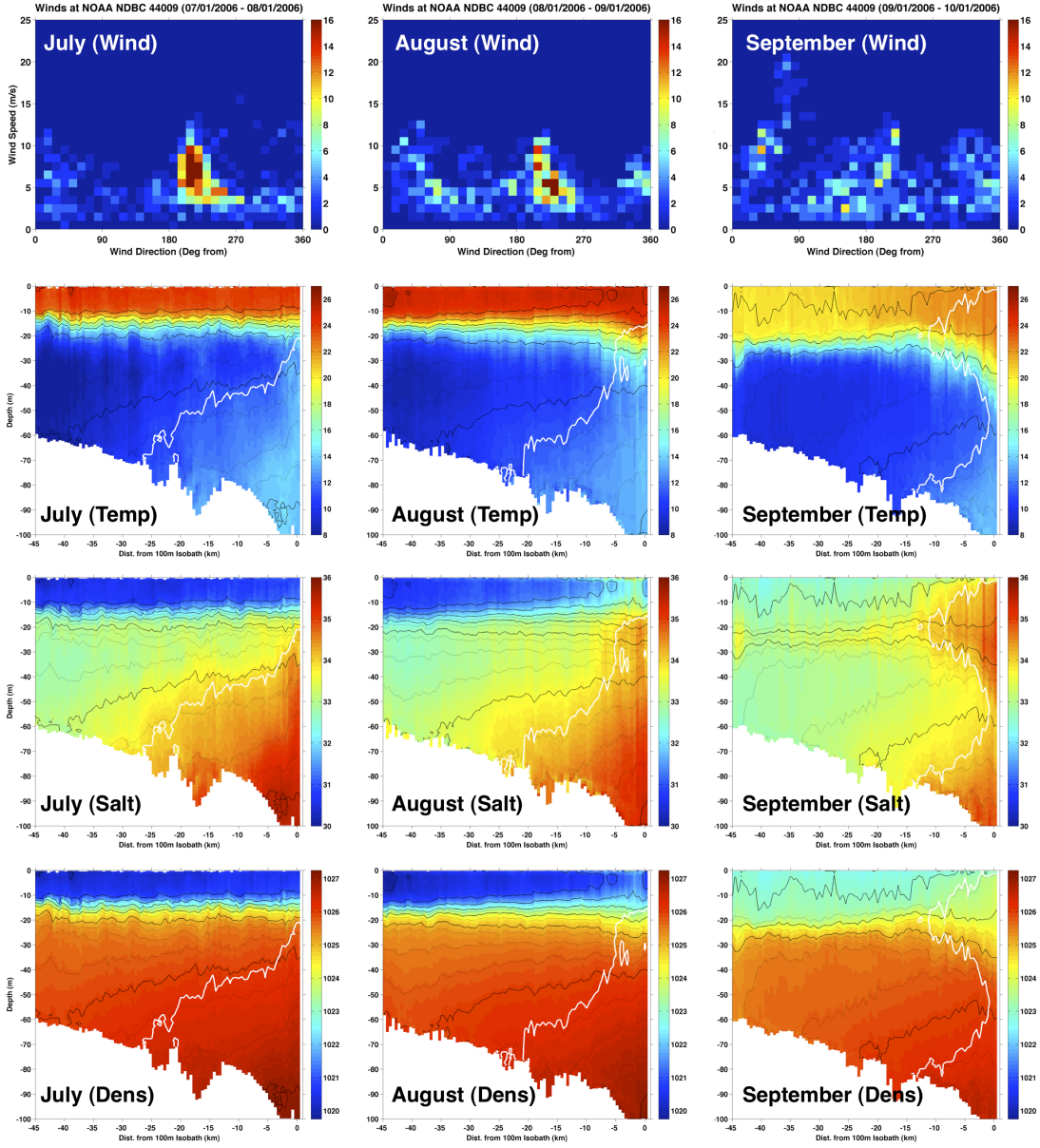

Figure 3.6: (a) - (c) Histogram of winds for July, August and September 2006 measured at NOAA NDBC Buoy 44009. x-axis is the direction of the wind from which it is coming, y-axis is the speed of the wind. Winds during July is predominantly from the southwest with progressively more frequent and stronger northeast winds in August and September. September winds is more scattered compared to July and August. (d) - (f) Mean temperature cross-shelf sections for July, August and September. (g) - (i) Mean salinity cross-shelf sections for July, August and September. (j) - (l) Mean density cross-shelf sections for July, August and September. The white lines are salinity 34 contour, the black lines are density contour lines.

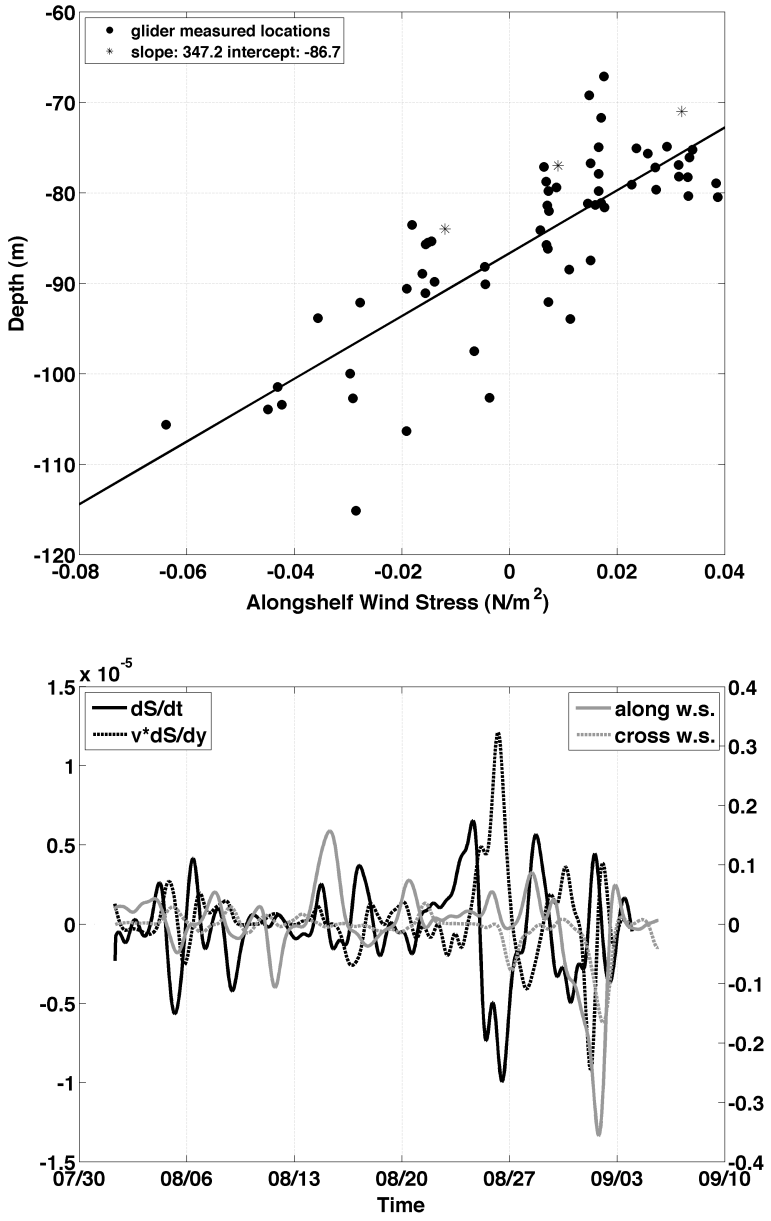

Figure 3.7: (a) The location of the foot of the shelf-slope front versus along-shelf wind stress. The dots represent measurement from individual glider transect and the stars are the monthly mean position of the foot of the SSF. The linear regression is calculated using the individual glider transects. (b) $\partial S/\partial t$ and $v * \partial S/\partial y$ are plotted as a function of time (black). The along-shelf and cross-shelf wind stress are also overlaid (grey).

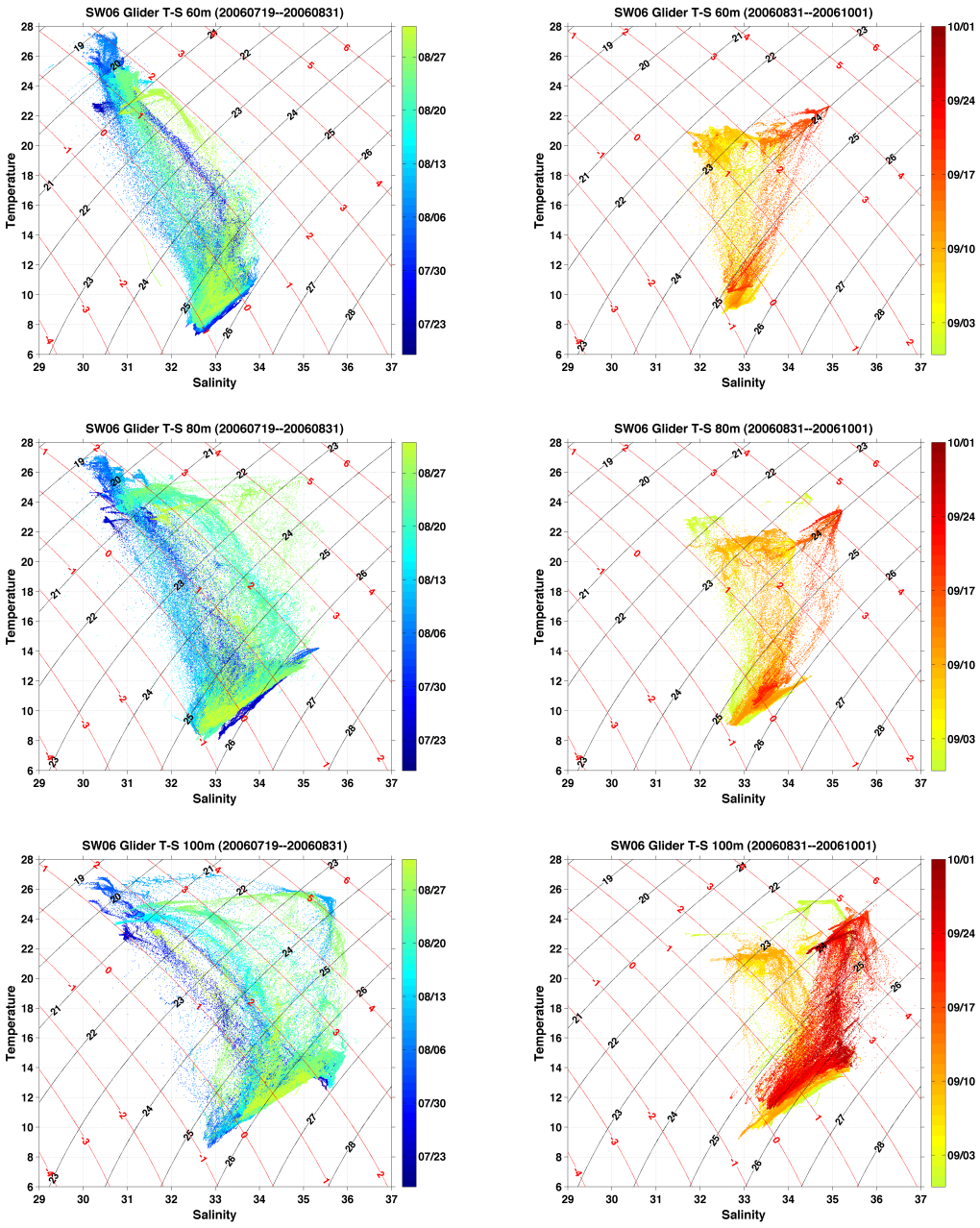

Figure 3.8: Intraseasonal evolution of the Temperature-Salinity structure at (a) - (b) 60 m isobath, (c) - (d) 80 m isobath, and (e) - (f) 100 m isobath.

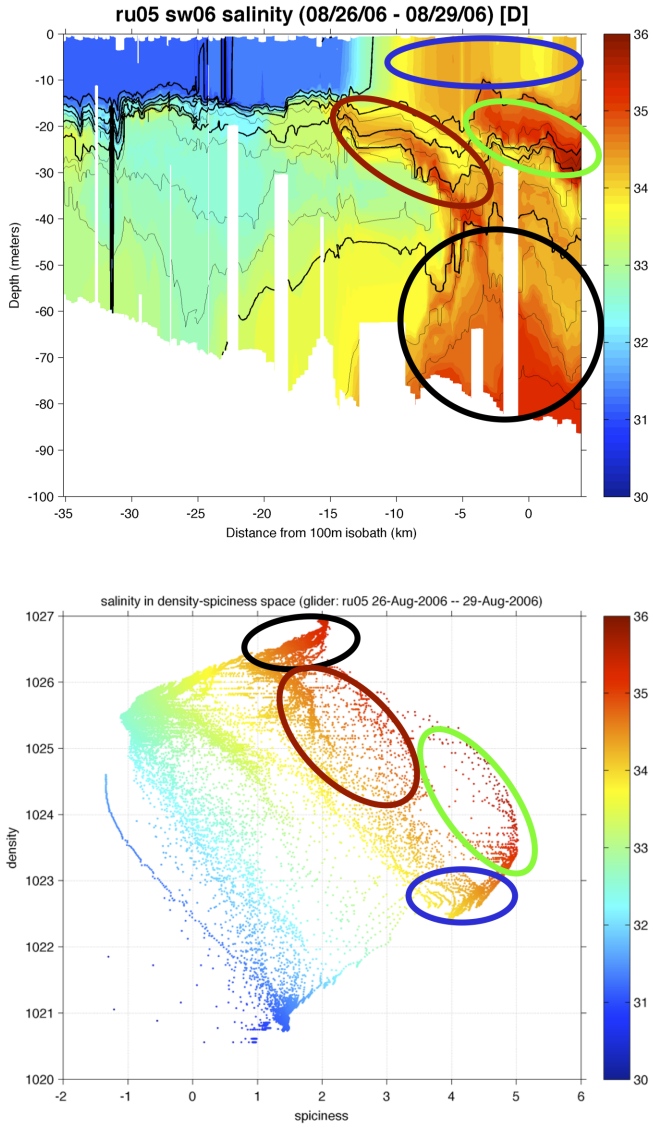

Figure 3.9: Four types of intrusions observed during SW06 at the outer NJ Shelf. (a) A salinity cross shelf section from glider RU05 near the main mooring line (August 26 - 29, 2006). The four intrusion types are surface (blue), pycnocline (green), sub-pycnocline (red) and bottom (black). The density contour (thick black lines) counting from bottom to top are: 1026, 1025, 1024, 1023 and 1022 (outcropping at the surface). (b) Data from the same transect but viewed in Density-Spiciness space. The four intrusion types are color coded in the same fashion.

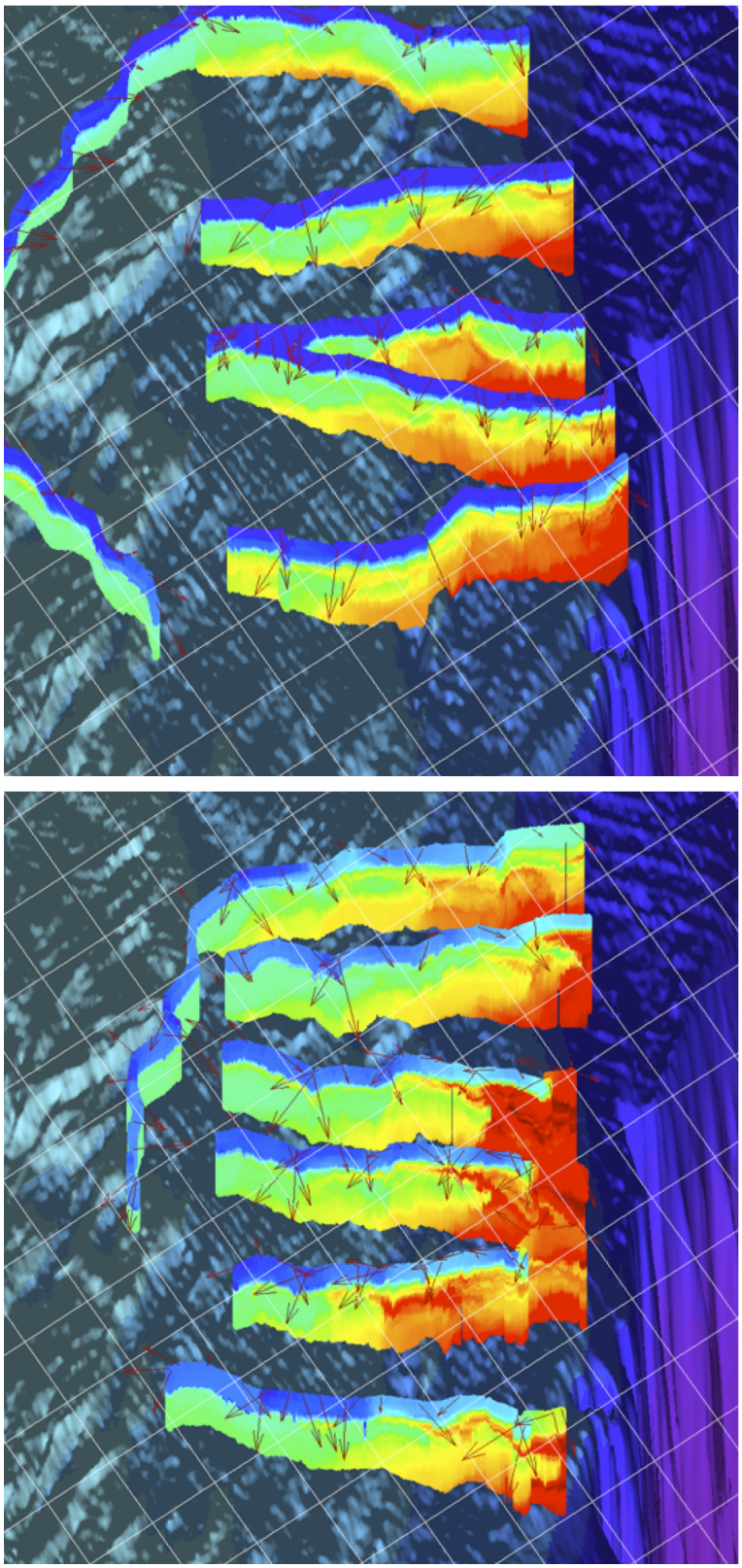

Figure 3.10: 3-D view of the SW06 glider experiment. The red arrows are the depth-averaged currents measured by gliders during each surfacing segment. Color indicates salinity ranging from 30 to 36. (a) Early August. (b) Late Aug.

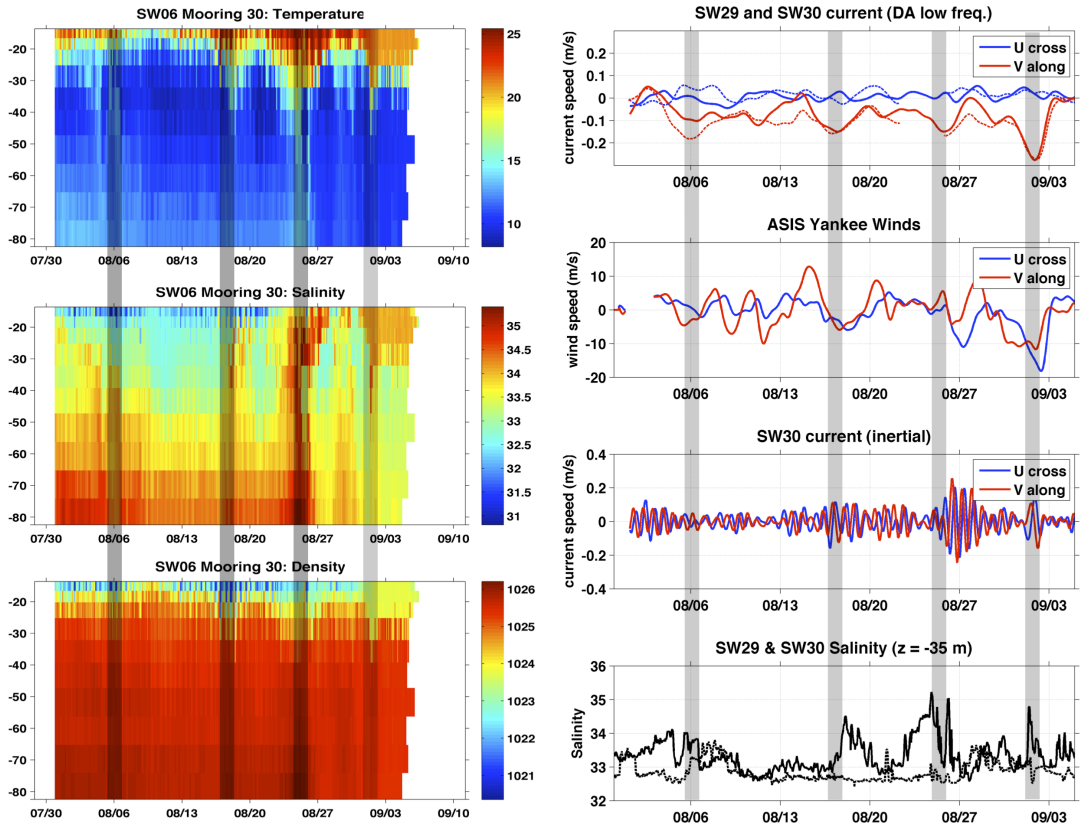

Figure 3.11: Hydrography and currents for moorings SW30 located near the 80 m isobath and SW29 located near the 60 m isobath. (a) Temperature (SW30), (b) Salinity (SW30), (c) Density (SW30), (d) Low-passed depth-averaged currents for SW30 (solid) and SW29 (dashed). Red is along-shelf flow, blue is cross-shelf flow. (e) Low-passed winds at buoy 'Yankee' (collocated with SW30), blue is cross-shelf, red is along-shelf. (f) Inertial current at SW30 at 15 m, (g) Salinity for SW30 (solid) and SW29 (dashed) at 35 m depth.

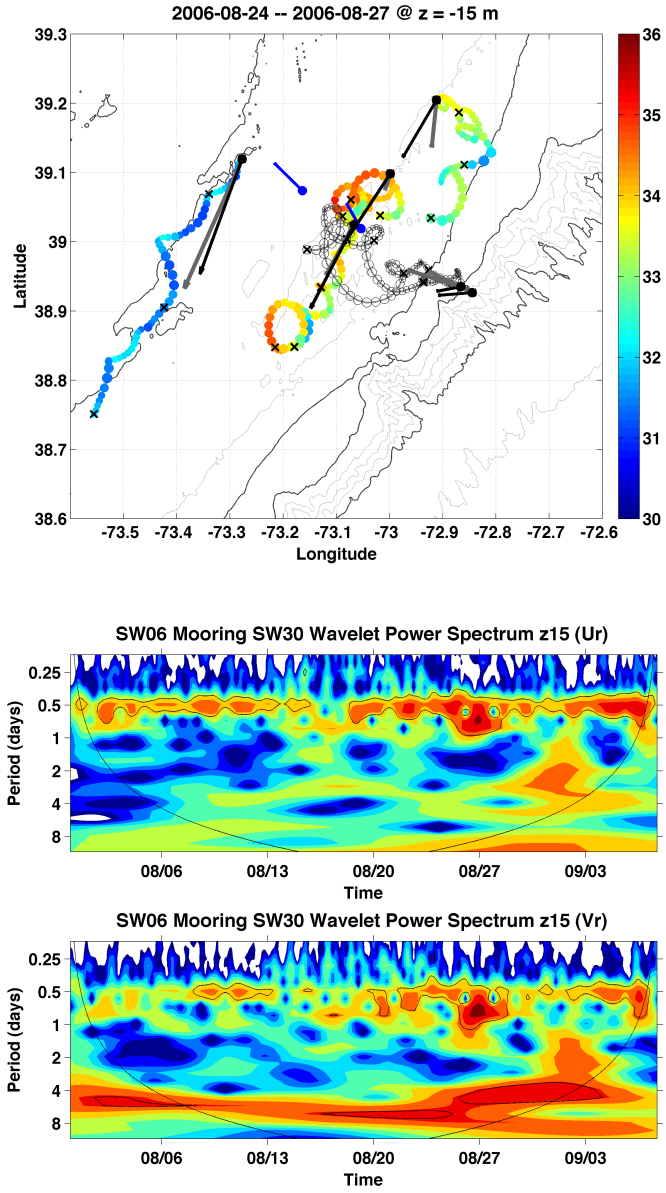

Figure 3.12: (a) Progressive vector diagram for velocity and salinity at 15 m for SW06 moorings. 3-day averaged depth-averaged velocity is plotted as black arrows and 3-day averaged velocity at 15 m is plotted as grey arrows. 3-day averaged wind velocity is plotted as blue arrows. Black crosses mark every 24 hours within the 3-day period. (b) Wavelet decomposition of the cross-shelf and the along-shelf current at 15 m depth for SW30 during August 2006. The 95% confidence interval for statistically significant wavelet power is contoured in black.

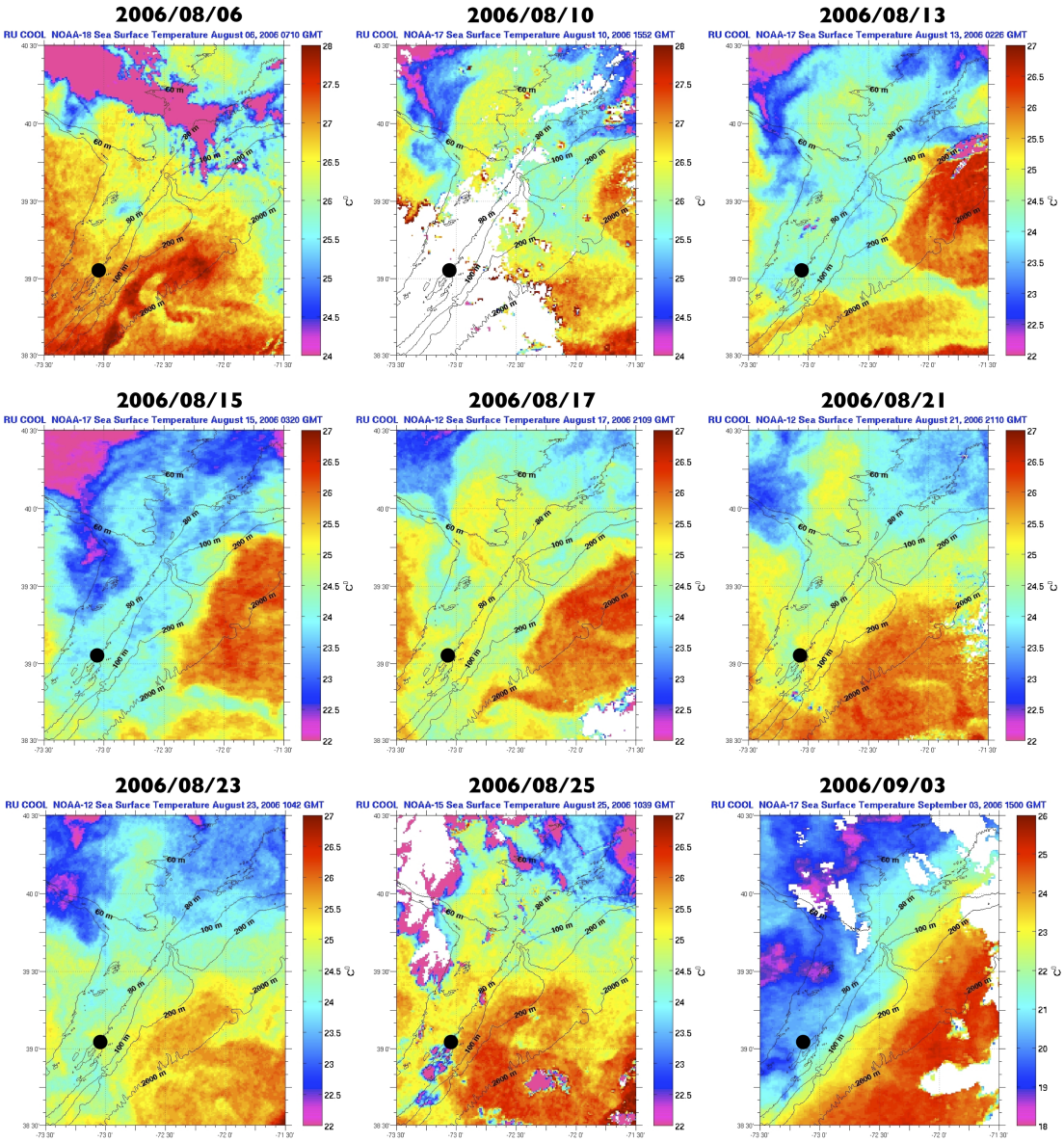

Figure 3.13: SST for August near the SW06 study region. Two eddies traveled through the sampling area. Black dot indicates the center of the mooring array.

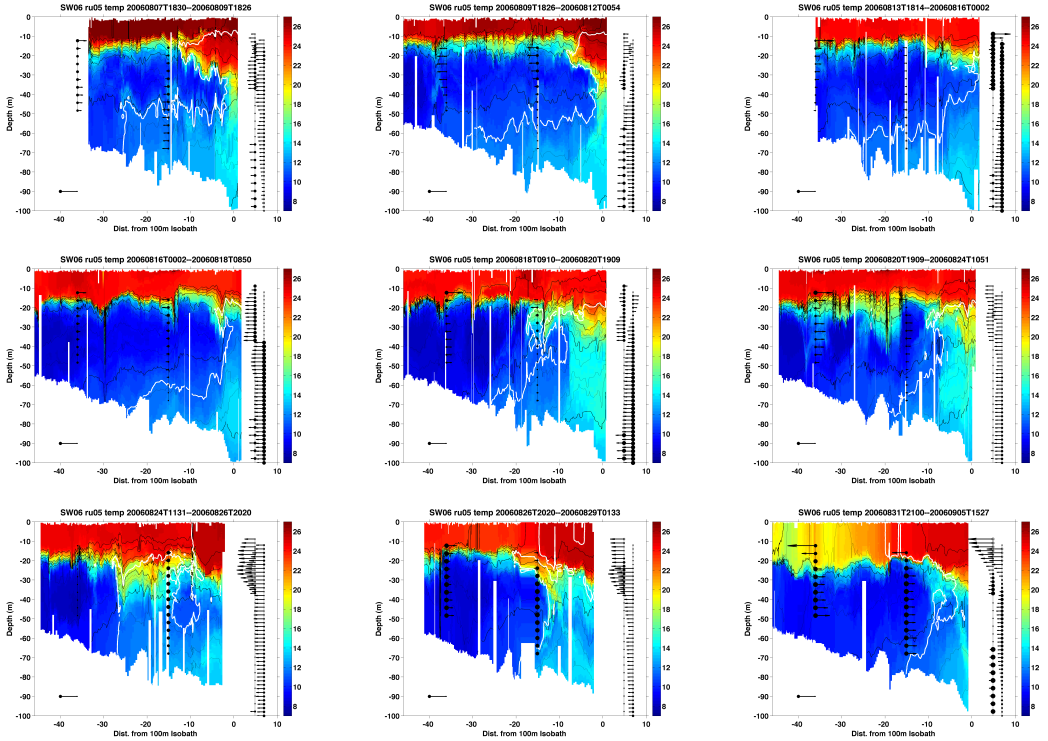

Figure 3.14: Combined (glider) temperature and (mooring) currents plot for the SW06 study region. Current data from moorings in the main cross-shelf line (SW29, SW30, SW42 and SW43) are plotted in the cross-shelf direction (arrows) and along-shelf direction (circle-cross and circle dots). The currents for the 24 hours prior to the closest crossing between the glider and each mooring are averaged and plotted. (a) Aug 7-9, (b) Aug 9-12, (c) Aug 13-16, (d) Aug 16-18, (e) Aug 18-20, (f) Aug 20-24, (g) Aug 24-26, (h) Aug 26-29, and (i) Aug 31 - Sep 03

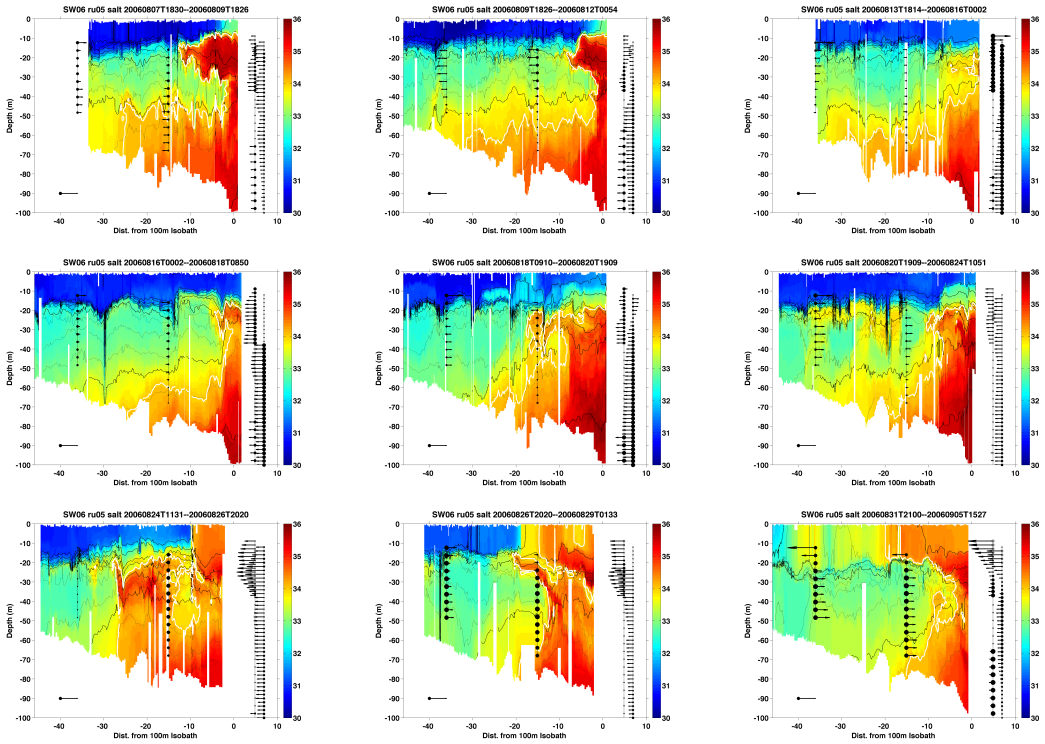

Figure 3.15: Same as sections as the temperature in Figure 3.14, but for salinity.

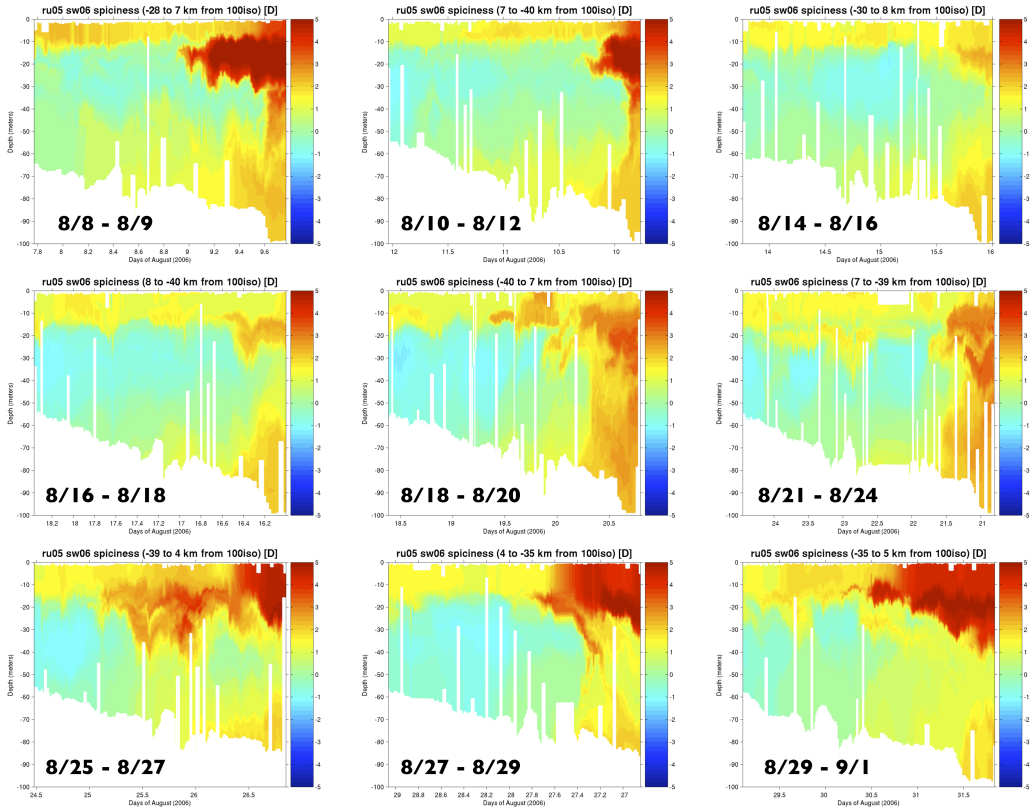

Figure 3.16: Cross-shelf sections of spiciness calculated from glider RU05 just south of the SW06 cross-shelf mooring array. Spiciness is a good indicator of pycnocline intrusions which tend to weaken the strength of the pycnocline.

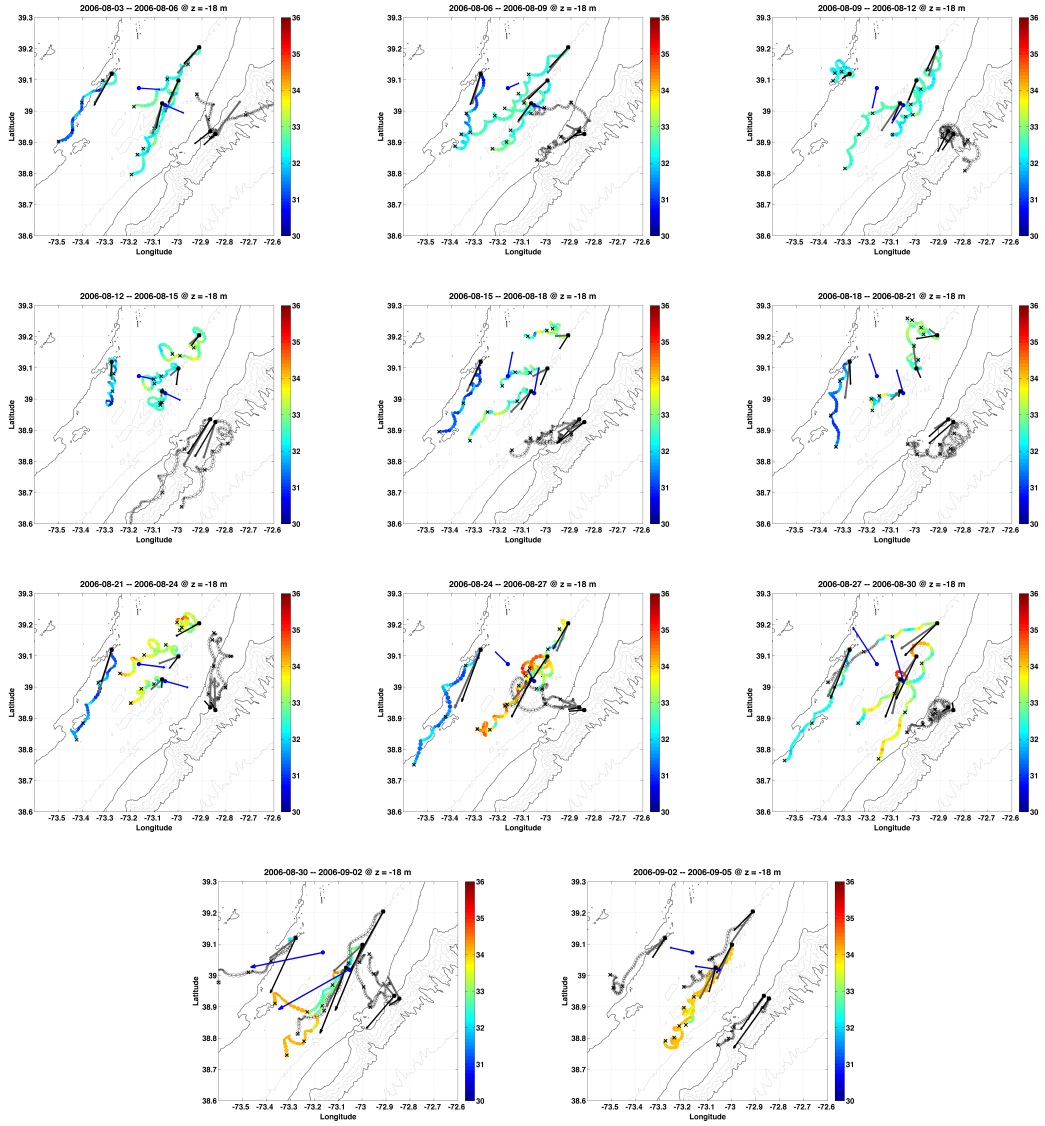

Figure 3.17: Progressive vector diagram for velocity and salinity at 18 m for SW06 moorings. 3-day averaged depth-averaged velocity is plotted as black arrows and 3-day averaged velocity at 18 m is plotted as grey arrows. 3-day averaged wind velocity is plotted as blue arrows. Black crosses mark every 24 hours within the 3-day period. (a) Aug 3 - 6, (b) Aug 6 - 9, (c) Aug 9 - 12, (d) Aug 12 - 15, (e) Aug 15 - 18, (f) Aug 18 - 21, (g) Aug 21 - 24, (h) Aug 24 - 27, (i) Aug 27 - 30, (j) Aug 30 - Sep 2, and (k) Sep 2 - 5.

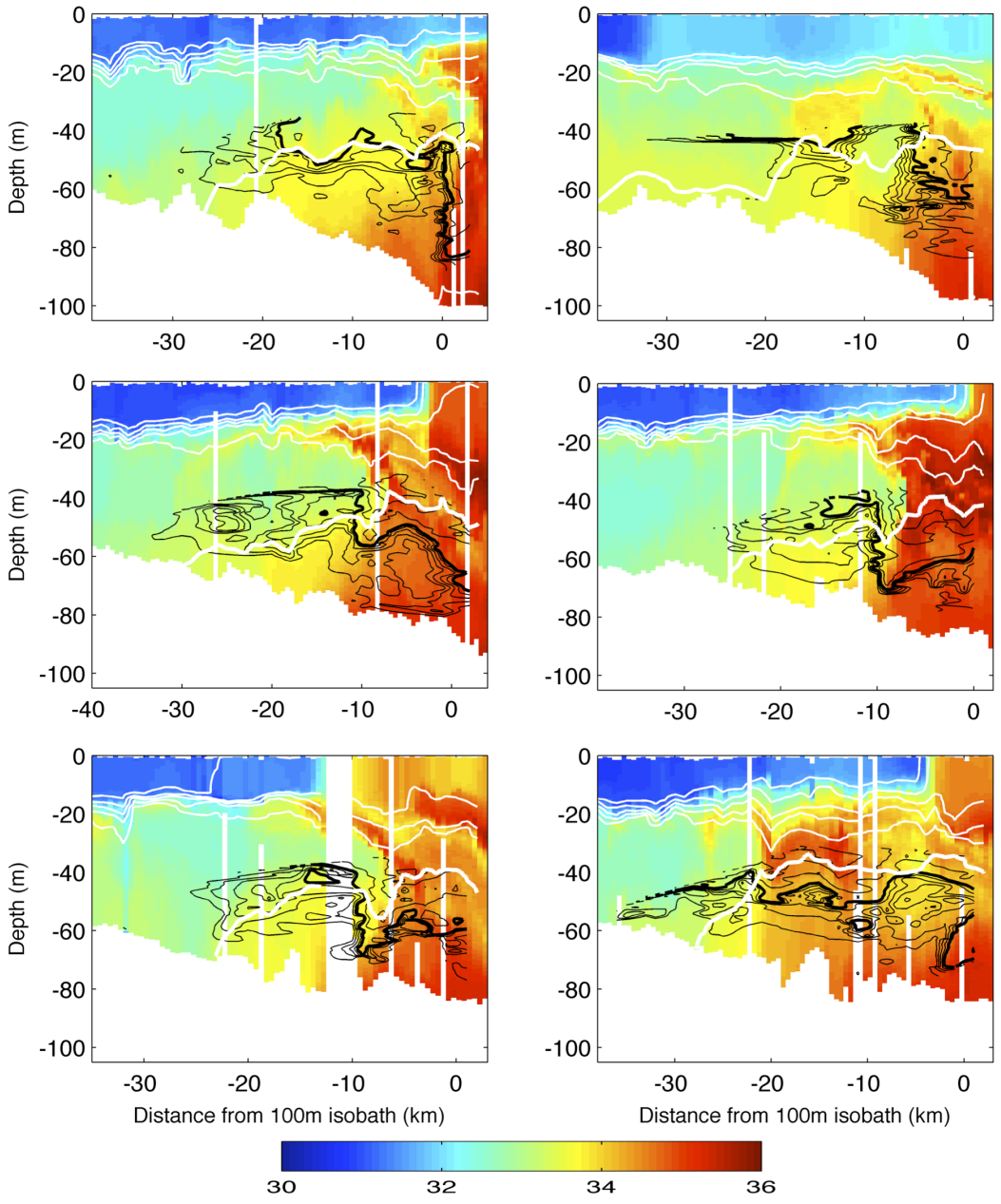

Figure 3.18: Testing for Bottom Boundary Layer Detachment on SW06 glider transects in late August 2006 using Accumulated Temperature Change test (*Pickart*, 2000).

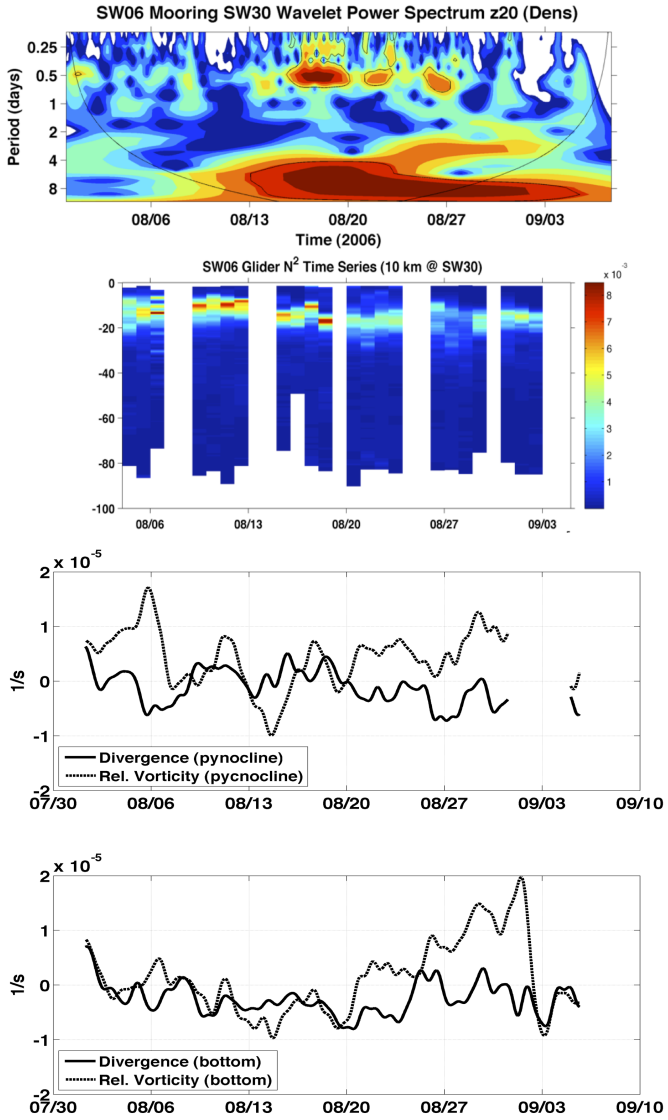

Figure 3.19: (a) Wavelet power spectrum of density at 20 m depth measured at SW30. Strong baroclinic tidal oscillation during Aug 17-19 correspond to a maximum in Non-Linear Internal Wave activity as well (*Shroyer*, 2010). (b) Stratification variability near SW30 constructed for nearest sets of glider data. An averaging circle of 10 km radius is used for the calculating stratification from gliders. Stratification near the 80 m isobath is a maximum at the same time of strong baroclinic tides and NLIW activity. (c) Divergence and the relative vorticity of flow near the pycnocline at SW30. (d) Divergence and the relative vorticity of flow in the bottom layer at SW30.

Chapter 4

Observations of bottom boundary layer detachment and secondary circulation at the MAB shelf-slope front

4.1 Introduction

The shelf-slope front (SSF) marks the boundary between the fresh shelf water and the saltier slope water. On the shallow and wide Mid-Atlantic Bight (MAB), the SSF is marked by the 34 isohaline (*Manning*, 1991) and it typically resides near the shelfbreak with the foot of the front located near the 80 m isobath during the summer on the New Jersey Shelf (*Burrage and Garvine*, 1988; *Linder and Gawarkiewicz*, 1998). The structure of the SSF is strongly affected by buoyancy-driven secondary circulation processes such as bottom boundary layer (BBL) detachment, cross-shelf-slope transport, and upwelling/downwelling. The combined along-shelf, cross-shelf and vertical flow due to these processes determine the delivery and the distribution of heat, salt and nutrients in the water column at the outershelf/shelfbreak region. Offshore forcing such as eddies and rings also exert significant influence on the structure of the SSF through the advection of offshore watermasses onto the outershelf in the form of salinity intrusions (*Churchill et al.*, 2003). Asymmetry in the SSF jet flow structure and the development of multiple near surface and bottom frontal jets are known signs of eddy-front interaction (*Gawarkiewicz et al.*, 2001).

Secondary circulation near the SSF has been studied using both observations

and models. Specifically upwelling driven by BBL detachment on the shoreward side of the SSF has been observed using suspended bottom material (*Barth et al.*, 1998). Modeling studies have shown that surface and bottom convergence/divergence near the SSF due to the cross-shelf transport of buoyancy can drive BBL detachment and form vertical circulation cells on opposing sides of the front (*Chapman and Lentz*, 1994; *Gawarkiewicz and Chapman*, 1992). A method of detecting BBL detachment using simple cross-shelf hydrographic CTD sections by tracking temperature changes along a set of isopycnals was developed by *Pickart* (2000). Local minimum in the contours of accumulated temperature change (ATC) were shown to follow the detached BBL's. Because the vertical mixing and buoyancy flux from the detached BBL is important for building and maintaining the shelf-slope front, the ATC method provides a way to track the location of the front using only hydrographic measurements. *Linder et al.* (2004) applied this technique to study the seasonal behavior of BBL detachment near the SSF using select hydrographic sections from the PRIMER experiments and found that detached BBL was seen extending higher in the water column in winter than summer due to seasonal stratification.

Although the previous studies have explored how individual physical forcing mechanisms affect the SSF, the combined effect of intense seasonal stratification and offshore ring/eddy forcing on the SSF and associated secondary circulation has not been well studied. Such study requires repeated hydrographic sampling that can resolve the cross-shelf structure of the front on the order of $1 - 5$ km during times of strong offshore forcing. To date, only a few ship-based experiments have been able to provide the necessary high resolution datasets (*Barth et al.*, 1998; *Gawarkiewicz et al.*, 2001).

Sustained seasonal cross-shelf glider surveys such as the Shallow Water 2006 Joint Experiment (SW06) (*Tang et al.*, 2009; *Gong et al.*, 2010) provided a unique dataset ideal for studying secondary circulation at the SSF under this combined scenario. 2006 was one of the most stratified summers on the New Jersey Shelf in the past decade and two slope water eddies carrying Gulf Stream water approached the New Jersey shelfbreak in August. This study will focus on a period when the SSF was interacting with an approaching slope water eddy and explore how secondary circulation can affect salinity distribution at the outershelf.

4.2 Data and Methods

A subset of the observational data from the SW06 Joint Experiment (August 15-21, 2006) was used for this study. All data times are referenced to the Coordinated Universal Time (UTC). Three Slocum gliders (each carrying a CTD), eight oceanographic moorings (two wind buoys, six moorings with Acoustic Doppler Current Profilers (ADCP), and four moorings with Conductivity-Temperature chains) were deployed. The glider tracks and mooring locations are shown in Figure 4.1. The inverted 'T' mooring array is overlaid on the bathymetry contours. The innershelf is to the northwest and the shelfbreak is to the southeast. The dark isobaths in each figure from left to right are the 60, 100, 200, and 1000 m isobaths. The mooring current vector coordinate system was rotated 34 degrees clockwise to align with the along-shelf and cross-shelf geographic axes. Positive is offshore in the x direction and upshelf in the y direction. The hourly averaged current data from the moorings were low-passed using a Hamming filter with a cutoff of 33 hours. Sea Surface Temperature (SST) maps from the NOAA Advanced Very High Resolution Radiometer (AVHRR) satellites were used to track

nearby slope water eddies or warm core rings (WCR).

Three gliders, RU10 (northern), RU11 (central), and RU05 (southern), each completed cross-shelf transects during the study time period. The cross-shelf axis is zero-referenced to the 100 m isobath. Negative is shoreward and positive is seaward. The glider transects are separated 15-30 km in the along-shelf direction (Figure 4.1(d)). Each glider carried a Seabird CTD package for making hydrographic measurements. The southern two glider sections (RU11 and RU05), flying from inshore to offshore, were completed within 3 hours of each other. The distance between these two gliders was approximately 10 km in the alongshelf direction. Time-averaged currents for one diurnal period (24.8 hours) before the closest glider approach to each mooring are calculated and overlaid on the glider hydrographic sections. This helps to show how the currents were related to the observed hydrographic features. The length of the black arrows in the temperature and salinity cross-sections indicate the cross-shelf flow speeds and the size of the dot (or cross) indicate the downshelf (or upshelf) flow speeds at the specified ADCP depth bins.

4.3 Results

The Sea Surface Temperature (SST) maps for the outer New Jersey Shelf for August 15 and 19, 2006 are shown in Figure 4.1(a) and 4.1(b). The mooring locations are overlaid on the SST images (black dots). Intense stratification with a density difference of 4 kg/m^3 in less than 5 m in the vertical was observed at the pycnocline. The outershelf underwent a change from being shelf-water dominated (cool) to slope-water (warm) dominated in 4 days, driving changes in the position, flow, and structure of the SSF.

During the shelf-water dominated period (August 15-18), a single thermohaline

interface (-4 km) representing the SSF was observed in the RU05 section south of the cross-shelf mooring array (Figure 4.2(a), 4.2(b)). Most of the slope-water on the shelf resided in the bottom layer, with little non-bottom slope-water observed shoreward of the SSF. The maximum temperature and salinity difference across the interface was approximately 2 °C (12 vs. 14) and 1 to 1.5 (33 vs. 34), respectively. The thermohaline interface extends from the bottom layer to just below the seasonal pycnocline. Depth-averaged flow was generally downshelf with a speed of 15 to 20 cm/s at the 80 m isobath and 20 to 30 cm/s at the shelfbreak.

During the ring-influenced period (August 18-21), a WCR with a diameter of 100 km and sub-mesoscale structures (such as filaments) on the scale of 5-20 km was seen in the shelfbreak region of the SW06 study area (Figure 4.1(b)). Current measurements from SW30 showed that downshelf flow at all depths was weakened and a significant cross-shelf flow component developed during this time (Figure 4.1(d)). Glider temperature and salinity cross-sections obtained just north (RU11) (Figure 4.2(e)) and south (RU05) (Figure 4.2(h)) of the cross-shelf mooring array showed that the SSF was further inshore (-20 km) than the earlier shelfwater influenced period (-5 km) (Figure 4.2(b)). The two transects (RU11 and RU05) were separated by 10 km in the alongshelf and were completed within 3 hours of each other. Both had salinity intrusions of similar extent and magnitude as well as a double fronted thermohaline interface observed at similar cross-shelf locations. The foot of the first interface was located near the 65 m isobath (-35 km), and it extended seaward to the 75 m isobath (-20 km). The width of the interface was approximately 5 km. The maximum temperature and salinity difference across the gradient was approximately 4 °C (8 vs. 12) and 0.6 to 1 (33 vs. 34), respectively. Shoreward of the interface, the isotherms and isopycnals were compressed

with cold pool water just below the pycnocline. Seaward of the interface, the isotherms and isopycnals were depressed downward and warmer water from the thermocline was brought into the interior of the water column (Figure 4.2(g)). The foot of the second gradient was located near the 80 m isobath, approximately 10 km from the 100 m isobath, and it extended upward nearly vertically, reaching a depth of 30 m. The second interface was sharper with a width of < 5 km. The temperature and salinity difference across the second gradient was approximately 2.5 °C (12 vs 14.5) and 1 (34 vs 35), respectively. Similar patterns of isotherm compression and depression were observed on opposing sides of this interface as well. In the regions between the two thermohaline gradients, intrusions of salty slope water were observed just below the seasonal pycnocline. Offshore of the second thermohaline interface, intrusions of slope water were seen throughout the entire lower water column. A previous study using datasets from the GULFEX 1 and POGO-2 experiments also saw a summertime double thermohaline frontal interface (*Szuts and Gawarkiewicz*, 2000). Near-bottom cross-shelf temperature and salinity was used to visualize the frontal gradients. A similar plot here showed the two regions of sharper thermohaline gradients at cross-shelf distances of -27 km and -8 km (Figure 4.3(b)). A third glider, RU10, 30 km to the north (data not shown), had a much different hydrographic section with significantly less developed intrusions. This suggests that the alongshelf correlation scale for the NJ outershelf was more than 10 km but less than 30 km.

The presence of warm and salty water, with apparent connections to both the thermocline and the BBL in the interior water column below the seasonal pycnocline, meant secondary circulation such as downwelling or upwelling was likely taking place near the SSF. A known driver of secondary circulation at the shelf-slope frontal region

is the detachment of the BBL. (*Gawarkiewicz and Chapman*, 1992). The mean current vectors at the mid-shelf and shelfbreak moorings indicate a flow convergence zone developing in between the midshelf and shelfbreak moorings (Figure 4.1(d)). Modeling of cross-shelf buoyancy transport due to Ekman advection of the BBL by *Chapman and Lentz* (1994) showed that thermal wind shear in the along-shelf flow can result in cross-shelf flow convergence just shoreward of the cross-shelf density front.

BBL detachment and upwelling/downwelling in the frontal region can be detected using high resolution cross-shelf hydrographic sections. One method is to track the accumulated temperature change (ATC) along a range of isopycnals (*Pickart*, 2000). The height of the minimum in ATC contours indicates the height of the detached BBL. The ATC contours overlaying cross-shelf salinity measurements for SW05 during the period before the WCR and the period after are shown in Figure 4.2(b), 4.2(e), and 4.2(h). All the ATC cross-section plots show elevated ATC contour lines just shoreward of the SSF. The ATC analysis during the second time period suggests the possibility of two regions of BBL detachments. The inshore one rises to a depth of 25-30 m, just below the thermocline and the offshore one rises to a depth of 40 m, just below the salinity intrusions.

Another way of visualizing the secondary circulation, such as upwelling due to BBL detachment or downwelling from the thermocline, is to track the vertical temperature gradient, dT/dz. There are two main sources of dT/dz on the summer stratified shelf, the seasonal pycnocline and the BBL. The seasonal thermocline located near 20 m of depth is a region of strongly positive dT/dz, showing decreasing temperature with increasing depth. The upper boundary of the BBL, on the other hand, is a region of

negative dT/dz exhibiting a sharp increase in temperature with increasing depth (Figure 4 of *Pickart* (2000)). Example temperature profiles from SW06 glider data at the mid- and outershelf are shown in Figure 4.3. The thickness of non-detached BBL can vary between 5 to 20 m above the bottom (*Linder et al.*, 2004), the gliders saw a BBL thickness of 10 m. In the case of a quiescent stably stratified shelf with non-detached BBL, the two sources of vertical temperature gradient mentioned above should be the dominant features at the pycnocline and near the bottom. On the other hand if buoyancy driven BBL detachment or downwelling from the thermocline do occur, the local maxima of the vertical temperature gradient would appear in the interior of the water column.

Cross-shelf sections of dT/dz are plotted for RU11 and RU05 transects to track secondary circulation in the core SW06 study region (Figure 4.2, right column). The dT/dz sections show the expected positive dT/dz in the thermocline region but they also show two regions of negative dT/dz rising from the bottom through the interior of the water column, connecting with the base of the pycnocline (Figure 4.2(f), 4.2(i)), indicative of upwelling tendencies. The locations of the local maxima of negative dT/dz match the BBL detachment/upwelling regions as indicated in the ATC plots. According to modeling study of *Chapman and Lentz* (1994) this would imply that the frontal interfaces are just seaward of these upwelling regions. In the regions in between the two BBL detachment upwelling zones, regions of positive dT/dz are pushed down from the thermocline, suggesting downwelling tendencies (Figure 4.2(i)) on opposite side of the SSF. The hydrography on opposing sides of the two cross-shelf frontal interfaces supports this picture. The temperature cross-sections in Figure 4.2(d) and Figure 4.2(g) clearly shows the downward advection/mixing of warm water from the pynocline

into the water column interior near the 80 and 100 m isobaths. For both interfaces, the pycnocline was depressed on the seaward side and elevated on the shoreward side (Figure 4.2(d)). The upwelling and downwelling circulation observed in the SSF region is consistent with two circulation cells setting up near the two thermohaline interfaces of the SSF.

4.4 Discussion and Summary

This study found two thermohaline interfaces separating three different water masses on the outer continental shelf of the central Mid-Atlantic Bight during the summer stratified season. The thermohaline interfaces appears to be associated with the shelf-slope front (SSF), and a 10-15 km shoreward movement of the front was observed during a 4 day period as a small WCR approached. The feature was coherent for greater than 10 km but less than 30 km in the alongshelf. Two previous studies using different datasets have characterized similar hydrographic features at the outershelf. *Lentz et al.* (2003) classified the three watermasses observed on the flank of George's Bank using a salinity criteria: shelf ($S < 33.6$), shelf-slope front water (SSFW) ($33.6 < S < 35$), and slope water ($S > 35$). The intrusion of the SSFW onto the southern flank of the bank was associated with the presence of WCR's (*Churchill et al.*, 2003). *Szuts and Gawarkiewicz* (2000) found a double front on the southern MAB with similar cross-frontal change in temperature and salinity as found here. They identified shelf ($S < 33.2$), upper slope ($33.2 < S < 35.2$), and Gulf Stream water ($S > 35.2$) in the study area. Although result of this study is compatible with either classification and interpretation, it emphasizes the effect of mesoscale offshore forcing on the double interface of the SSF frontal structure.

Hydrographic analysis showed that there were extensive sub-pycnocline salinity intrusions when the SSF was further inshore. The twin thermohaline fronts suggest there were alternating zones of upwelling and downwelling. Secondary circulation drives the vertical transport of material at the shelf-slope frontal region. Stratification and slope water eddy acted as opposing forces. Under weakly stratified regimes, idealized shelf models have shown that upwelling on the shoreward side of the shelf-slope front is due to flow convergence in the BBL and downwelling on the seaward side of the shelf-slope front is due to flow divergence in the BBL (*Chapman and Lentz*, 1994). Near-surface divergent and convergent flow on opposing sides of the shelf-slope front had also been observed when shelf was weakly stratified, $N^2 \sim 1-2\times10^{-4}\ 1/s^2$ (estimated from Figure 5 and 6 of *Gawarkiewicz et al.* (2001)). BBL detachment on the other hand can shut down at a previously observed threshold of $N^2 > 1.7\times10^{-4}\ 1/s^2$ on the MAB shelf (*Linder et al.*, 2004). Here the observed seasonal stratification of $N^2 \sim 10^{-2}\ 1/s^2$ therefore would inhibit any secondary circulation through the pycnocline. On the other hand, below the pycnocline, stratification can be weak enough to support upwelling and downwelling near the SSF connecting the BBL and the pycnocline, potentially delivering nutrients and other material from the bottom into the lower euphotic zone.

The upwelling due to BBL detachment was shown to take place at both SSF interfaces using the method of ATC and a new method of the inspection of the vertical temperature gradient sections. Downwelling from the thermocline was observed through inspection of the temperature section. The evidence of upwelling and downwelling was consistent with having two circulation cells on opposite sides of the SSF. Modeling study of *Chapman and Lentz* (1994) suggests that such cells are a result of simply buoyancy driven flow. Whether the existence of a nearby eddy or ring is necessary to sustain this

secondary circulation pattern on the MAB shelf remains an open question. This study provided the first spatial constraint on the along-shelf scale of the double interface of the SSF during the stratified season ($10km < l < 30km$), and an upper bound estimate of the feature growth time scale ($\sim$ 4 days).

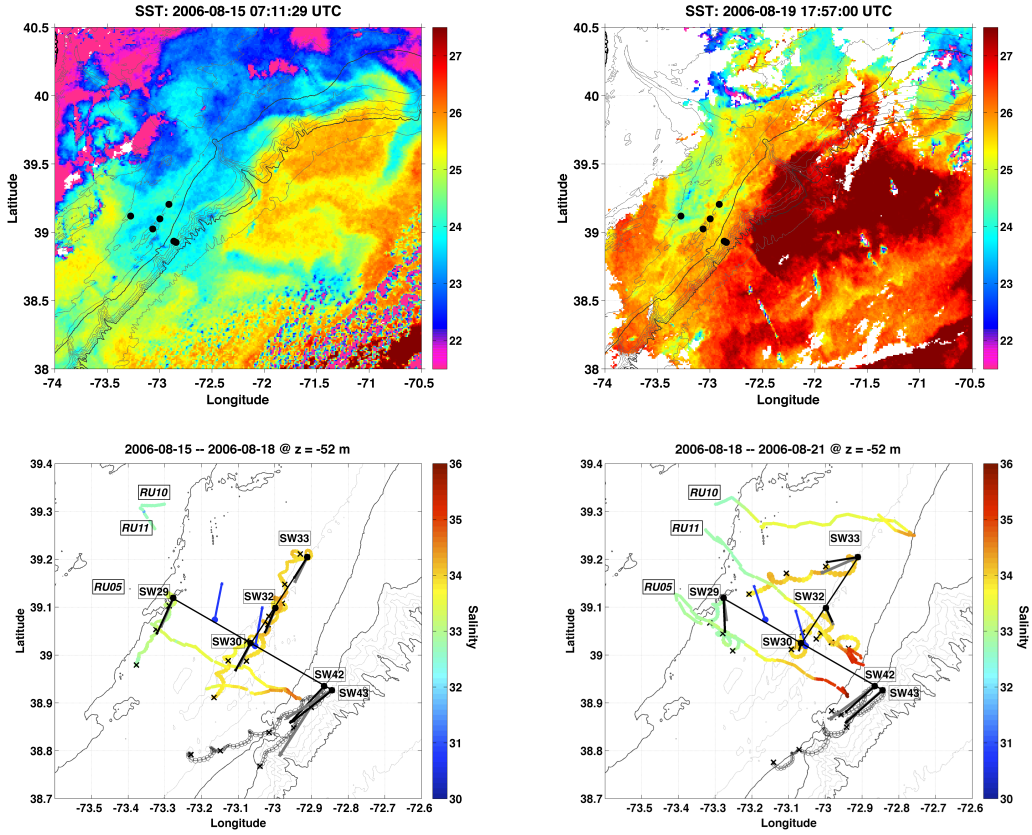

Figure 4.1: Sea Surface Temperature for the SW06 region on (a) August 15, 2006 and (b) August 19, 2006. (c) and (d) show maps of the moorings (black), wind buoys (blue), and glider tracks for August 15-18 and August 18-21, respectively. The three gliders from north to south are: RU10, RU11 and RU05. The progressive vector diagrams for velocity, colored by salinity, are plotted for each mooring. Progressive vectors at moorings without salinity measurements are shown in grey. The 3-day mean current velocity vectors (black arrows are depth averaged; grey arrows are for specified depths at 52 m) and wind velocity vectors (blue) are plotted. Black crosses on the progressive vector tracks mark every 24 hours.

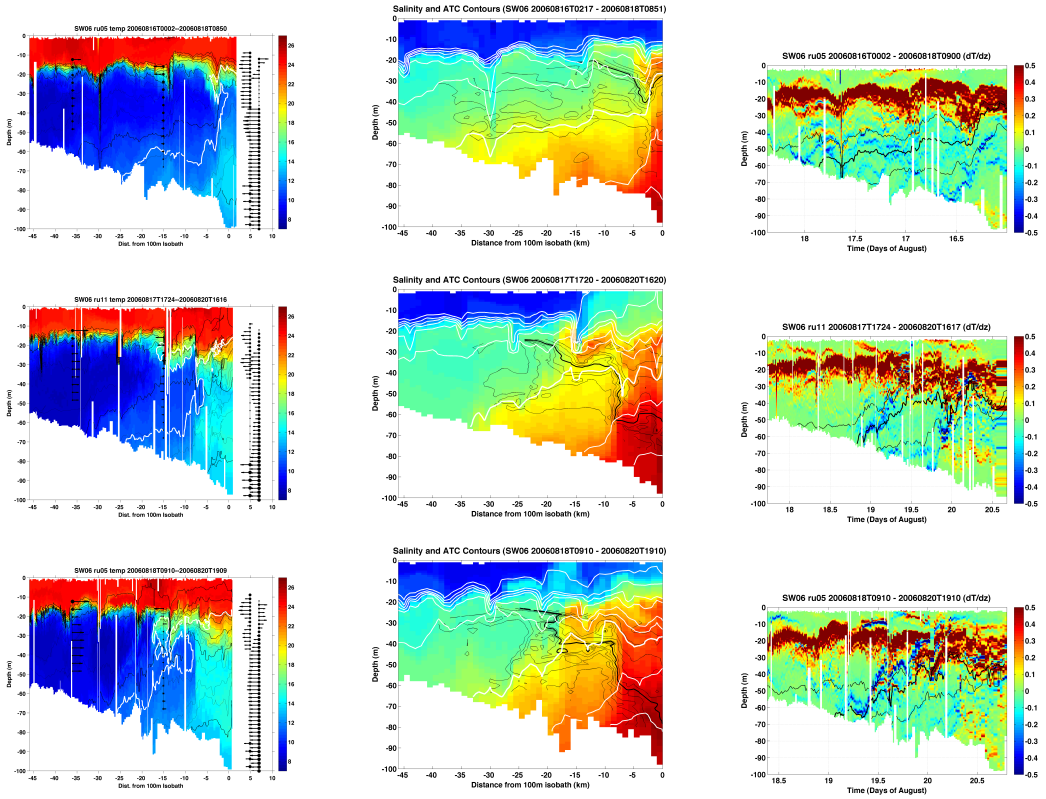

Figure 4.2: Temperature (left column), salinity with accumulated temperature change (ATC) contours (middle column), and vertical temperature gradient dT/dz (right column) cross-shelf sections for gliders RU11 and RU05 before (top row) and during an eddy approach (middle and bottom rows). The two glider transects were separated by approximately 10 km in the along-shelf. The black lines are density contours (1026 kg/m^3 highlighted) and the white line is the 34 isohaline in temperature and temperature gradient plots. Black lines are ATC contour lines in the salinity sections (0.5 highlighted). White lines are isopycnals (1026 kg/m^3 highlighted). (a) Temperature for RU05 (Aug 16-18), (b) salinity with ATC for RU05 (Aug 16-18), (c) dT/dz for RU05 (Aug 16-18). (d) Temperature for RU11 (Aug 18-21), (e) salinity with ATC for RU11 (Aug 18-21), (f) dT/dz for RU11 (Aug 18-21). (g) Temperature for RU05 (Aug 18-21), (h) salinity with ATC for RU05 (Aug 18-21), (i) dT/dz for RU05 (Aug 18-21).

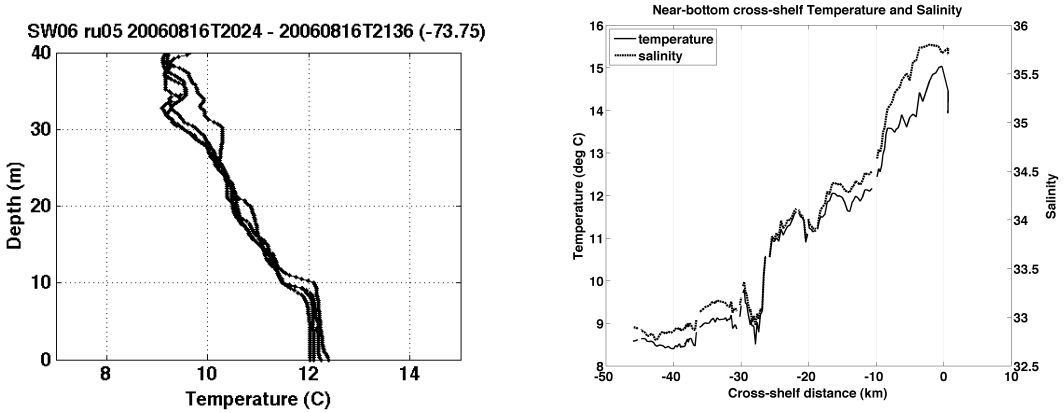

Figure 4.3: (a) Bottom referenced temperature profiles for the lower 40 m of the water column on the New Jersey Shelf for mid-August 2006. Temperature inversions characteristic of the BBL the outer-shelf was seen at a depth of approximately 10 m above the bottom. (b) Along-bottom temperature and salinity for the cross-shelf glider RU05 transect during 8/18/06 and 8/21/06. Steep changes in both temperature and salinity were seen at two cross-shelf locations, one near -27 km and the other near -8 km in the cross-shelf.

Chapter 5

Conclusions

Through the analysis of datasets from a sustained HF-Radar surface current mapping network and an observatory-enabled oceanographic experiment at the outer New Jersey shelf during the stratified season, this study characterized the subtidal mesoscale variability of several key physical forcing mechanisms and the oceanographic response at the mid- to outer NJ Shelf. Higher stratification resulted in surface current turning more to the right of the wind. Cross-shelf offshore transport was mainly driven by winds from onshore during the winter and upwelling winds from downshelf during the summer. Along-shelf transport during the transition seasons of spring and autumn was mainly driven by along-shore winds from the upshelf.

During the stratified season, variability in the outershelf hydrography was governed by river discharge, wind forcing, and offshore forcing such rings and eddies. Different types of intrusions occurred at the shelf-slope front (SSF) at the shelfbreak. Large volumes of surface fresh water, as was the case for summer 2006, could push the shelf surface layer offshore of the shelfbreak. Slope water eddies directly controlled the extent and intensity of pycnocline intrusions and they could indirectly affect intrusions below the pycnocline through its control on the location of the SSF. The offshore eddies and rings could be tracked using Sea Surface Temperature maps. The location of the

foot of the SSF was correlated with along-shelf wind stress. The SSF had characteristic alongshelf length alongshelf scales of 10-30 km and cross-shelf scales of 5-20. It could vary significantly on time scales of 2 days or less. BBL detachment near the SSF played an important role driving secondary circulation at the outershelf. Upwelling and downwelling associated with the SSF could take place at multiple frontal interfaces. The persistent salinity intrusions at the outershelf and the significant eddy/ring influence suggested that the shelf-slope interface was highly porous and variable during the summer stratified season. Mixing brought by late season storms could entrain slope watermasses on the shelf. Future studies assessing the rate of cross-shelf-slope exchange and how climate change might affect such rates require the proper measurement and parametrization of these important forcing factors operating at meso- and submesocales.

Bibliography

Allen, J. R. (1981), Beach erosion as a function of variations in the sediment budget, Sandy Hook, New Jersey, U.S.A, *Earth Surface Processes and Landforms*, *6*(2), 139–150, 10.1002/esp.3290060207.

Allen, J. S. (1980), Models of Wind-Driven Currents on the Continental Shelf, *Annual Review of Fluid Mechanics*, *12*(1), 389–433, doi:doi:10.1146/annurev.fl.12.010180.002133.

Barrick, D. E. (1971a), Theory of HF/VHF propagation across the rough sea. Part I: The effective surface impedance for a slightly rough highly conducting medium at grazing incidence, *Radio Science*, *6*, 517–526.

Barrick, D. E. (1971b), Theory of HF/VHF propagation across the rough sea. Part II: Application to HF/VHF propagation above the sea, *Radio Science*, *6*, 527–533.

Barth, J. A., D. Bogucki, S. D. Pierce, and P. M. Kosro (1998), Secondary circulation associated with a shelfbreak front, *Geophysical Research Letters*, *25*(15), 2761–2764, 5.

Barth, J. A., D. Hebert, A. C. Dale, and D. S. Ullman (2004), Direct observations of along-isopycnal upwelling and diapycnal velocity at a shelfbreak front, *Journal of Physical Oceanography*, *34*(3), 543–565, 34.

Beardsley, R. C., and W. C. Boicourt (1981), On estuarine and continental-shelf circulation in the Middle Atlantic Bight, in *Evolution of Physical Oceanography: Scientific Surveys in Honor of Henry Stommel*, edited by B. A. Warren and C. Wunsch, pp. 198–235, MIT Press.

Beardsley, R. C., and C. D. Winant (1979), On the Mean Circulation in the Mid-Atlantic Bight, *Journal of Physical Oceanography*, *9*(3), 612–619.

Beardsley, R. C., W. C. Boicourt, and D. Hanson (1976), Physical Oceanography of the Mid-Atlantic Bight, *J. Limnol. Ocean., Spec. Symp.*, *2*, 20–34.

Beardsley, R. C., D. C. Chapman, K. H. Brink, S. R. Ramp, and R. Schlitz (1985), The Nantucket Shoals Flux Experiment (NSFE79). Part I: A Basic Description of the Current and Temperature Variability, *Journal of Physical Oceanography*, *15*(6), 713–748.

Bigelow, H. B. (1933), Studies of the waters on the continental shelf, Cape Cod to Chesapeak Bay. I. The cycle of temperature, *Papers in Physical Oceanography and Meteorology*, *2*(4).

Bigelow, H. B., and M. Sears (1935), Studies of the waters on the continental shelf, Cape Cod to Chesapeak Bay. II. Salinity, *Papers in Physical Oceanography and Meteorology*, *4*(1).

Biscaye, P. E., C. N. Flagg, and P. G. Falkowski (1994), The Shelf Edge Exchange Processes Experiment, Seep-Ip - an Introduction to Hypotheses, Results and Conclusions, *Deep-Sea Research Part Ii-Topical Studies in Oceanography*, *41*(2-3), 50.

Boicourt, W. C., and P. W. Hacker (1976), Circulation on the Atlantic continental shelf of the United States, Cape May to Cape Hatteras, *Mem. Soc. R. Sci. Liege Ser.*, *6e*(10), 187–200.

Bumpus, D. F. (1973), A description of the circulation on the continental shelf of the east coast of the United States, *Progress in Oceanography*, *6*, 111–157.

Burrage, D. M., and R. W. Garvine (1988), Summertime Hydrography at the Shelfbreak Front in the Middle Atlantic Bight, *Journal of Physical Oceanography*, *18*(10), 1309–1319.

Byoung-Ju, C., and J. L. Wilkin (2007), The Effect of Wind on the Dispersal of the Hudson River Plume, *Journal of Physical Oceanography*, *37*(7), 1878–1897.

Castelao, R., O. Schofield, S. Glenn, R. Chant, and J. Kohut (2008a), Cross-shelf transport of freshwater on the New Jersey shelf, *Journal of Geophysical Research-Oceans*, *113*(C7), 12, doi:C07017 10.1029/2007jc004241, iSI Document Delivery No.: 328LJ Times Cited: 0 Cited Reference Count: 48.

Castelao, R., S. Glenn, O. Schofield, R. Chant, J. Wilkin, and J. Kohut (2008b), Seasonal evolution of hydrographic fields in the central Middle Atlantic Bight from glider observations, *Geophysical Research Letters*, *35*, 10.1029/2007GL032335.

Chant, R. J., S. M. Glenn, E. Hunter, J. Kohut, R. F. Chen, R. W. Houghton, J. Bosch, and O. Schofield (2008), Bulge formation of a buoyant river outflow, *Journal of Geophysical Research-Oceans*, *113*(C1), 16, doi:C01017 10.1029/2007jc004100.

Chapman, D. C., and R. C. Beardsley (1989), On the Origin of Shelf Water in the Middle Atlantic Bight, *Journal of Physical Oceanography*, *19*(3), 384–391.

Chapman, D. C., and H. C. Graber (1997), Validation of HF Radar measurements, *Oceanography*, *10*, 76–79.

Chapman, D. C., and S. J. Lentz (1994), Trapping of a Coastal Density Front by the Bottom Boundary-Layer, *Journal of Physical Oceanography*, *24*(7), 1464–1479, 28.

Churchill, J. H. (1985), Intrusions of Outer Shelf and Slope Water Within the Nearshore Zone off Long Island, New York, *Limnology and Oceanography*, *30*(5), 972–986, 0024-3590 Article type: Full Length Article / Full publication date: Sep., 1985 (198509). / Copyright 1985 American Society of Limnology and Oceanography.

Churchill, J. H., J. P. Manning, and R. C. Beardsley (2003), Slope water intrusions onto Georges Bank, *Journal of Geophysical Research-Oceans*, *108*(C11), 24 8012.

Csanady, G. T. (1976), Mean Circulation in Shallow Seas, *Journal of Geophysical Research*, *81*(6), 5389–5399.

Delworth, T. L., and M. E. Mann (2000), Observed and simulated multidecadal variability in the Northern Hemisphere, *Climate Dynamics*, *16*(9), 661–676, 10.1007/s003820000075.

Dzwonkowski, B., J. T. Kohut, and X. H. Yan (2008a), Sub-inertial surface flow field over the shelf of the central Mid-Atlantic Bight, *Continental Shelf Research*, in Revision.

Dzwonkowski, B., J. T. Kohut, and X. H. Yan (2008b), Seasonal differences in wind-driven cross-shelf forcing and response relationships in the shelf surface layer of the central Mid-Atlantic Bight, *Journal of Geophysical Research-Oceans*, in Revision.

Dzwonkowski, B., J. T. Kohut, and X. H. Yan (2009), Sub-inertial surface flow field over the shelf of the central Mid-Atlantic Bight, *Continental Shelf Research*.

Ekman, V. W. (1905), On the influence of the earth's rotation on ocean current, *Ark. Mat. Astron. Fys.*, *2*, 1–53.

Fairbanks, R. G. (1982), The Origin of Continental Shelf and Slope Water in the New York Bight and Gulf of Maine: Evidence from H2 18O/H2 16O Ratio Measurements, *Journal of Geophysical Research*, *87*, doi:10.1029/JC087iC08p05796.

Fewings, M., S. J. Lentz, and J. Fredericks (2008), Observations of Cross-Shelf Flow Driven by Cross-Shelf Winds on the Inner Continental Shelf, *Journal of Physical Oceanography*, *38*(11), 2358–2378.

Flagg, C. N., R. W. Houghton, and L. J. Pietrafesa (1994), Summertime Thermocline Salinity Maximum Intrusions in the Mid-Atlantic Bight, *Deep-Sea Research Part Ii-Topical Studies in Oceanography*, *41*(2-3), 325–, 11.

Flagg, C. N., L. J. Pietrafesa, and G. L. Weatherly (2002), Springtime hydrography of the southern Middle Atlantic Bight and the onset of seasonal stratification, *Deep-Sea Research Part Ii-Topical Studies in Oceanography*, *49*(20), 4297–4329, 29.

Flagg, C. N., M. Dunn, D. P. Wang, H. T. Rossby, and R. L. Benway (2006), A study of the currents of the outer shelf and upper slope from a decade of shipboard ADCP observations in the Middle Atlantic Bight, *Journal of Geophysical Research-Oceans*, *111*(C6), 49 C06003.

Flament, P. (2002), A state variable for characterizing water masses and their diffusive stability: spiciness, *Progress in Oceanography*, *54*(1-4), 493–501, doi: DOI: 10.1016/S0079-6611(02)00065-4.

Fong, D. A., and W. R. Geyer (2002), Response of a river plume during an upwelling favorable wind event, *J. Geophys. Res.*, *106*, 10.1029/2000JC900134.

Fratantoni, P. S., and R. S. Pickart (2003), Variability of the shelf break jet in the Middle Atlantic Bight: Internally or externally forced?, *J. Geophys. Res.*, *108*(C5), 3166, doi:10.1029/2002jc001326.

Fratantoni, P. S., R. S. Pickart, D. J. Torres, and A. Scotti (2001), Mean structure and dynamics of the shelfbreak jet in the Middle Atlantic Bight during fall and winter , *Journal of Physical Oceanography*, *31*(8), 2135–2156, 36.

Garvine, R. W. (2004), The vertical structure and subtidal dynamics of the inner shelf off New Jersey, *Journal of Marine Research*, *62*(3), 337–371, 39.

Garvine, R. W., K. C. Wong, G. G. Gawarkiewicz, R. K. McCarthy, R. W. Houghton, and I. Aikman, F. (1988), THE MORPHOLOGY OF SHELFBREAK EDDIES, *J. Geophys. Res.*, *93*(C12), 15,593–15,607, doi:10.1029/JC093iC12p15593.

Gawarkiewicz, G. (1991), Linear Stability Models of Shelfbreak Fronts, *Journal of Physical Oceanography*, *21*(4), 471–488, doi:doi:10.1175/1520-0485(1991)021¡0471:LSMOSF¿2.0.CO;2.

Gawarkiewicz, G., and D. C. Chapman (1992), The Role of Stratification in the Formation and Maintenance of Shelf-Break Fronts, *Journal of Physical Oceanography*, *22*(7), 753–772.

Gawarkiewicz, G., T. G. Ferdelman, T. M. Church, and G. W. Luther (1996a), Shelfbreak frontal structure on the continental shelf north of Cape Hatteras, *Continental Shelf Research*, *16*(14), 1751–1773, 23.

Gawarkiewicz, G., F. Bahr, R. C. Beardsley, and K. H. Brink (2001), Interaction of a slope eddy with the shelfbreak front in the Middle Atlantic Bight, *Journal of Physical Oceanography*, *31*(9), 2783–2796, 24.

Gawarkiewicz, G. G., C. A. Linder, J. F. Lynch, A. E. Newhall, and J. J. Bisagni (1996b), A surface-trapped intrusion of slope water onto the continental shelf in the mid-Atlantic bight, *Geophysical Research Letters*, *23*(25), 3763–3766, 16.

Glenn, S., and O. Schofield (2009), Growing a Distributed Ocean Observatory: Our View from the COOL Room, *Oceanography*, *22*(2), 112–129.

Glenn, S., et al. (2004), Biogeochemical impact of summertime coastal upwelling on the New Jersey Shelf, *J. Geophys. Res.*, *109*, 10.1029/2003JC002265.

Glenn, S., C. Jones, M. Twardowski, L. Bowers, J. Kerfoot, J. Kohut, D. Webb, and O. Schofield (2008), Glider observations of sediment resuspension in a Middle Atlantic Bight fall transition storm, *Limnology and Oceanography*, *53*(5), 2180–2196.

Gong, D., and S. Glenn (submitted), Observations of bottom boundary layer detachment and secondary circulation at the MAB shelf-slope interface, *Geophysical Research Letters*.

Gong, D., S. Glenn, R. Chant, J. Wilkin, and J. Kohut (2006), NJ Turnpike–Dynamics of the Hudson Shelf Valley, *Ocean Sci. Meet. Suppl.*, *87*(36).

Gong, D., J. T. Kohut, and S. M. Glenn (2010), Seasonal climatology of wind-driven circulation on the New Jersey Shelf, *J. Geophys. Res.*, *115*(C4).

Gordon, A. L., and F. Aikman III (1981), Salinity Maximum in the Pycnocline of the Middle Atlantic Bight, *Limnology and Oceanography*, *26*(1), 123–130, 0024-3590 Article type: Full Length Article / Full publication date: Jan., 1981 (198101). / Copyright 1981 American Society of Limnology and Oceanography.

Graber, H. C., E. A. Terray, M. A. Donelan, W. M. Drennan, J. C. Van Leer, and D. B. Peters (2000), ASIS—A New Air-Sea Interaction Spar Buoy: Design and Performance at Sea, *Journal of Atmospheric and Oceanic Technology*, *17*(5), 708–720.

Griffa, A. (1996), Applications of stochastic particle models to oceanographic problems., in *Stochastic Modelling in Physical Oceanography*, vol. 113, edited by R. Adler, P. Muller, and B. Rozovskii, Birkhauser Boston, Cambridge, MA.

Hare, J. A., J. A. Quinlan, F. E. Werner, B. O. Blanton, J. J. Govoni, R. B. Forward, L. R. Settle, and D. E. Hoss (1999), Larval transport during winter in the SABRE study area: results of a coupled vertical larval behaviour–three-dimensional circulation model, *Fisheries Oceanography*, *8*, 57.

Hare, J. A., J. H. Churchill, R. K. Cowen, T. J. Berger, P. C. Cornillon, P. Dragos, S. M. Glenn, J. J. Govoni, and T. N. Lee (2002), Routes and rates of larval fish transport from the southeast to the northeast United States continental shelf, *Limnology and Oceanography*, *47*(6), 1774–1789, 62.

Harris, C. K., B. Butman, and P. Traykovski (2003), Winter-time circulation and sediment transport in the Hudson Shelf Valley, *Continental Shelf Research*, *23*(8), 801–820.

Houghton, R. W., and J. Marra (1983), Physical/Biological Structure and Exchange Across the Thermohaline Shelf/Slope Front in the New York Bight, *Journal of Geophysical Research*, *88*(C7), 4467–4481.

Houghton, R. W., and M. Visbeck (1998), Upwelling and convergence in the Middle Atlantic Bight shelfbreak front, *Geophysical Research Letters*, *25*(15), 2765–2768, 4.

Houghton, R. W., R. Schlitz, R. C. Beardsley, B. Butman, and J. L. Chamberlin (1982), The Middle Atlantic Bight Cold Pool: Evolution of the Temperature Structure During Summer 1979, *Journal of Physical Oceanography*, *12*(10), 1019–1029.

Houghton, R. W., D. B. Olson, and P. J. Celone (1986), Observation of an Anticyclonic Eddy near the Continental Shelf Break South of New England, *Journal of Physical Oceanography*, *16*(1), 60–71.

Hunter, E., R. Chant, L. Bowers, S. Glenn, and J. Kohut (2007), Spatial and temporal variability of diurnal wind forcing in the coastal ocean, *Geophysical Research Letters*, *34*(3), hunter, Eli Chant, Robert Bowers, Louis Glenn, Scott Kohut, Josh 29 L03607.

Keen, T. R., and S. M. Glenn (1994), A Coupled Hydrodynamic–Bottom Boundary Layer Model of Ekman Flow on Stratified Continental Shelves, *Journal of Physical Oceanography*, *24*(8), 1732–1749.

Keen, T. R., and S. M. Glenn (1995), A Coupled Hydrodynamic–Bottom Boundary Layer Model of Storm and Tidal Flow in the Middle Atlantic Bight of North America, *Journal of Physical Oceanography*, *25*(3), 391–406.

Kennelly, M. A., R. H. Evans, and T. M. Joyce (1985), Small-Scale Cyclones on the Periphery of a Gulf Stream Warm-Core Ring, *J. Geophys. Res.*, *90*(C5), 8845–8857, doi:10.1029/JC090iC05p08845.

Kerfoot, J., O. Schofield, S. M. Glenn, H. G. Arango, C. Haldeman, C. Jones, and D. Pingal (2010), Correction and Comparison of Pumped and Non-Pumped CTD sensors on the Slocum Glider, *Eos Trans. AGU*, *91*(26), Ocean Sci. Meet. Suppl., Abstract IT35B–03.

Kerr, R. A. (2000), A North Atlantic Climate Pacemaker for the Centuries, *Science*, *288*(5473), 1984–1985, doi:10.1126/science.288.5473.1984.

Knebel, H. J., and E. C. Spiker (1977), Thickness and age of surficial sand sheet, Baltimore Canyon Trough area., *American Association of Petroleum Geologists Bulletin*, *61*, 861–871.

Kohut, J. T., S. M. Glenn, and R. J. Chant (2004), Seasonal current variability on the New Jersey inner shelf, *Journal of Geophysical Research-Oceans*, *109*(C7), 45 C07S07.

Kohut, J. T., S. M. Glenn, and J. D. Paduan (2006a), Inner shelf response to Tropical Storm Floyd, *Journal of Geophysical Research-Oceans*, *111*(C9), kohut, Josh T. Glenn, Scott M. Paduan, Jeffrey D. C09S91.

Kohut, J. T., H. J. Roarty, and S. M. Glenn (2006b), Characterizing observed environmental variability with HF Doppler radar surface current mappers and acoustic Doppler current profilers: Environmental variability in the coastal ocean, *IEEE Journal of Oceanic Engineering*, *31*(4), 876–884, kohut, Josh T. Roarty, Hugh J. Glenn, Scott M. 19.

Kuzmina, N., B. Rudels, T. Stipa, and V. Zhurbas (2005), The Structure and Driving Mechanisms of the Baltic Intrusions, *Journal of Physical Oceanography*, *35*(6), 1120–1137.

Lentz, S. J. (2001), The Influence of Stratification on the Wind-Driven Cross-Shelf Circulation over the North Carolina Shelf, *Journal of Physical Oceanography*, *31*(9), 2749–2760.

Lentz, S. J. (2003), A climatology of salty intrusions over the continental shelf from Georges Bank to Cape Hatteras, *Journal of Geophysical Research-Oceans*, *108*(C10), 32 3326.

Lentz, S. J. (2008a), Observations and a Model of the Mean Circulation over the Middle Atlantic Bight Continental Shelf, *Journal of Physical Oceanography*, *38*(6), 1203–1221.

Lentz, S. J. (2008b), Seasonal Variations in the Circulation over the Middle Atlantic Bight Continental Shelf, *Journal of Physical Oceanography*, *38*(7), 1486–1500.

Lentz, S. J., and J. H. Trowbridge (1991), The Bottom Boundary Layer Over the Northern California Shelf, *Journal of Physical Oceanography*, *21*(8), 1186–1201.

Lentz, S. J., R. C. Beardsley, J. D. Irish, J. Manning, P. C. Smith, and R. A. Weller (2003), Temperature and salt balances on Georges Bank February—August 1995, *J. Geophys. Res.*, *108*(C11), 8006, doi:10.1029/2001jc001220.

Linder, C. A., and G. Gawarkiewicz (1998), A climatology of the shelfbreak front in the Middle Atlantic Bight, *Journal of Geophysical Research-Oceans*, *103*(C9), 18,405–18,423, 41.

Linder, C. A., G. G. Gawarkiewicz, and R. S. Pickart (2004), Seasonal characteristics of bottom boundary layer detachment at the shelfbreak front in the Middle Atlantic Bight, *Journal of Geophysical Research-Oceans*, *109*(C3), 20 C03049.

Linder, C. A., G. G. Gawarkiewicz, and M. Taylor (2006), Climatological estimation of environmental uncertainty over the middle Atlantic bight shelf and slope, *Ieee Journal of Oceanic Engineering*, *31*(2), 308–324, linder, Chistopher A. Gawarkiewicz, Glen G. Taylor, Maureen 24.

Lueck, R. G. (1990), Thermal inertia of conductivity cells: Theory., *Journal of Atmospheric and Oceanic Technology*, *7*, 741–755.

Madsen, O. S. (1977), A Realistic Model of the Wind-Induced Ekman Boundary Layer, *Journal of Physical Oceanography*, *7*(2), 248–255.

Manning, J. (1991), Middle Atlantic Bight salinity: interannual variability, *Continental Shelf Research*, *11*(2), 123–137.

Mooers, C. N. K., J. Fernandez-Partagas, and J. F. Price (1976), Meteorological forcing fields of the New York Bight (first year's progress report), *Tech. rep.*, Rosenstiel School of Marine and Atmospheric Science, University of Miami.

Mooers, C. N. K., R. W. Garvine, and W. W. Martin (1979), Summertime Synoptic Variability of the Middle Atlantic Shelf Water/Slope Water Front, *Journal of Geophysical Research*, *84*(C8), 4837–4854.

Morgan, C. W., and J. M. Bishop (1977), An Example of Gulf Stream Eddy-Induced Water Exchange in the Mid-Atlantic Bight, *Journal of Physical Oceanography*, *7*(3), 472–479.

Morison, J., R. Andersen, N. Larson, E. Asaro, and T. Boyd (1994), The Correction for Thermal-Lag Effects in Sea-Bird CTD Data, *Journal of Atmospheric and Oceanic Technology*, *11*(4), 1151–1164.

Mountain, D. G. (2003), Variability in the properties of Shelf Water in the Middle Atlantic Bight, 1977Äì1999, *J. Geophys. Res.*, *108*, 10.1029/2001JC001044.

Nelson, W. R., M. C. Ingham, and W. E. Schaaf (1977), Larval transport and year-class strength of Atlantic menhaden. Brevoortia tyrannus, *Mar. Fish. Serv. Fish. Bull.*, *75*, 23–41.

Newhall, A. E., et al. (2007), Acoustic and Oceanographic Observations and Configuration Information for the WHOI Moorings from the SW06 Experiment, *Tech. Rep. 4*, Woods Hole Oceanographic Institution.

Ohlmann, C., P. White, L. Washburn, E. J. Terrill, B. Emery, and M. P. Otero (2007), Interpretation of coastal HF radar-derived surface currents with high-resolution drifter data, *Journal of Atmospheric and Oceanic Technology*, *24*, 666–680, doi: 10.1175/JTECH1998.1.

Pawlowicz, R., R. C. Beardsley, and S. J. Lentz (2002), Classical Tidal Harmonic Analysis Including Error Estimates in MATLAB using T_TIDE, *Computers and Geosciences*, *28*, 929–937.

Perlin, A., J. N. Moum, and J. M. Klymak (2005), Response of the bottom boundary layer over a sloping shelf to variations in alongshore wind, *J. Geophys. Res.*, *110*, 10.1029/2004JC002500.

Pickart, R. S. (2000), Bottom boundary layer structure and detachment in the shelfbreak jet of the Middle Atlantic Bight, *Journal of Physical Oceanography*, *30*(11), 2668–2686, 18.

Pingree, R. D. (1979), Baroclinic eddies bordering the celtic sea in late summer, *Journal of the Marine Biological Association of the UK*, *59*(03), 689–703, doi: doi:10.1017/S0025315400045677.

Pollard, R., and L. Regier (1992), Vorticity and Vertical Circulation at an Ocean Front, *Journal of Physical Oceanography*, *22*(6), 609–625.

Posmentier, E. S., and R. W. Houghton (1981), Springtime evolution of the New England shelf break front, *Journal of Geophysical Research*, *86*(C5), 4253–4259.

Quinlan, J. A., B. O. Blanton, T. J. Miller, and F. E. Werner (1999), From spawning grounds to the estuary: using linked individual-based and hydrodynamic models to interpret patterns and processes in the oceanic phase of Atlantic menhaden Brevoortia tyrannus life history, *Fisheries Oceanography*, *8*, 224.

Ramp, S. R., R. C. Beardsley, and R. Legeckis (1983), An Observation of Frontal Wave Development on a Shelf-Slope/Warm Core Ring Front Near the Shelf Break South of New England, *Journal of Physical Oceanography*, *13*(5), 907–912.

Schofield, O., et al. (2008), The Decadal View of the Mid-Atlantic Bight from the COOLroom: Is Our Coastal System Changing?, *Oceanography*, *23*(4), 108–117.

Shroyer, E. (2010), Nonlinear internal waves on the continental shelf, Ph.D. thesis, Oregon State University.

Sobarzo, M., R. K. Shearman, and S. Lentz (2007), Near-inertial motions over the continental shelf off Concepción, central Chile, *Progress In Oceanography*, *75*(3), 348–362, doi: DOI: 10.1016/j.pocean.2007.08.021.

Song, T., D. B. Haidvogel, and S. M. Glenn (2001), Effects of topographic variability on the formation of upwelling centers off New Jersey: A theoretical model, *J. Geophys. Res.*, *106*(C5), 9223–9240.

Stewart, R. H., and J. W. Joy (1974), HF radio measurements of surface currents, *Deep-Sea Research Part I-Oceanographic Research Papers*, *21*, 1039–1049.

Szuts, Z., and G. Gawarkiewicz (2000), Variability of Thermohaline Structure in the Shelfbreak Front in the Southern Middle Atlantic Bight.

Tang, D., et al. (2009), Shallow Water '06 – A Joint Acoustic Propagation / Nonlinear Internal Wave Physics Experiment, *Oceanography*, *20*(4), 156–167.

Teague, C. C. (1971), High Frequency Resonant Scattering Techniques for the Observation of Directional Ocean-Wave Spectra, Ph.D. thesis.

Thieler, E. R., B. Butman, W. C. Schwab, M. A. Allison, N. W. Driscoll, J. P. Donnelly, and E. Uchupi (2007), A catastrophic meltwater flood event and the formation of the Hudson Shelf Valley, *Palaeogeography, Palaeoclimatology, Palaeoecology*, *246*(1), 120–136, doi: DOI: 10.1016/j.palaeo.2006.10.030.

Tilburg, C. E. (2003), Across-Shelf Transport on a Continental Shelf: Do Across-Shelf Winds Matter?, *Journal of Physical Oceanography*, *33*(12), 2675–2688.

Torrence, C., and G. P. Compo (1998), A Practical Guide to Wavelet Analysis, *Bulletin of the American Meteorological Society*, *79*, 61–78.

Trowbridge, J., and S. Lentz (1991), Asymmetric Behavior of an Oceanic Boundary Layer above a Sloping Bottom, *Journal of Physical Oceanography*, *21*(8), 1171–1185.

Ullman, D. S., J. O'Donnell, J. Kohut, T. Fake, and A. Allen (2006), Trajectory prediction using HF radar surface currents: Monte Carlo simulations of prediction uncertainties, *J. Geophys. Res.*, *111*, 10.1029/2006JC003715.

Voorhis, A. D., D. C. Webb, and R. C. Millard (1976), Current Structure and Mixing in the Shelf/Slope Water Front South of New England, *J. Geophys. Res.*, *81*(21), 3695–3708, doi:10.1029/JC081i021p03695.

Werner, F. E., J. A. Quinlan, B. O. Blanton, and R. A. Luettich (1997), The role of hydrodynamics in explaining variability in fish populations, *Journal of Sea Research*, *37*(3-4), 195–212, doi: DOI: 10.1016/S1385-1101(97)00024-5.

Whitney, M. M., and R. W. Garvine (2005), Wind influence on a coastal buoyant outflow, *J. Geophys. Res.*, *110*, 10.1029/2003JC002261.

Winant, C. D. (1980), Coastal Circulation and Wind-Induced Currents, *Annual Review of Fluid Mechanics*, *12*(1), 271–301, doi:doi:10.1146/annurev.fl.12.010180.001415.

Wright, W. R., and C. E. Parker (1976), A Volumetric Temperature/Salinity Census for the Middle Atlantic Bight, *Limnology and Oceanography*, *21*(4), 563–571.

Xu, Y., R. Chant, D. Gong, R. Castelao, S. Glenn, and O. Schofield (2009), Inter-annual dynamics in the seasonal phytoplankton dynamics in the Mid-Atlantic Bight.

Yankovsky, A. E., and R. W. Garvine (1998), Subinertial Dynamics on the Inner New Jersey Shelf during the Upwelling Season, *Journal of Physical Oceanography*, *28*(12), 2444–2458.

Yankovsky, A. E., R. W. Garvine, and A. Münchow (2000), Mesoscale Currents on the Inner New Jersey Shelf Driven by the Interaction of Buoyancy and Wind Forcing, *Journal of Physical Oceanography*, *30*(9), 2214–2230.

Yoder, J. A., S. E. Schollaert, and J. E. O'Reilly (2002), Climatological phytoplankton chlorophyll and sea surface temperature patterns in continental shelf and slope waters off the northeast US coast, *Limnology and Oceanography*, *47*(3), 672–682, 39.

Zhang, W. G., J. L. Wilkin, and R. J. Chant (2009), Modeling the Pathways and Mean Dynamics of River Plume Dispersal in the New York Bight, *Journal of Physical Oceanography*.

Vita

Donglai Gong

EDUCATION

2010 Oct. Ph.D. Oceanography, School of Environmental and Biological Sciences, Rutgers University, New Brunswick, NJ.

2004 Feb. S.M. Physics, Massachusetts Institute of Technology, Cambridge, MA.

2001 Jan. B.S. Physics, B.A. Mathematics, with Highest Honor, Rutgers University, New Brunswick, NJ.

RESEARCH AND TEACHING

2010-2012 Postdoctoral Scholar, Ocean and Climate Change Institute, Woods Hole Oceanographic Institution

2009 Sum. Educator, 4-H: Science, Engineering, and Technology Camp–Coral Oasis Oceans and Lakes, Rutgers University

2009 Spr. Lecturer, Ocean Science Inquiries–Carbon Cycle, Renewable Energy and Humans, Rutgers University

2007 Fall Guest Lecturer, Human Ecology, Rutgers University

2007 Spr. Education and Outreach Assistant, Communicating Ocean Sciences to Informal Audiences (COSIA) in collaboration with Liberty Science Center

2006 Spr. Teaching Assistant, Department of Marine and Coastal Sciences, Rutgers University

2005-2010 Research Assistant, Department of Marine and Coastal Sciences, Rutgers University

2004 Research Engineer, Coastal Ocean Observations Lab, Institute of Marine and Coastal Sciences, Rutgers University

2001-2004 Research Assistant, Center for Space Research, Department of Physics, MIT

2001 Spr. Research Assistant, Department of Physics and Astronomy, Rutgers University

PUBLICATIONS

Gong, D., J. T. Kohut, and S. M. Glenn (2010), Seasonal climatology of wind-driven circulation on the New Jersey Shelf, J. Geophys. Res., 115, C04006, doi:10.1029/2009JC005520.

O. Schofield, R. Chant, B. Cahill, R. Castelao, D. Gong, A. Kahl, J. Kohut, M. Montes-Hugo, R. Ramadurai, P. Ramey, Y. Xu, S. Glenn (2008), The Decadal View of the Mid-Atlantic Bight from the COOLroom: Is Our Coastal System Changing?, Progress in Oceanography, 23 (4), 108-117.

S. Glenn, O. Schofield, R. Chant, J. Kohut, H. Roarty, J. Bosch, L. Bowers, D. Gong and J. Kerfoot (2007), Wind-Driven Response of the Hudson River Plume and its Effect on Dissolved Oxygen Concentration, Environmental Research, Engineering and Management, No.1(39)

M. E. Gershenson, D. Gong, and T. Sato (2001), Millisecond electron-phonon relaxation in ultrathin disordered metal films at millikelvin temperatures, Appl. Phys. Lett., 79, 2049

Y. Fan, D. Gong (2000), On the Twist of Emerging Flux Loops in the Solar Convection Zone, Solar Phys., 192, 141